

# LIVE-LOAD TESTING AND FINITE-ELEMENT MODELING OF A FRACTURE CRITICAL BRIDGE

FINAL REPORT  
2016

Submitted by:

Jake L. Morrill, M.S.

Paul J. Barr, P.E., Ph.D.

Marvin W. Halling, P.E., Ph.D.

Utah State University  
4110 Old Main Hill  
Logan, UT 84322-4110

External Project Manager

Joshua Sletten  
Utah Department of Transportation  
4501 South 2700 West  
Salt Lake City, UT 84129

*This report has been published as a thesis  
for the degree of Master of Science in Civil & Environmental Engineering,  
Utah State University.*

In cooperation with

Rutgers, The State University of New Jersey  
And  
Utah Department of Transportation  
And  
U.S. Department of Transportation  
Federal Highway Administration

## **Disclaimer Statement**

The contents of this report reflect the views of the authors, who are responsible for the facts and the accuracy of the information presented herein. This document is disseminated under the sponsorship of the Department of Transportation, University Transportation Centers Program, in the interest of information exchange. The U.S. Government assumes no liability for the contents or use thereof.

The Center for Advanced Infrastructure and Transportation (CAIT) is a National UTC Consortium led by Rutgers, The State University of New Jersey. Members of the consortium are the University of Delaware, Utah State University, Columbia University, New Jersey Institute of Technology, Princeton University, University of Texas at El Paso, Virginia Polytechnic Institute and the University of South Florida. The Center is funded by the U.S. Department of Transportation.

TECHNICAL REPORT STANDARD TITLE PAGE		2. Government Accession No.		3. Recipient's Catalog No.	
1. Report No. <b>CAIT-UTC-NC12</b>					
4. Title and Subtitle <b>LIVE-LOAD TESTING AND FINITE-ELEMENT MODELING OF A FRACTURE CRITICAL BRIDGE</b>			5. Report Date <b>June 2016</b>		
7. Author(s) <b>Jake L. Morrill</b>			6. Performing Organization Code <b>CAIT/Utah State University</b>		
9. Performing Organization Name and Address <b>Utah State University 4110 Old Main Hill Logan, UT 84322-4110</b>			8. Performing Organization Report No. <b>CAIT-UTC-NC12</b>		
12. Sponsoring Agency Name and Address <b>Center for Advanced Infrastructure and Transportation Rutgers, The State University of New Jersey 100 Brett Road Piscataway, NJ 08854</b>			10. Work Unit No.		
			11. Contract or Grant No. <b>DTRT13-G-UTC28</b>		
15. Supplementary Notes <b>U.S. Department of Transportation/OST-R 1200 New Jersey Avenue, SE Washington, DC 20590-0001</b>			13. Type of Report and Period Covered <b>Final 9/1/14-6/30/16</b>		
			14. Sponsoring Agency Code		
16. Abstract <p>The Utah Transportation Center, in conjunction with CAIT at Rutgers, sponsored a study that investigated the distribution factors and load ratings of a continuous, steel-girder bridge. The SH-52 Bridge over the Snake River is located on the Idaho-Oregon border near Payette, Idaho. The bridge was built in the 1950's and presently supports two lanes of traffic.</p> <p>A finite-element model of the bridge was calibrated with the results from a live-load test. For the live-load test, the bridge was instrumented at nine longitudinal cross section locations with 62 strain gauges attached on the girders, stringers, and intermediate diaphragms. The live-load was applied with two heavy trucks that were driven along three predetermined load paths.</p> <p>The calibrated finite-element model was used to quantify moment distribution factors and load ratings for the bridge. The finite-element distribution factors were compared to those calculated according to the AASHTO Standard and AASHTO LRFD Specifications. The distribution factors from both AASHTO codes were found to be unconservative for the girders and overly conservative for the stringers.</p> <p>The model was also used to quantify the effect of the transverse diaphragm members on the live-load distribution. Distribution factors were calculated with and without the diaphragm members. The diaphragms were found to increase the distribution of moments by over 20% for both positive and negative moments.</p>					
17. Key Words <b>Bridge, steel, live load, distribution, load ratings</b>			18. Distribution Statement <b>No restrictions</b>		
19. Security Classification (of this report) <b>Unclassified</b>		20. Security Classification (of this page) <b>Unclassified</b>		21. No. of Pages <b>154</b>	22. Price
Form DOT F 1700.7 (8-69)					

## ACKNOWLEDGMENTS

I would like to thank Dr. Paul J. Barr for his help and patience for the countless times I stopped by his office or emailed him for help. I would not have been able to complete this project without his guiding influence. I would also like to thank the other professors on my committee, Dr. Marc Maguire and Dr. Joseph A. Caliendo for their role in the approval process. I also recognize the help and guidance of other professors and classmates who helped me and influenced me throughout my academic career.

I would also like to thank Bridge Diagnostics, Inc. for performing the live-load test and providing their data and report to us at USU. The live-load data was essential to be able to calibrate the finite-element model, and the report was very helpful in many aspects of this study.

Lastly, I would like to thank my parents for their continued love and support for me as I completed this project. They instilled in me the importance of gaining an education and were even so helpful as traveling to the bridge with me and making sure I had everything I needed for my thesis defense. I could not have made it this far without them.

Jake Morrill

## TABLE OF CONTENTS

Chapter 1.	INTRODUCTION .....	1
1.1	Context .....	1
1.2	Research Objectives .....	2
1.3	Organization of Report .....	3
Chapter 2.	REVIEW OF LITERATURE .....	4
2.1	Using Diagnostic Load Tests for Accurate Load Rating of Typical Bridges (Chajes, Shenton III) ..	4
2.2	Live-Load Test Comparison and Load Ratings of a Posttensioned Box Girder Bridge (Hodson, Barr, and Pockels, 2013) .....	4
2.3	Modeling the Response of Fracture Critical Steel Box-Girder Bridges (Barnard, Hovell, Sutton, Mouras, Neuman, Samaras, Kim, Williamson, and Frank) .....	6
2.4	Load Path Evaluation of the I-40 Bridge (Idriss, and Jauregui) .....	9
2.5	Inspection and Management of Bridges with Fracture-Critical Details (Connor, Dexter, and Mahmoud, 2005) .....	11
2.6	Ultimate Capacity Destructive Testing and Finite-Element Analysis of Steel I-Girder Bridges (Bechtel, McConnell, and Chajes, 2011) .....	12
Chapter 3.	LIVE-LOAD TEST .....	15
3.1	Bridge Description .....	15
3.2	Instrumentation and Load Paths .....	28
3.3	Live-Load Test Results .....	35
Chapter 4.	FINITE ELEMENT ANALYSIS .....	43
4.1	Description of Finite Element Model .....	43
4.2	Finite Element Live-Load Test .....	51
4.3	FE Model Results .....	53
4.4	Transverse Comparison of Strain .....	65
Chapter 5.	DISTRIBUTION FACTORS AND LOAD RATINGS .....	71
5.1	Comparison of Distribution Factors .....	71
5.2	Comparison of Distribution Factors with and without Diaphragm Bracing .....	81
5.3	Load Ratings .....	82
Chapter 6.	SUMMARY AND CONCLUSIONS .....	97
6.1	Summary .....	97
6.2	Conclusions .....	98
6.3	Recommendations for Additional Research .....	99

Chapter 7. REFERENCES ..... 101

Chapter 8. APPENDICES ..... 103

    APPENDIX A: INSTRUMENTATION ..... 103

    APPENDIX B: CAPACITY CALCULATIONS ..... 107

    APPENDIX C: DISTRIBUTION FACTOR CALCULATIONS ..... 121

    APPENDIX D: DISTRIBUTION FACTORS CALCULATIONS WITHOUT CROSS BRACING..... 135

    APPENDIX E: LOAD RATING CALCULATIONS ..... 144

## LIST OF TABLES

Table 3.1 Stringer Section Dimensions .....	20
Table 3.2 Load Cases and Live-Load Parameters .....	33
Table 3.3 Stringer-Deck Composite Action .....	39
Table 3.4 Maximum and Minimum Girder Stress Responses .....	40
Table 3.5 Maximum and Minimum Stringer Stress Responses .....	41
Table 5.1 Multiple Presence Factor vs. Lane Loading .....	72
Table 5.2 Distribution Factors for AASHTO Standard Specifications .....	73
Table 5.3 AASHTO LRFD Distribution Factors for Single Lane Loading .....	77
Table 5.4 AASHTO LRFD Distribution Factors for Double Lane Loading .....	77
Table 5.5 Finite-Element Positive Moment Distribution Factors.....	79
Table 5.6 Comparison of Positive Moment Distribution Factors.....	80
Table 5.7 Comparison of Negative Moment Distribution Factors .....	81
Table 5.8 Finite-Element Positive Moment Distribution Factors with and without Diaphragm Members	82
Table 5.9 Finite-Element Negative Moment Distribution Factors with and without Diaphragm Members .....	82
Table 5.10 Input Values for Compactness Checks .....	86
Table 5.11 Input Values for Equations 17, 18, and 19 .....	87
Table 5.12 Input Values for Girder Positive Moment Capacity .....	89
Table 5.13 Girder Positive Moment Capacity .....	90
Table 5.14 Input Values for the Requirement of Equation 27 .....	90
Table 5.15 Input Values for Equation 28.....	91
Table 5.16 Input Values to obtain $R_b$ .....	92
Table 5.17 Stringer Positive Moment Capacities .....	92
Table 5.18 Input Values for Equation 30.....	93
Table 5.19 Input Values for Equation 31.....	94
Table 5.20 Girder Negative Moment Capacities .....	95
Table 5.21 Summary of Girder and Stringer Capacities.....	95
Table 5.22 Summary of Positive Moment Load Rating Parameters .....	95
Table 5.23 Summary of Negative Moment Load Rating Parameters .....	96

## LIST OF FIGURES

Figure 3.1 SH-52 Bridge Over the Snake River .....	15
Figure 3.2 Bridge Span Lengths .....	16
Figure 3.3 Deck Cross Sectional Dimensions .....	16
Figure 3.4 Elevation View of Typical Bridge Railing .....	17
Figure 3.5 Pictures of Roller, Pinned, and Roller in Fixed Shoe Bearings .....	17
Figure 3.6 Girder Cross-Sectional Dimensions .....	18
Figure 3.7 Cover Plate Distances and Stiffeners .....	19
Figure 3.8 Stringer Cross-Sectional Dimensions .....	20
Figure 3.9 Stringer Layout .....	20
Figure 3.10 Vertical and Longitudinal Stiffeners near Pier 2 .....	21
Figure 3.11 Typical Cross Section at Locations of Vertical Diaphragms .....	22
Figure 3.12 Picture of Vertical and Transverse Diaphragms Members .....	23
Figure 3.13 Elevation View of Approach Span with Dimensions .....	24
Figure 3.14 Picture of Approach Span .....	24
Figure 3.15 Elevation View of Piers 1 and 4, and 2 and 3 .....	25
Figure 3.16 Plan View of Pier Caps 1 and 4, 2, and 3 .....	26
Figure 3.17 Plan View of Footings 1 and 4, 2, and 3 .....	27
Figure 3.18 Section A-A Instrumentation .....	29
Figure 3.19 Instrumentation at Section F-F .....	30
Figure 3.20 Truck Dimensions .....	31
Figure 3.21 Load Path Layout .....	32
Figure 3.22 Live-Load Test .....	34
Figure 3.23 Example Plot of Neutral Axis vs. Longitudinal Position for Girder 2 .....	36
Figure 3.24 Stinger-Deck Level of Composite Action .....	38
Figure 3.25 Response at Section A-A due to Approach Spans .....	40
Figure 3.26 Response Comparison between Crawl Speed and Normal Speed Data .....	42
Figure 4.1 3-D View of SH-52 Bridge Over the Snake River Finite-Element Model .....	46
Figure 4.2 Extruded View of Bridge Substructure .....	47
Figure 4.3 Extruded View of Cover Plates near Piers 2 and 3 .....	48
Figure 4.4 Bridge Vertical Diaphragm .....	49
Figure 4.5 Finite-Element Live-Load Test .....	53
Figure 4.6 Deformed Shape of Analyzed Bridge with Truck near Mid Span .....	54
Figure 4.7 Stress Response vs. Longitudinal Position in Girder 1 at Section E-E .....	56
Figure 4.8 $R^2$ Correlation and Slope of Line for Measured vs. FE Data for Girder 1 .....	56
Figure 4.9 Stress Response vs. Longitudinal Position in Girder 2 at Section E-E .....	57
Figure 4.10 $R^2$ Correlation and Slope of Line for FE vs. Measured Data .....	57
Figure 4.11 Stress Response vs. Longitudinal Position in Stringer 1 at Section E-E, Load Path Y2 .....	58
Figure 4.12 $R^2$ Correlation and Slope of Line for FE vs. Measured Data .....	59
Figure 4.13 Stress Response vs. Longitudinal Position in Stringer 2 at Section E-E, Load Path Y2 .....	59

Figure 4.14 $R^2$ Correlation and Slope of Line for FE vs. Measured Data .....	60
Figure 4.15 Correlation for Girders at Sections E-E and B-B and for Stringers at Section E-E .....	61
Figure 4.16 Diaphragm Reference Figure .....	62
Figure 4.17 Stress Response vs. Longitudinal Position in Floor Beam .....	62
Figure 4.19 Example Stress Response in Bottom Right Beam .....	63
Figure 4.18 Example Stress Response in the Right Diagonal Diaphragm Member .....	63
Figure 4.20 Correlation of all Load Paths for Transverse Diaphragm Members .....	64
Figure 4.21 $R^2$ Correlation for all Load Paths and all Structural Supporting Members .....	65
Figure 4.22 Transverse Strain Distribution in Bottom Flanges for Load Path Y1 .....	66
Figure 4.23 Transverse Strain Distribution in Top Flanges for Load Path Y1 .....	67
Figure 4.24 Transverse Strain Distribution in Bottom Flanges for Load Path Y .....	67
Figure 4.25 Transverse Strain Distribution for Top Flanges in Load Path Y3 .....	68
Figure 4.26 Transverse Strain Distribution in Top Flanges with Snooper at 91.44 m (300 ft) for Load Path Y1 .....	69
Figure 4.27 Transverse Strain Distribution in Top Flanges with Snooper at 91.44 m (300 ft) for Load Path Y1 .....	69
Figure 4.28 Strain Distribution in Bottom Flanges with Snooper at 91.44 m (300 ft) for Load Path Y3 .....	70
Figure 4.29 Transverse Strain Distribution in Top Flanges with Snooper at 91.44 m (300 ft) in Load Path Y3 .....	70
Figure 5.1 Schematic Drawing of the Lever Rule .....	75
Figure 5.2 Schematic Drawing of an HS-20 Truck .....	77

# CHAPTER 1. INTRODUCTION

## 1.1 Context

The Utah Transportation Center (UTC) located on the campus of Utah State University (USU), sponsored a study to investigate the differences in distribution factors calculated according to the AASHTO bridge design specifications and the results of a calibrated finite-element model of a fracture-critical, steel I-girder bridge. Load ratings were also calculated based on the results of the finite-element model. Bridge Diagnostics Inc. (BDI) performed the diagnostic load testing for this project and subsequently provided the data to researchers at USU. BDI was originally contracted by the Idaho Transportation Department to perform a live-load test on the SH-52 Bridge over the Snake River near Payette, Idaho. The bridge was instrumented with strain gauges at nine longitudinal cross-section locations. Two trucks combined for three loading scenarios; a snoop truck was driven individually, and side-by-side and in tandem with a gravel truck. The loading scenarios occurred at three predetermined transverse positions that were selected to maximize the loading experienced by each supporting steel beam. Data from the sensors was recorded with the corresponding longitudinal position of the truck(s).

Calibrated finite-element models provide a more accurate description of actual bridge behavior in comparison to the AASHTO bridge design specifications. The AASHTO specifications provide simplified equations that have been found to be conservative and therefore less accurate. The results of the finite-element analyses tend to improve the load ratings, ease restrictions, and provide more accurate data for maintenance or replacement requirements assigned to a bridge.

Many studies involving finite-element analysis have been performed on various kinds of bridges. Hodson, Barr, and Pockels (2013) examined a post-tensioned box girder bridge. Idris

and Jauregui created a finite-element model and studied the effects of alternate load paths on a two-girder, fracture-critical, steel bridge. Yanadori and Barr (2004) used a finite-element model to study the static and dynamic behavior of a continuous, steel, I-girder bridge. The SH-52 Bridge over the Snake River is unique because it is an old, steel I-girder, fracture critical bridge, with two large fabricated exterior girders, and two smaller, rolled wide flange section, interior stringers. This cross-section does not fit into the standard cross-sectional shapes defined in the AASHTO specifications.

## **1.2 Research Objectives**

This research compared the distribution factors and load ratings calculated according to the AASHTO Standard and AASHTO LRFD Specifications to the distribution factors obtained from a finite-element model that was calibrated with a live-load test. Load ratings for the bridge were calculated using the dead and live load response in the beams from the calibrated model. Additionally, the effects of the intermediate diaphragm members were investigated. Since the finite-element model was three dimensional, the diaphragms members could be removed, and their impact on the distribution of moments was quantified.

The AASHTO Standard Specifications (2002) provide a simplified equation for calculating distribution factors for interior beams, and a procedure (the lever rule) and limiting equation for the distribution factors for exterior beams of steel I-girder bridges. The equations and procedure do not take into account member stiffness, span length, deck thickness, or system behavior of the bridge. The procedures and equations from the AASHTO LRFD Specifications (2010) take into account more parameters such as member stiffness, span length, and deck thickness, but are based on standard cross-sectional shapes where the beam stiffness is

approximately constant. Calibrated finite-element models can provide more accurate distribution factors by accounting for member stiffness, span length, deck thickness, and system behavior, as well as the variability in composite behavior present between the deck and the supporting beams.

### **1.3 Organization of Report**

For this research, a 3-D finite-element model was created using CSiBridge 2015 version 17.3.0 (Computers and Structures, Inc., 2015). The model was calibrated using live-load data. The model was subsequently used to find distribution factors and load ratings for the bridge. The report is organized in this manner:

- Chapter 2 presents a review of previous studies relating to live-load diagnostic testing and finite-element model calibration.
- Chapter 3 details the bridge specifications, member instrumentation, and live-load test.
- Chapter 4 describes the finite-element model, the results of the model, and the calibration to live-load data.
- Chapter 5 discusses the calculations and comparison of distribution factors calculated according to the AASHTO Standard Specifications (2002), AASHTO LRFD Specifications (2010), and the finite-element analysis, as well as the calculation of the load ratings.
- Chapter 6 provides a summary of the research, conclusions, and recommendations for future work.

## CHAPTER 2. REVIEW OF LITERATURE

### 2.1 Using Diagnostic Load Tests for Accurate Load Rating of Typical Bridges (Chajes, Shenton III)

This study examined the effectiveness of diagnostic-load tests to improve the accuracy of bridge load ratings. Many bridges are approaching the end of their intended design life. Due to limited resources and other restraints, constructing new bridges is not always feasible. However, various calculations to determine bridge design life are often conservative by nature. A load rating derived exclusively from theoretical calculations is one calculation that can be very conservative. A diagnostic-load test will allow bridge engineers to assign bridges a more accurate rating, and potentially preserve the life of the bridge. A diagnostic-load test is performed by placing strain gages or transducers at various specified locations along the length of the bridge. One or more heavy vehicles are driven along the length of the bridge at speeds between 8-16 kph (5-10 mph) along predetermined lines. Dynamic load effects may be determined by driving the vehicles along the same load paths at the posted speed limit. Strain data is collected and stored for each pass made by the vehicles. The results of the test are used to quantify maximum member forces. Additionally, the data is used to determine the effects of lateral load distribution, support fixity, composite action, and secondary members. These effects along with the load test results are then used to calculate a more accurate load rating for the bridge.

### 2.2 Live-Load Test Comparison and Load Ratings of a Posttensioned Box Girder Bridge (Hodson, Barr, and Pockels, 2013)

In this study a post-tensioned, box girder bridge, was examined. A live-load test was performed with 56 strain gauges being attached to various locations on the superstructure of the

bridge. An HS20-44 design truck was driven along three separate load paths, and was repeated twice to ensure reproducible results. The results from this live-load test were compared to the results from a nearly identical live-load test performed 20 years earlier. It was found that the bridge exhibited less strain in the most recent live-load test despite the design truck being slightly heavier. The reduction in strain is attributed to improved bridge stiffness over time. After in-situ testing was complete, a finite-element model of the bridge was created. Aside from comparing the response of the bridge to the results of the previous live-load test, the test also allowed the researchers to validate the finite-element model with the recorded strain data. The strains from the live-load data and the finite-element model were compared and a coefficient of correlation of 0.95 was calculated between the two data sets. The overall finite-element strain was found to be less than the live-load test strain by 9%. While slightly unconservative, the finite-element strain values were sufficiently close to accurately predict the distribution factors and load ratings for the bridge.

The finite-element model was used to find the maximum positive and negative moments by modeling the truck loads as concentrated loads on the load paths. From these maximum moments, moment distribution factors were computed and compared to those obtained based on the AASHTO LRFD Specifications. The AASHTO LRFD distribution factors and the finite-element distribution factors were similar for the interior girders. The finite-element and the AASHTO LRFD distribution factors for the exterior girders were significantly different, however, with the AASHTO factors being 34.1% more conservative. The inventory and operating load ratings were subsequently calculated using the validated finite-element model.

The load ratings found using the finite-element model were 13.7% larger than those calculated using the AASHTO LRFD specifications.

### **2.3 Modeling the Response of Fracture Critical Steel Box-Girder Bridges (Barnard, Hovell, Sutton, Mouras, Neuman, Samaras, Kim, Williamson, and Frank)**

This research examined the tendency of some fracture-critical bridges (FCBs) to have load redundancy, meaning they continue to function after a fracture-critical member (FCM) completely fractures. While many FCBs will collapse when a FCM fails, there are also examples to the contrary. Some FCBs have continued to carry normal loads until their fractures were inadvertently discovered. Due to safety concerns, FCBs require more frequent, labor intensive, and costly inspections. A FCB must be inspected every six months, and receive a full inspection every two years. In the costly full inspection (about \$400,000 per day), every welded connection to a FCM must be examined. For these reasons, bridge owners have begun to question the necessity of the more strict FCB inspection requirements for every FCB.

This study was funded by the Federal Highway Administration and the Texas Department of Transportation (TxDOT). It was performed at the University of Texas at Austin. Texas has particular interest in this subject because TxDOT owns and operates over 50,000 bridges, many of which are fracture-critical. In this study, only twin steel box-girder bridges, a common FCB design, were considered.

This research extensively examined redundancy in load paths of FCBs using a variety of techniques. A full-scale twin steel box-girder bridge was built and tested. Large specimens were also tested in the laboratory to experimentally calculate the strength of specific bridge

components. Additionally, structural analysis was performed using hand calculations, and computer simulations.

The constructed full-scale bridge was designed to replicate a worst-case scenario. The bridge was simply supported, thus lacking any inherent redundancy that statically indeterminate structures experience. All external braces that could have contributed to redistributing loads were removed after construction. Bridge railing was constructed with expansion joints which limited their ability to contribute to overall bridge strength. Lastly, the bridge had a horizontal plan curve, and the exterior girder was the one that experienced the fracture in testing.

The first test was performed by detonating an explosive to rapidly cut through the bottom flange of the exterior girder, replicating what the bridge would experience in fracture. The equivalent of an HS-20 truck load was positioned straight above the fracture location. Despite the fracture, the bridge deflected less than 25 mm (1 in.). In the second test the fracture in the exterior girder was extended up until 83% of the web was pre-fractured. The bridge was again loaded directly above the fracture with the equivalent of an HS-20 truck and only deflected 178 mm (7 in.). The final test the bridge underwent was ultimate loading capacity. The bridge was loaded with 1615 kN (363,000 lbs.) before collapsing, or five times larger than the legal truck load.

Along with field testing, finite-element (FE) models were created and subsequently compared to the field test results. The results from the FE models correlated well with the collected field test data. The results from the first test that the FE models experienced showed a deflection of 133 mm (5.23 in.) which was slightly less than the 143 mm (5.64 in.) deflection experienced in the field test. This result was considered acceptable. In the second test, the FE

models predicted a vertical deflection that was only 2% larger than was measured for the intact, interior girder. However, the models predicted a deflection that was 23% higher than was measured for the fractured, exterior girder. In the simulated third test the FE models successfully predicted the failure modes observed during the field test, and predicted a similar ultimate load capacity. Additionally, the FE models successfully predicted prominent bridge component failures, which were experienced during the second and third tests.

Using the FE model, the authors investigated how variations of parameters affected ultimate load capacity. Shear stud length, horizontal curvature, bridge span length, and structural indeterminacy were studied to determine their effect on the strength of the bridge. Pull-out strength of stud connections had a large effect on bridge failure after the girder was fractured. The capacity of shear studs to resist pull-out increased with length. It was found that as the radius of horizontal curvature decreased, deflections in the fractured girder increased. The research also showed that deflection in the fractured girder correlated more with the span length-to-depth ratio, than with span length alone. Lastly, it was found that structural indeterminacy positively affected the overall load bearing capacity. These findings confirmed that redundancy exists in twin steel box-girder bridges.

The AASHTO LRFD Bridge Design Specifications classify twin steel box-girder bridges as fracture critical. This research examined the redundancy that exists in this type of bridge. The authors conclude that after further research efforts, revisions to the AASHTO specifications regarding twin steel box-girder bridges should be considered. More appropriate inspection and maintenance requirements could be prescribed, and save millions of dollars in maintenance and inspection costs.

#### **2.4 Load Path Evaluation of the I-40 Bridge (Idriss, and Jauregui)**

This study investigated alternate load paths present in two-girder, fracture-critical, steel bridges. The research examined one main girder of one three-span section of the I-40 Bridge over the Rio Grande in Albuquerque, New Mexico. For the purposes of the study, the bridge was tested both analytically and experimentally. First, a 3-D finite-element (FE) model was created and tested, and secondly a field test was performed. The bridge section was tested both before, and after receiving a near full depth crack. The results of the two testing methods were recorded and compared.

The authors created a 3-D FE model of the bridge section using SAP90 software. In the FE model, each individual bridge component was modeled using a variety of options available in the program. The fracture was modeled by disconnecting the web and bottom flange elements of the girder, at the crack. The crack was 1.83 m (6 ft) deep, extending from the connection of the floor beam to the girder, down through the bottom flange of the girder. The FE model was loaded with the equivalent of an HS-18.35 truck, above the location of fracture.

To check the accuracy of the SAP90 3-D model, two additional computer models were created, and hand calculations were performed. The two separate 2-D models were created using SAP90 and RISA 2-D. Hand calculations were performed using the method of consistent deformations. Upon comparison, it was determined that the 3-D model correlated well with the 2-D models and hand calculations, with some slight discrepancies.

The results of the analytical models predicted that, despite the crack, the structure would remain stable. The principal alternate load path was the damaged girder itself. Acting as a cantilever, the load was redistributed to the interior support. Most of the load was redistributed

longitudinally, while a smaller portion was redistributed transversely across the deck, floor beams, and bracing system to the intact girder. The predicted after-fracture deflection at the mid span of the intact girder, due to the live load, was 12 mm (0.48 in.).

For the field test, the bridge section was also tested in both pristine, and fractured conditions. First, the bridge was loaded and measurements were collected while the bridge was still in pristine condition. Next, the girder was manually cut to create the fractured condition. The cut extended up 1.83 m (6 ft) from the bottom of the 3.05 m (10 ft) girder, matching the fracture used in the analytical models. The bridge section was then loaded with the same truck load, and measurements for strain, deflection, and load redistribution were collected. The after-fracture deflection at the mid span due to the live load was 13mm (0.50 in.).

After testing was completed, the results from the analytical and experimental tests were compared. The two sets of results correlated well, with the analytical model sufficiently predicting strains, deflections, and load redistributions for both the pristine and fractured conditions. Additionally, the analytical test was also accurate in predicting that, under the specified loads, no yielding would occur.

The authors found that computer modeling was very valuable in studying the behavior of the bridge section, and analytical models can be used to successfully predict bridge response. It was concluded that after fracture, the bridge transformed into a new, but stable structure. The main load path after fracture was the damaged girder. The fractured girder was converted from a continuous beam into two cantilever beams connected just above the crack. A smaller portion of the load was redistributed transversely across the bridge, to the other intact girder. This mainly occurred near the location of the crack. Lastly, it was concluded that connections are important

to ensure redundancy in a structure. The connections allowed the floor beams to redistribute the load transversely.

## **2.5 Inspection and Management of Bridges with Fracture-Critical Details (Connor, Dexter, and Mahmoud, 2005)**

The objective of this project was to search for, find, document, and compile current knowledge of fracture-critical bridges (FCBs). Information was gathered from thirty-four states and three Canadian provinces containing FCBs, which responded to a survey. The collected information was used for three main purposes: (1) identify gaps in existing literature; (2) determine best practices in defining, identifying, documenting, inspecting, and managing FCBs; (3) identify research needs.

A bridge is defined as “a structure, including supports, erected over a depression or an obstruction . . . having an opening measured along the center of the roadway of more than 20 feet” (AASHTO LRFD Bridge Design Specifications). A FCB refers to a bridge that has fracture-critical members (FCMs). These members are defined in the AASHTO LRFD Bridge Design Specifications as “component[s] in tension whose failure is expected to result in the collapse of the bridge or the inability of the bridge to perform its function.” Eleven percent of steel bridges in the United States are classified as FCBs.

Due to lack of clarity in the literature, bridge owners are not consistent in classifying bridges as fracture-critical. In California alone, substantial disagreement was observed in FCB classification. Additionally, there were significant differences in the classification of the same bridge style as fracture-critical or non-fracture-critical between those states and provinces that responded to the survey.

FCBs pose a greater risk for collapse, as such they require more frequent and in-depth inspections. Because frequency and depth of inspections are generally based on bridge classification, it is important that they are classified correctly. Inspection of FCBs is on average two to five times more expensive than inspection of non-FCBs. FCBs are commonly inspected more frequently than those without FCMs, which also raises bridge maintenance costs.

Hands-on inspection of FCBs has been effective in revealing numerous fatigue and corrosion problems that had otherwise been undetected. However, hands-on inspections are not needed in all cases, and frequency of such tests could be based on risk factors. The survey found that sufficient training for bridge inspectors is available, but additional training is needed for bridge engineers. It was also noted that increased efforts are needed to document and archive previous bridge failures and problems.

Several needs for additional research were identified. Differing interpretations of FCB classification exist. Depth and frequency of inspections for individual FCBs vary. The extent of serviceability of already cracked FCBs is also largely unknown. Efforts should be made to further understand and study FCBs in order to update and unify existing definitions and design specifications.

## **2.6 Ultimate Capacity Destructive Testing and Finite-Element Analysis of Steel I-Girder Bridges (Bechtel, McConnell, and Chajes, 2011)**

This study compared the ultimate capacity of bridges with their design capacity according to AASHTO code. The ultimate capacity of a 1/5 scale-model bridge was quantified by performing an ultimate capacity destructive test. The results of the test were compared to the

results of a finite-element (FE) analysis of the same scaled bridge to determine correlation and deficiencies of the FE model.

Destructive tests of full-scale bridges have been performed since the 1970's. The results have overwhelmingly shown that the ultimate capacity of the tested bridges is greater (often significantly) than the design capacity. It is widely accepted that the increased bridge strength in relation to design capacity is because of current design and rating procedures. Current practices consider individual member component resistance instead of system-level resistance. Due to the fact that loads redistribute through redundant load paths, system-level behavior is what in reality occurs. Advances in computer technology have facilitated the more accurate system-level analysis. However, additional testing is needed to validate assumptions made in creating FE models. Increased accuracy in predicting ultimate bridge capacity through system-level analyses will potentially have a large impact on economic design, and bridge ratings.

Although very useful, full-scale bridge destructive testing is rare because of testing costs, and available bridges. Consequently, it is convenient to construct a scale-model bridge which can be tested in a laboratory. The authors used dimensional analysis to create a 1/5 scale-model of a skewed four-girder steel bridge. The bridge was designed and built according to the AASHTO LRFD Design Specifications and based on the Delaware River and Bay Authority Bridge 7R. The bridge was tested using two 996.4 kN (100 ton) jacks, and a single 597.84 kN (60 ton) jack. These were used to resemble the three axles of an AASHTO design truck. The jacks were placed over an interior girder to reduce the chance of punching shear and to monitor load redistribution. Through testing it was determined that the scale-model bridge reached its ultimate capacity when loaded with an equivalent of 22 trucks.

A FE model of the bridge was created and the results were compared to those found in testing. This allowed the authors to evaluate the techniques and assumptions used in creating the FE model. The FE bridge model was found to reach its ultimate capacity when loaded with 21 trucks. The overall results showed that the FE model correlated well with the scale-model bridge. Despite the correlation, differences between the FE and scale-model bridges were discovered in the yielding point of the girders. It was hypothesized that the girders in the scale-model test yielded sooner due to stresses experienced during construction.

It was concluded that many more destructive tests must be performed to accurately predict the post-elastic response of bridges. When response can be accurately predicted, it will allow engineers to design and evaluate bridges to their system-level capacities. This in turn will provide increased knowledge of when bridges need to be replaced or repaired.

## CHAPTER 3. LIVE-LOAD TEST

### 3.1 Bridge Description

The SH-52 Bridge over the Snake River is located on the Idaho-Oregon border near Payette, ID. The SH-52 Bridge is part of a two-lane highway system providing one lane of vehicles in the east and west direction. The bridge carries traffic across the Snake River, and is shown in *Figure 3.1*. It was originally designed for H15-S12-44 loading, and was constructed in the 1950's. The bridge was designed and constructed using five spans; three main spans (Spans 1, 2, and 3) and two approach spans (Spans A1 and A2). Span 1 is supported by piers 1 and 2, Span 2 is supported by piers 2 and 3, and Span 3 by piers 3 and 4. Spans A1 and A2 are supported by the abutments on the shore and piers 1 and 4, respectively. Spans 1 and 3 are 56.24 m (184.5 ft) long, Span 2 is 72.92 m (239.25 ft) long, and each approach span is 12.19 m (40 ft) long, as shown in *Figure 3.2*. The total bridge length is approximately 185.39 m (608.25 ft).



*Figure 3.1 SH-52 Bridge Over the Snake River*

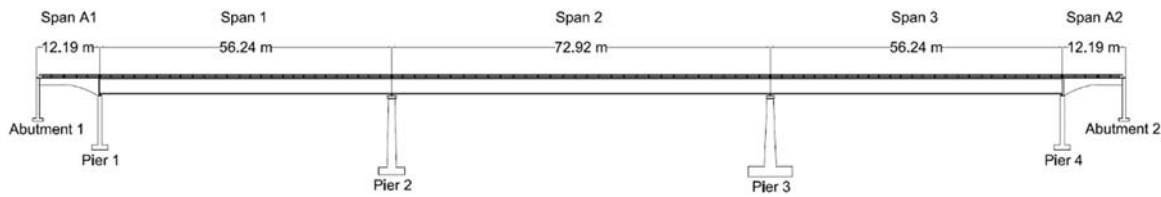


Figure 3.2 Bridge Span Lengths

The roadway deck of the three continuous main spans (spans 1 through 3), is supported with a twin girder and stringer system. The deck is supported with reinforced concrete, T-beam sections over the approach spans. The deck width is 9.30 m (30.5 ft), with a roadway width of 7.92 m (26.0 ft). The deck has an overall depth of 165.1 mm (6.5 in.) with an asphalt wearing surface of 12.7 mm (0.5 in.). The curb is 393.7 mm (15.5 in.) thick and 647.7 mm (25.5 in.) wide on each side. The bridge railing has a height of 0.89 m (35 in.), and is comprised of L101.6x101.6x9.5 mm (4x4x3/8 in.) angle sections that span between railing posts. The maximum railing span length is 2.44 m (8.0 ft). A cross-section of the deck is shown in *Figure 3.3*, and the bridge railing is shown in *Figure 3.4*.

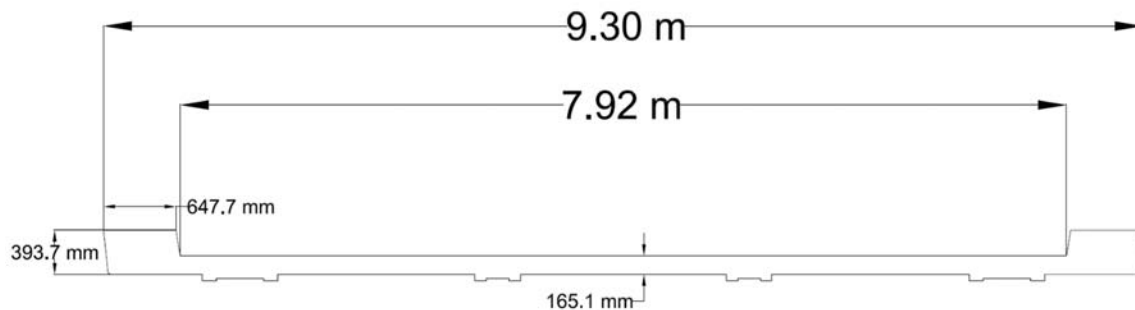


Figure 3.3 Deck Cross Sectional Dimensions

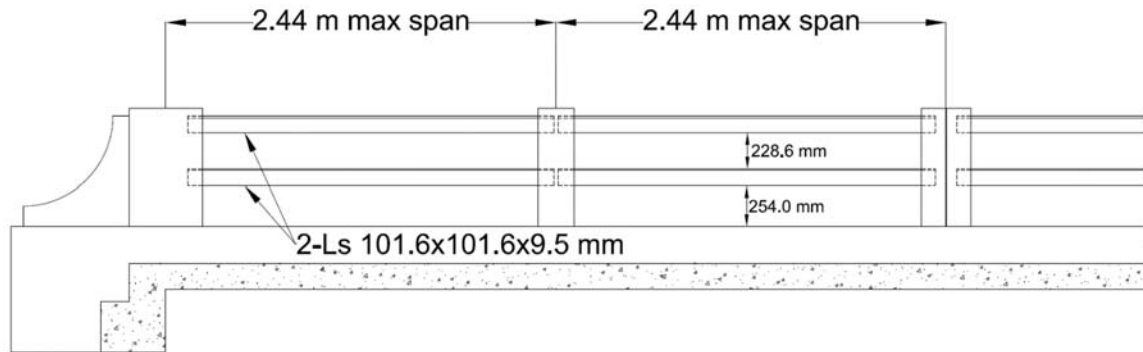


Figure 3.4 Elevation View of Typical Bridge Railing

For the twin girder and stringer system, the girders support the deck on the outside while the stringers support the deck near the middle, transversely. The stringers are spaced 2.31 m (7.56 ft) in from the girders on either side of the bridge, and the spacing is 2.25 m (7.38 ft) between stringers. The girders are supported with bearings at their respective piers. The bearings on piers 1, 2, and 4 were designed as roller connections, and the bearing on pier 3 was designed as a pinned connection. The stringers are supported by a double angle floor beam (L101.6x88.9x15.88 mm, L4x3.5x5/8 in.) that connects to the girders. The bearings are shown in *Figure 3.5*.



Figure 3.5 Pictures of Roller, Pinned, and Roller in Fixed Shoe Bearings

Each girder was fabricated as a built up section, 2-L203.4x203.4x101.6 mm (L8x8x3/4 in.) angle sections were used as the flanges on the top and bottom of the girders, a 3.06 m x 12.7 mm (10.04 ft x 0.5 in.) plate was used as the girder web. A cross section of the girders is shown in *Figure 3.6*.

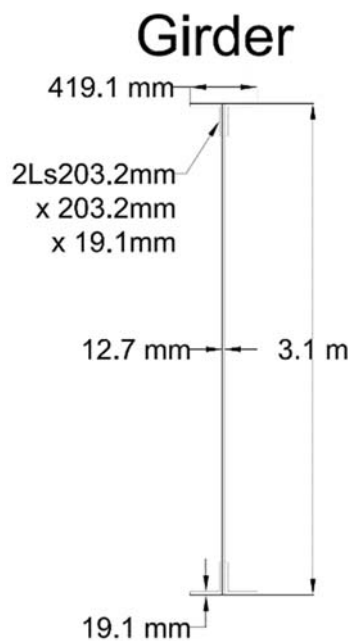


*Figure 3.6 Girder Cross-Sectional Dimensions*

Near piers 2 and 3, 508 mm x 19.1 mm (20 in. x 0.75 in.) cover plates were placed above and below the top and bottom flanges. As the girders become closer to the piers, two, then three cover plates were placed above and below the girder flanges. The bottom cover plate runs 17.80 m (58.40 ft), approximately 8.90 m (29.20 ft) to each side of piers 2 and 3. The middle cover plate spans 14.83 m (48.67 ft), and runs 7.42 m (24.33 ft) on each side of piers 2 and 3. The top cover plate spans 9.30 m (30.5 ft), running 4.65 m (15.25 ft) on each side of piers 2 and 3. The lengths of cover plates is the same on the top and the bottom of the girders. *Figure 3.7* shows the lengths of the cover plates.

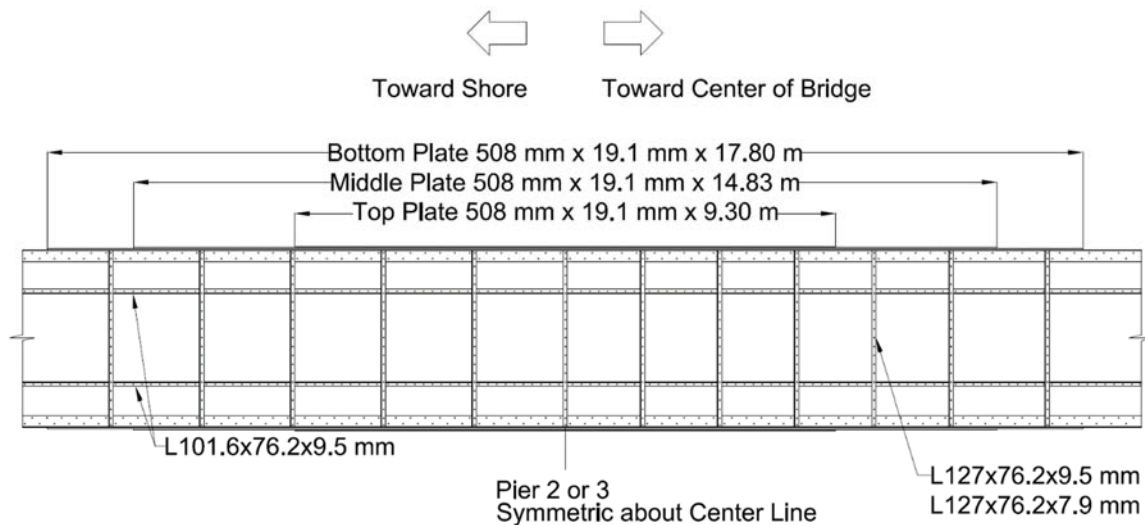


Figure 3.7 Cover Plate Distances and Stiffeners

For the stringers, three different rolled wide flange sections were used. On the west side (stringer S1), a 16 WF 45 section was used for the first 11.32 m (37.13 ft) from the beginning of Span 1. For the next 37.49 m (123.0 ft) a 16 WF 36 section was used. From that point to the bridge centerline (44.08 m, 144.63 ft), a 16 WF 40 section was used. This layout for S1 was symmetric about the centerline of the bridge. On the east side (stringer S2), a 16 WF 45 section spanned the first 7.81 m (25.0 ft). A 16 WF 36 section then spanned the next 49.99 m (164.0 ft). From that point to the centerline (35.09 m, 115.13 ft) a 16 WF 40 section was used. The layout for S2 was also symmetric about the centerline. Stringer cross sectional dimensions are shown in *Figure 3.8*. The stringer dimensional properties are listed in *Table 3.1*, and *Figure 3.9* shows in plan-view the layout of the stringers.

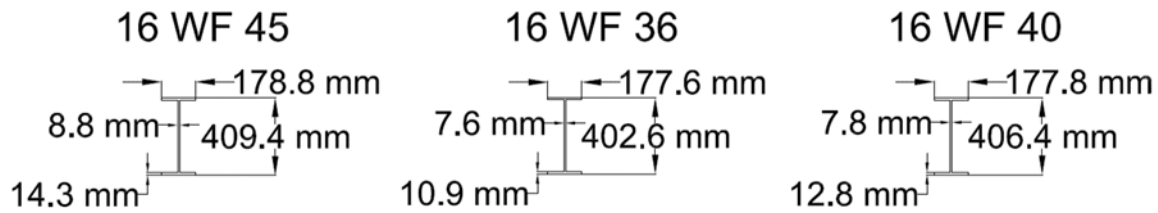


Figure 3.8 Stringer Cross-Sectional Dimensions

Table 3.1 Stringer Section Dimensions

Stringer Section	Height (mm)	Flange Width (mm)	Flange thickness (mm)	Web thickness (mm)
16 WF 45	409.4	178.8	14.3	8.8
16 WF 36	402.6	177.6	10.9	7.6
16 WF 40	406.4	177.8	12.8	7.8

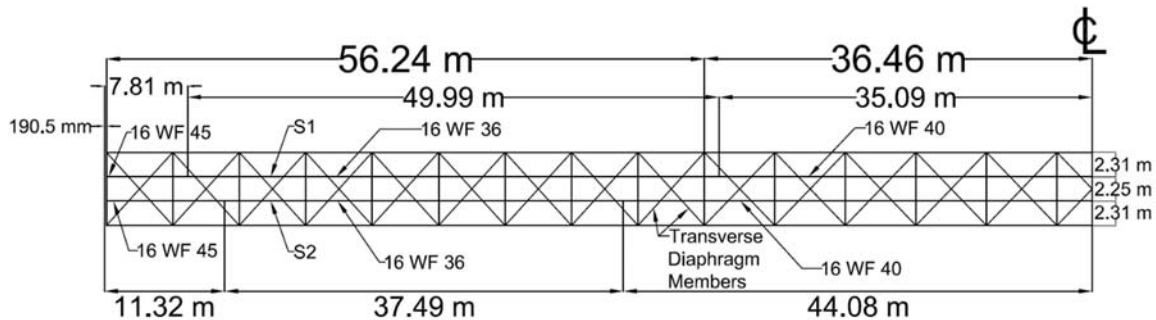


Figure 3.9 Stringer Layout

Additional capacity for the girders was provided by vertical and longitudinal stiffeners. Vertical stiffeners were placed on the inside and outside of the web, and generally spaced at 1.56 m (61.5 in.) and 1.66 m (65.25 in.) in spans 1 and 3, and 2, respectively. Longitudinal stiffeners were placed only on the outside, and near the top of the webs along the entire length of the bridge. However, close to piers 2 and 3, longitudinal stiffeners were also placed near the bottom of the webs. The longitudinal stiffeners were placed 0.53 m (1.75 ft) away from the flange angles at the top and bottom of the webs. For the vertical stiffeners, angle sections L127x76.2x9.5 mm

(L5x3x3/8 in.) and L127x76.2x7.9 mm (L5x3x5/16 in.) were generally used, with the exception of L152.4x101.6x11.1 mm (L6x4x7/16 in.) and L152.4x101.6x15.9 mm (L6x4x5/8 in.) sections being used for small segments near the piers. For the longitudinal stiffeners, the angle section L101.6x76.2x9.5 mm (L4x3x3/8 in.) was generally used, with L76.2x76.2x7.9 mm (L3x3x5/16 in.), and L101.6x76.2x11.1 mm (L4x3x7/16 in.) sections also being used for portions of the bridge. Vertical and longitudinal stiffeners near pier 2 are shown below in *Figure 3.10*.

The bridge diaphragms provide torsional resistance for the bridge. This resistance is supplied both transversely (as shown in *Figure 3.9 and Figure 3.12*) and vertically (*Figure 3.11 and Figure 3.12*). The transverse diaphragm connects the bottom flange of each girder diagonally. Six different angle sections were used, L127x88.9x7.9 mm (L5x3.5x5/16 in.), L127x76.2x7.9 mm (L5x3x5/16 in.), L127x127x11.1 mm (L5x5x7/16 in.), L127x88.9x11.1 mm (L5x3.5x7/16 in.), L127x127x12.7 mm (L5x5x1/2 in.), and L127x88.9x9.5 mm (L5x3.5x3/8 in.). The vertical diaphragms are spaced at 6.25 m (20.5 ft) in spans 1 and 3, and 6.63 m (21.75



*Figure 3.10 Vertical and Longitudinal Stiffeners near Pier 2*

ft) in span 2. The vertical diaphragm members are connected from the bottom of the floor beam to the bottom of the girders, and in between as shown in *Figure 3.11*. Seven different angle sections were used for the floor beam and vertical diaphragm, 2Ls 101.6x88.9x15.9 mm (2Ls 4x3.5x5/8 in.), 2Ls 152.4x88.9x9.5 mm (2Ls 6x3.5x3/8 in.), 2Ls 127x88.9x7.9 mm (2Ls 5x3.5x5/16 in.), 2Ls 101.6x88.9x7.9 mm (2Ls 4x3.5x5/16 in.), 2Ls 76.2x88.9x9.5 mm (2Ls 3x3.5x3/8 in.), 2Ls 101.6x101.6x9.5 mm (2Ls 4x4x3/8 in.), and L101.6x76.2x9.5 mm (L 4x3x3/8 in.).

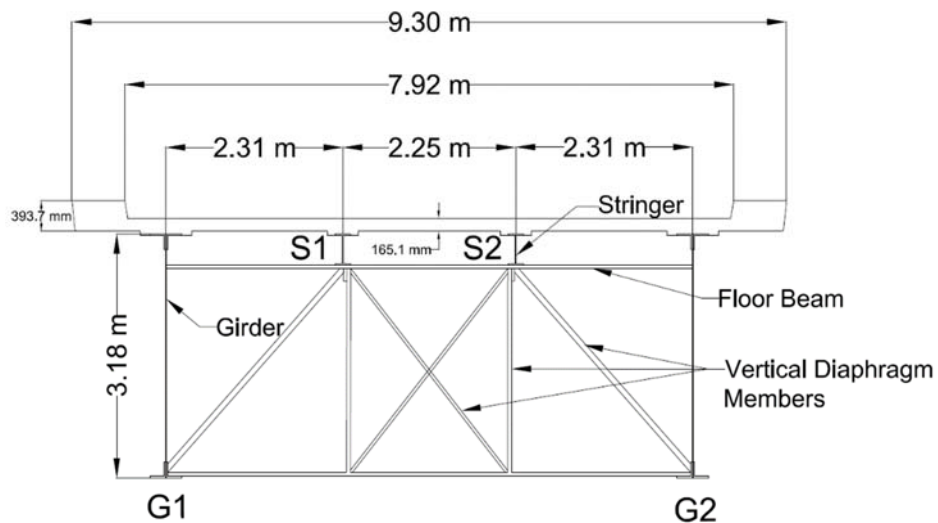


Figure 3.11 Typical Cross Section at Locations of Vertical Diaphragms



*Figure 3.12 Picture of Vertical and Transverse Diaphragms Members*

The two 12.19 m (40 ft), approach spans (A1 and A2 in *Figure 3.2*), were connected from the abutments on the shore to piers 1 and 4. The approach spans have a parabolic parametric variation, with a radius of 7.9 m (25.92 ft). The variation extends from the pier back toward the abutment 5.76 m (18.90 ft). The T-beams that support the deck are spaced transversely at 2.29 m (7.5 ft) on center. Longitudinally, the T-beams are 330.2 mm (13 in.) wide by 1.22 m (48 in.) deep from the abutment to the parametric variation, and then follow the variation. The approach span is shown below (*Figures 3.13 and 3.14*).

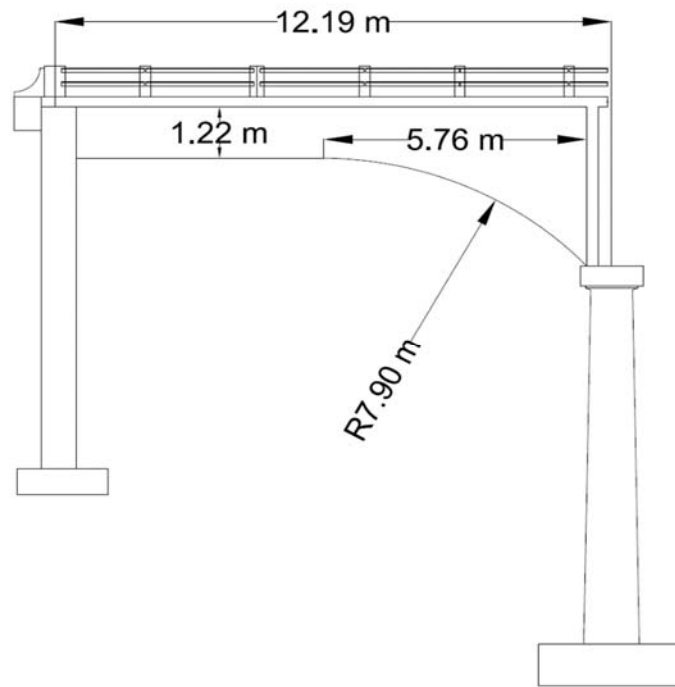
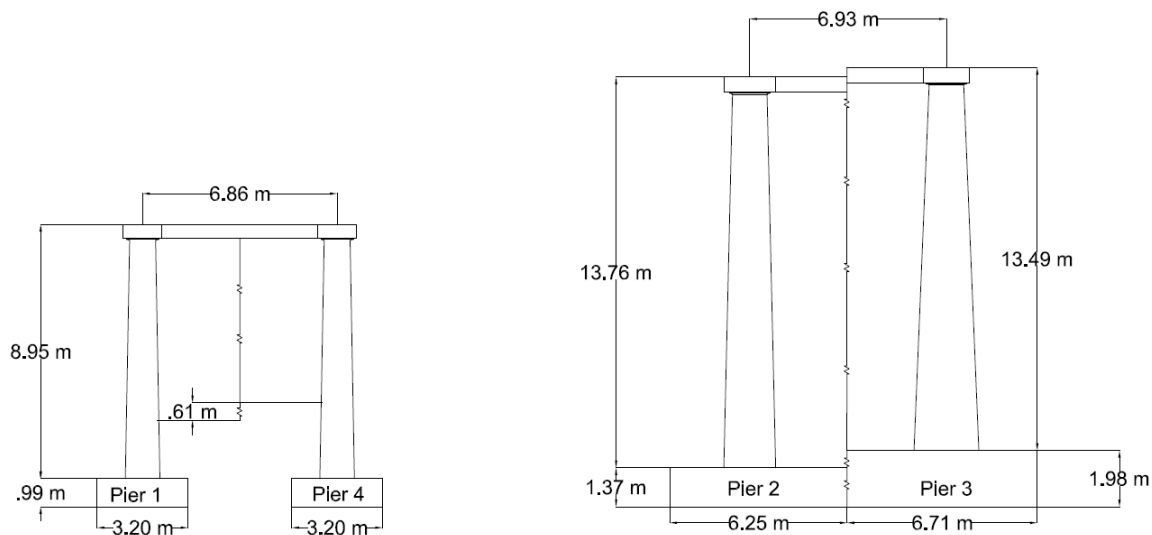


Figure 3.13 Elevation View of Approach Span with Dimensions



Figure 3.14 Picture of Approach Span

The superstructure of spans 1 through 3 is supported with four piers. The height of piers 1 and 4 is 8.95 m (29.37 ft). The bent diameter slopes from 0.91 m (3.0 ft) at the top to 1.22 m (4.0 ft) at the bottom. The height of pier 2 is 13.76 m (45.15 ft), and the bent diameter is 1.22 m (4.0 ft) at the top and 1.83 m (6.0 ft) at the bottom. Pier 3 is 13.49 m (44.25 ft) tall. The diameter of the bent is 1.22 m (4.0 ft) at the top and 2.29 m (7.5 ft) at the bottom. The piers are shown in *Figure 3.15*.



*Figure 3.15 Elevation View of Piers 1 and 4, and 2 and 3*

For piers one and four, the pier cap diameter at the columns is 1.37 m (4.5 ft), the cap thickness between bents is 1.22 m (4.0 ft) and spans 8.23 m (27.0 ft). The thickness of the wall between bents is 0.30 m (1.0 ft). The footings are not connected transversely, and their dimensions are 3.2 m (10.5 ft) by 3.2 m (10.5 ft) by 0.99 m (3.25 ft) high. For piers 2 and 3, the cap diameter at the columns is 1.60 m (5.25 ft), and the cap between the bents is 0.91 m (3.0 ft) thick. The wall between bents is 0.30 m (1.0 ft) and 0.46 m (1.5 ft) thick for piers 2 and 3,

respectively. The pier caps spanned 8.46 m (27.75 ft) for both piers. The footings for piers 2 and 3 were connected transversely. The footing for pier 2 is 12.50 m (41.0 ft) by 5.03 m (16.5 ft) by 1.37 m (4.5 ft) high, and the footing for pier 3 is 3.41 m (11.2 ft) by 8.53 m (28.0 ft) by 1.98 m (6.5 ft) high. The plan view of the pier caps is shown in *Figure 3.16*, and the plan view of the footings is shown in *Figure 3.17*.

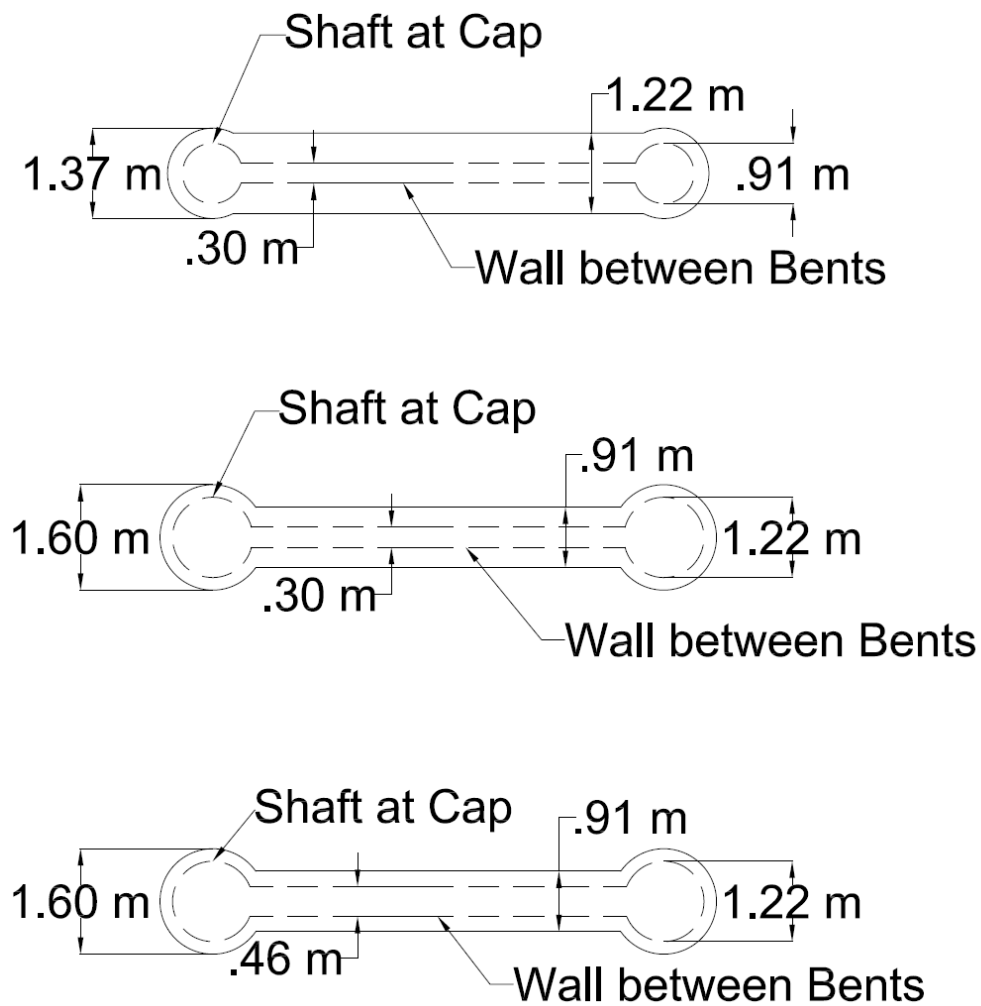


Figure 3.16 Plan View of Pier Caps 1 and 4, 2, and 3

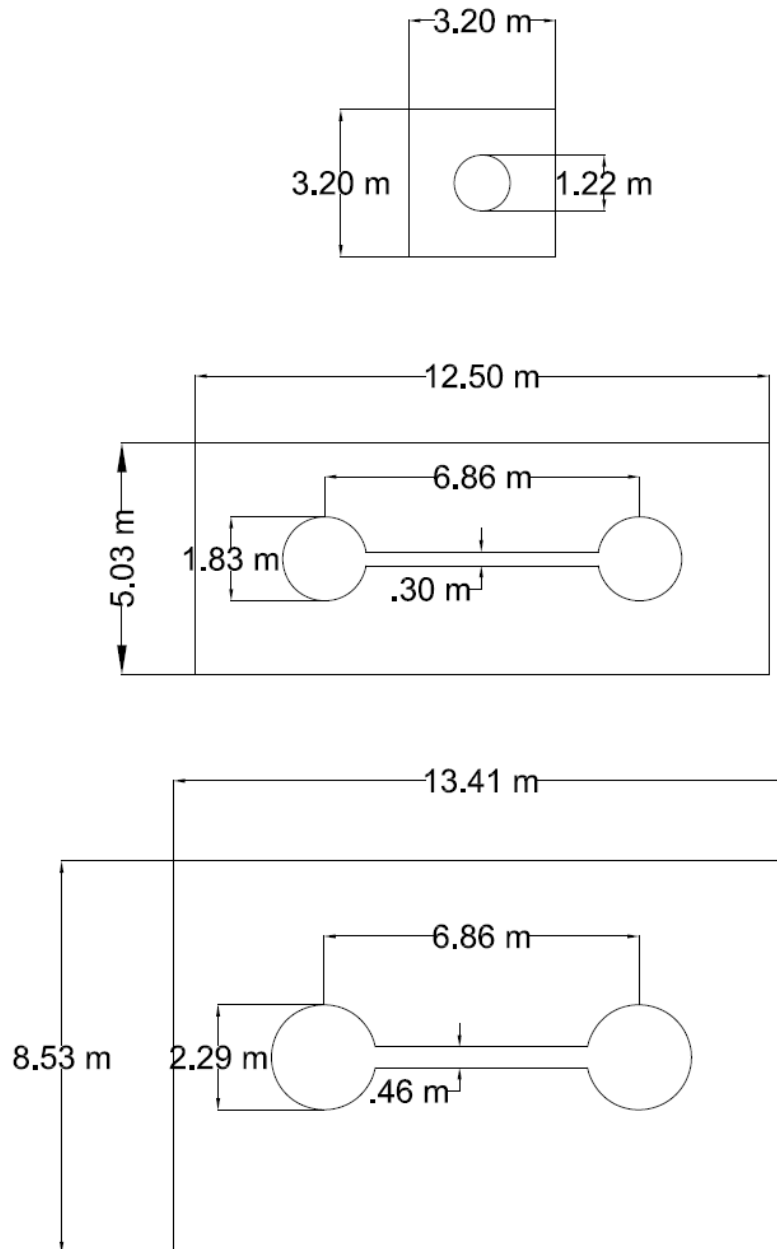


Figure 3.17 Plan View of Footings 1 and 4, 2, and 3

The ends of the bridge are supported by abutments on the shore. The height of abutment 1 is 8.77 m (28.78 ft), and the height of abutment 2 is 6.33 m (20.77 ft). The bents of either

abutment are not connected transversely, and the footing dimensions are 1.98 m (6.5 ft) by 1.98 m (6.5 ft) by 0.61 m (2.0 ft) tall.

All concrete for the bridge was specified as class “A” with a minimum breaking strength of 22.8 MPa (3,300 psi) in 28 days. The allowable stress for the reinforcing steel is 137.9 MPa (20 ksi). The structural steel for the stringers, girder webs, flange angles, cover plates, and splice material was specified as ASTM 242-46 low alloy steel, with an allowable stress of 186.2 MPa (27 ksi). The steel for the floor beam trusses, girder stiffeners, bearing details, and miscellaneous steel was specified to be A7-46 carbon steel with an allowable stress of 124.1 MPa (18 ksi).

### **3.2 Instrumentation and Load Paths**

A live-load test was performed on the SH-52 Bridge over the Snake River to quantify the in-situ behavior and accurate load ratings. The Idaho Transportation Department contracted Bridge Diagnostics Inc. (BDI) to perform the diagnostic load testing. BDI subsequently provided the data and results of the live load tests to researchers at USU. The test was performed on August 26 and 27, 2013.

To record the response due to live load, the bridge was instrumented with 62 surface-mounted strain transducers. The bridge was instrumented at nine longitudinal cross sections (A-A to I-I), and the layout of the instrumentation for each cross section is provided in the text and in Appendix A. The instrumentation locations were limited to the three main bridge spans, and did not include either of the 12.19 m (40 ft) approach spans.

Each longitudinal cross section was measured from a reference point, which was located at the start of Span 1 longitudinally, and at the east edge of the roadway width, transversely. Section A-A was located near the beginning of Span 1, measured longitudinally at 3.51 m (11.50

ft) from the reference location. Three strain transducers were attached to each girder. One strain transducer was placed on each girder web, with the five remaining transducers placed on the top and bottom flanges as shown in *Figure 3.18*. For *Figure 3.18* and *Figure 3.19*, the sensor identification number is listed first with the gauge number in parenthesis.

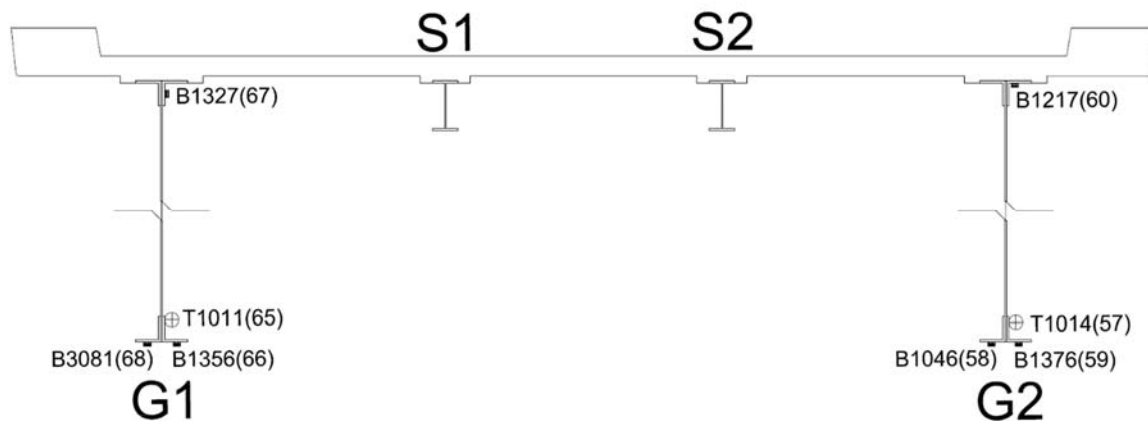


*Figure 3.18 Section A-A Instrumentation*

Section B-B was located at 28.50 m (93.50 ft) from the reference point, which was near the mid span of Span 1. This section was instrumented with eight transducers, three on G1, and five on G2. Six transducers were placed on the top and bottom flanges, and two were placed on the web of G2, as shown in *Figure A1*. Six strain transducers were placed near the end of Span 1 at Section C-C, measured longitudinally at 53.49 m (175.50 ft). The transducers were placed on the web and bottom flange of G1, and on the web, and both flanges of G2. The instrumentation for Section C-C is shown in *Figure A2*. Section D-D, (*Figure A3*) was measured at 59.56 m (195.42 ft) from the reference position and located near the beginning of Span 2. Both G1 and G2 had the same instrumentation. Two transducers were placed on the web, and one transducer was installed on the bottom flange.

Sections E-E (*Figure A4*), F-F (*Figure 3.19*), and G-G (*Figure A5*) were all located near the mid span of Span 2. Section E-E was instrumented at 94.18 m (309 ft) from the reference location. The site instrumentation included transducers on the top and bottom flanges of each girder, and transducers on the top and bottom flanges of each stringer (S1 and S2). Section F-F, measured at 95.40 m (313 ft) from the starting point was instrumented differently than any other cross section. Transducers were placed on stringers S1 and S2, one on each of the top and bottom flanges. Twelve more were placed on the surrounding diaphragm members. Six were offset 0.66 m (26 in.) to the south of S2, and the other six were offset 1.02 m (40 in.) to the north of S2, as shown in *Figure 3.12*. The labels “E” and “W” in the figure refer to the gauges placed on the east and west sides of the double angle diaphragm sections. Section G-G was measured at 96.62 m (317 ft) from the reference point. Four transducers were placed at Section G-G, one on the top and another on the bottom flange of each stringer.

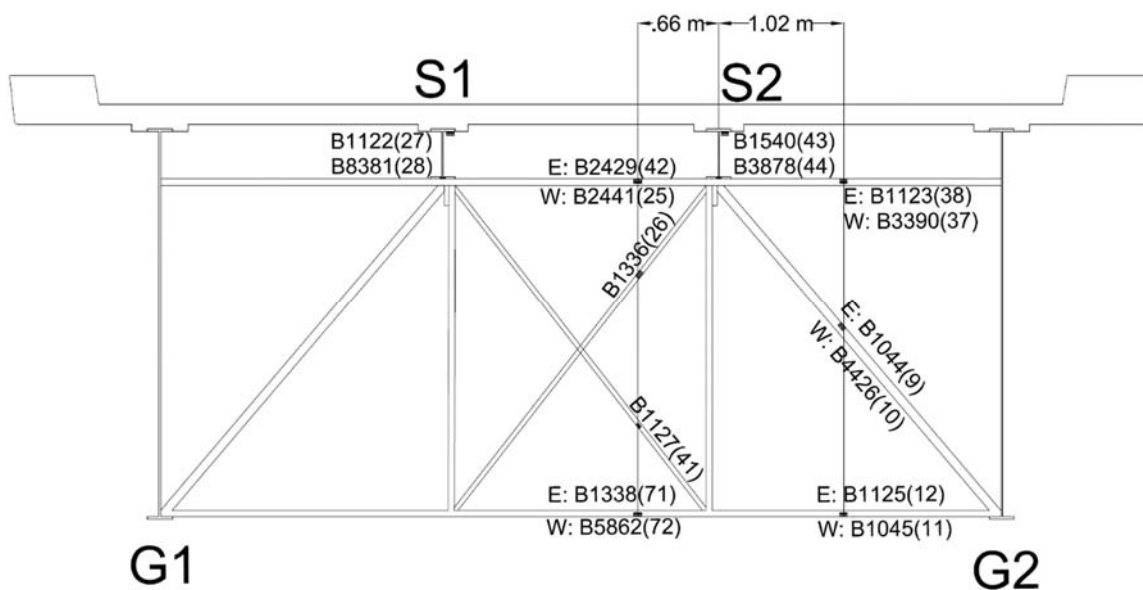


Figure 3.19 Instrumentation at Section F-F

Section H-H (*Figure A6*) was located at 125.86 m (412.92 ft) from the reference position, which was near the end of Span 2. Four transducers were installed, one transducer on the bottom flange and one on the web, of each girder. Section I-I (*Figure A7*) was the only cross section instrumented in Span 3, located near its end and measured at 182.65 m (599.25 ft) from the reference location. A transducer was installed on the top and bottom flanges of each girder.

After all the sensors were installed, the live-load tests were performed. Two vehicles were used to apply the external loads, a snooper and a gravel truck. The three-axle snooper truck weighed a total of 254.30 kN (57,170 lbs), with 91.72 kN and 81.29 kN (20,620 lbs and 18,275 lbs.) on the front, and each of the back two axles, respectively. The axle spacing was 6.38 m (20.92 ft) and 1.37 m (4.50 ft). The front axle width was 2.21 m (7.25 ft), and the back two axles were 2.22 m (7.29 ft) wide. The three-axle gravel truck weighed 234.45 kN (52,710 lbs), 67.45 kN (15,160 lbs) was located on the front axle, with 18.50 kN (18,770 lbs) on each of the back two axles. The axles were spaced at 5.0 m (16.42 ft) and 1.35 m (4.42 ft). The axle widths were 2.01 m (6.58 ft) and 2.16 m (7.08 ft) from front to back, respectively. The layout and dimensions of the snooper and gravel truck are shown in *Figure 3.20*.

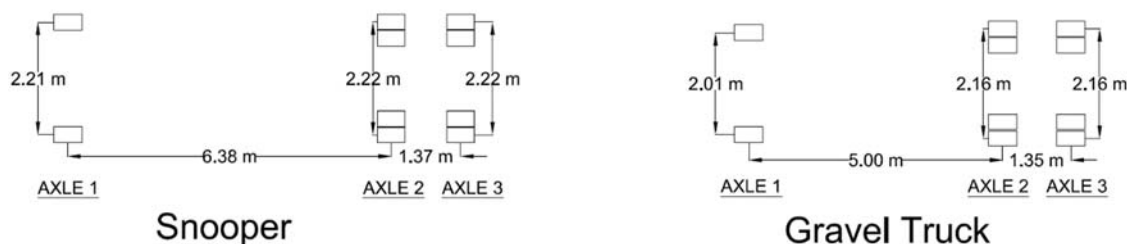


Figure 3.20 Truck Dimensions

The trucks were driven longitudinally along three separate load paths labeled Y1, Y2, and Y3. Each load path was measured transversely from the reference point. The offset distances were 0.61 m (2.0 ft), 5.03 m (16.50 ft), and 7.32 m (24.0 ft) for Y1, Y2, and Y3, respectively. Y1 was positioned such that the trucks traveled directly over girder G2 and stringer S2. Y2 was positioned for travel over both stringers, S1 and S2. Y3 was positioned for travel on top of S1 and G1. All tests were driven in the northwest direction with the center of the outside wheel being driven along the specified offset distances, as shown in *Figure 3.21*. Traffic was intermittently stopped so that no other loads contributed to the strain values measured while the trucks were driven across the bridge.

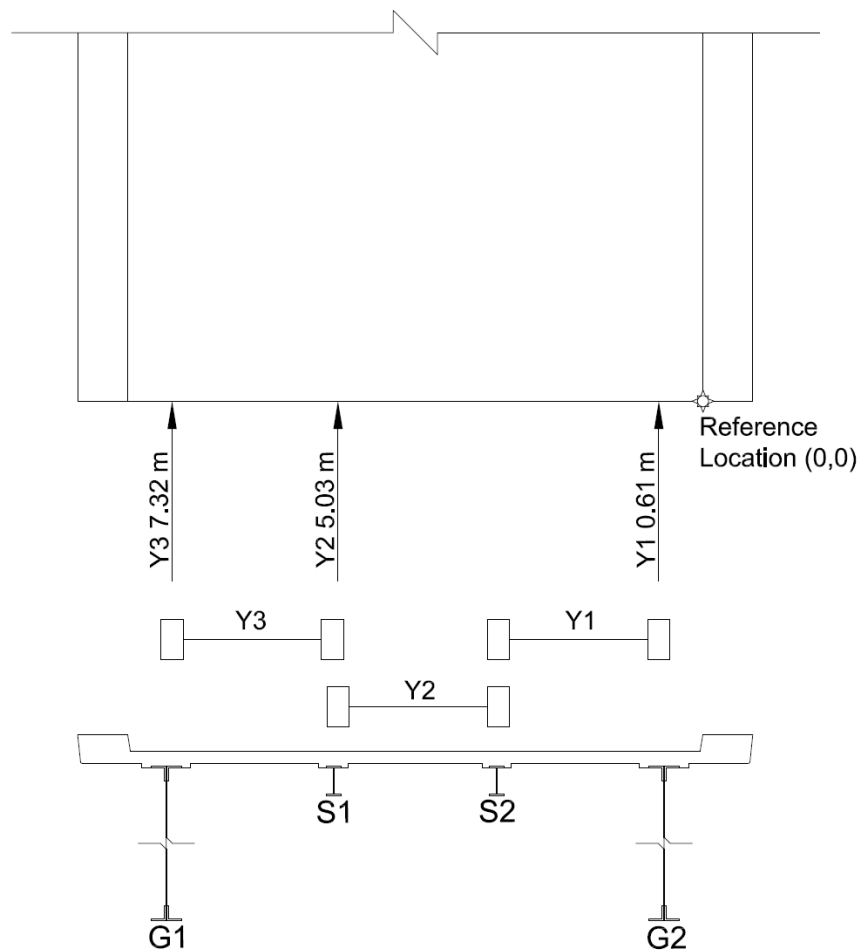


Figure 3.21 Load Path Layout

Data from each sensor was collected from twelve tests which were performed over three separate loading conditions. Data from eight of the twelve tests was provided, the eight tests were chosen because they were deemed the most accurate for each loading condition, along each load path. The eight chosen tests were 1, 3, 6, 7, 9, 10, 11, and 12. The majority of the tests were performed with the vehicles traveling at a crawl speed of 5-8 kph (3-5 mph), while one test (test 12) was driven at normal speed, 56 kph (35 mph). The bridge response data was recorded at a rate of 40 Hz for each sensor.

For tests 1, 3, and 6 the snoopers were driven at crawl speed along load paths Y1, Y2, and Y3, respectively. For test 7, the snoopers and the gravel truck were driven side-by-side at crawl speed, with the snoopers in path Y1, and the gravel truck in path Y3. For tests 9, 10, and 11 the two trucks were driven in tandem. For these tests, the snoopers pulled the gravel truck with 5.11 m (16.75 ft) between the back axle of the snoopers and the front axle of the gravel truck, along paths Y1, Y3, and Y2, respectively. For test 12 the snoopers were driven along path Y2 at normal speed. *Table 3.2* shows the loading scenarios for the chosen tests.

*Table 3.2 Load Cases and Live-Load Parameters*

<b>Load Case</b>	<b>Test</b>	<b>Load Path</b>	<b>Data Quality</b>
Snooper	1	Y1	Good
Snooper	3	Y2	Good
Snooper	6	Y3	Good
Side-by-Side	7	Y1 & Y3	Some Double Clicks
Tandem	9	Y1	Good
Tandem	10	Y3	Good
Tandem	11	Y2	Good
Snooper-Normal	12	Y2	Good

Values of strain were recorded along with the longitudinal truck position. This was done by using a BDI AutoClicker. The AutoClicker, which was installed near the front wheel, used a laser aimed directly at the wheel. A strip of reflective tape was installed on the wheel, and as the wheel rotated, the laser passed over the tape. When the laser passed the tape, a mark was recorded in the data which signified the position of the truck (Hodson, 2010). *Figure 3.22* shows the snoopers being driven across the bridge in the live-load test.



*Figure 3.22 Live-Load Test*

### 3.3 Live-Load Test Results

The collected data pertaining to longitudinal truck position and corresponding changes in strain from the live-load tests were analyzed for quality. Governing factors for test quality included: the absence of double clicking for the longitudinal truck position data, reproducible strain data between tests along the same load path, elastic behavior of the bridge (which meant that the strain values returned to zero after the truck was off the bridge), and the absence of any visible atypical responses which could indicate erroneous recording of data (B.D.I., 2013).

The longitudinal truck position data was considered to be of good quality except for some double clicks that were recorded during the side-by-side load testing. There was also some evidence of thermal drift in the recorded data. Thermal drift is common when using strain transducers. This is a result of the smaller transducers reacting much quicker to temperature change in comparison to the larger structural members they are attached to. Although often negligible, thermal drift had some effect on the recorded data because some of the live-load tests lasted several minutes while being exposed to the sun. In reviewing the test data it was determined that a maximum value of  $5 \mu\epsilon$  occurred due to thermal drift. To account for this, a linear drift offset subtraction method was used to correct the data (B.D.I., 2013).

Recorded values of strain were converted to stress using Hooke's Law ( $\sigma = E * \epsilon$ ), which were then used to determine the degree of composite behavior between the deck and its supporting beams. The degree of composite behavior between the deck and girders was determined by calculating the location of the neutral axis from the measured data and comparing it to the theoretical neutral axis. This procedure is presented below.

The height of the neutral axis was found by comparing stress at the top and the bottom of the girders, and finding the vertical location on the girder for which the stress was equal to zero. The principle of similar triangles was used for this calculation. *Figure 3.23* shows the measured neutral axis of the girder with respect to longitudinal location. *Equation 1* was used to find the measured neutral axis.

$$N.A. = \frac{\sigma_1}{\sigma_1 - \sigma_2} * h \quad (1)$$

Where:

$\sigma_1$  = stress at the bottom of the girder

$\sigma_2$  = stress at the top of the girder

$h$  = height of the girder of stringer

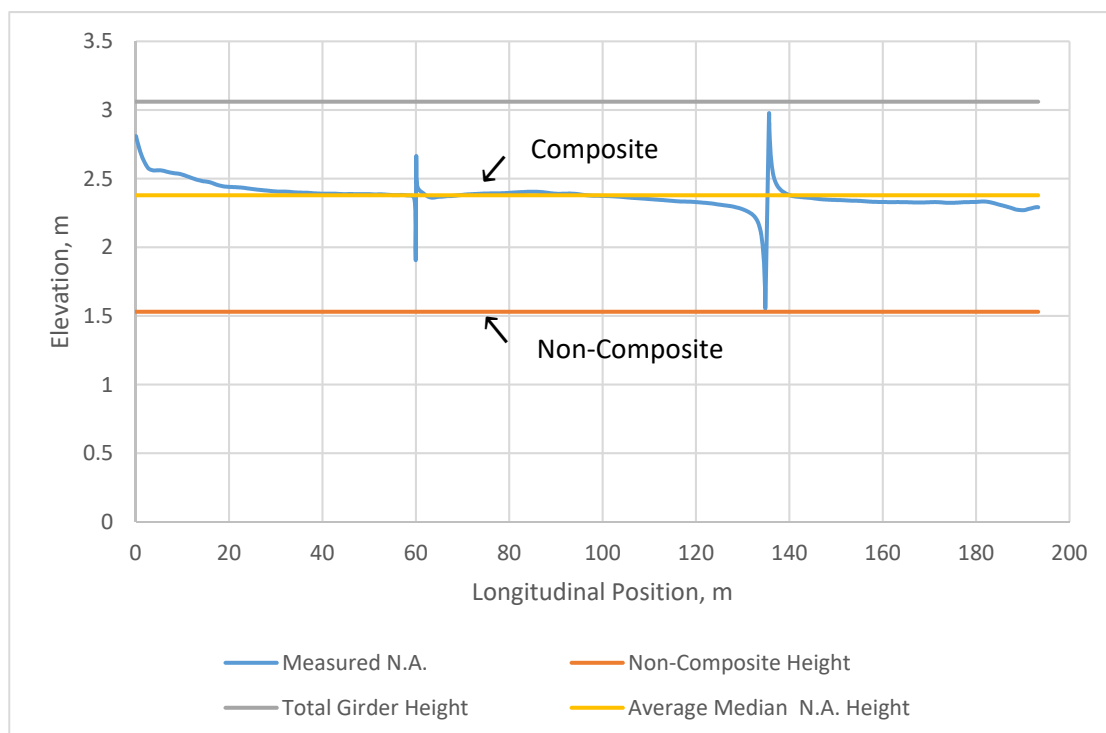


Figure 3.23 Example Plot of Neutral Axis vs. Longitudinal Position for Girder 2

The measured neutral axis was used to derive the tributary deck width for the girders through an iterative procedure. For this process, *Equation 2* was used.

$$\bar{Y} = \frac{\sum_{i=1}^n \bar{y} * A}{\sum_{i=1}^n A} \quad (2)$$

Where:

$\bar{Y}$  = the overall centroid of the girder-deck system

$\bar{y}$  = the centroid of each structural element

$A$  = the area of each structural element

A tributary deck width of 3.59 m (11.77 ft) was found for the girders, and 1.06 m (3.48 ft) for the stringers.

Because the stiffness of the girders is significantly larger than the stiffness of the stringers, the strain gauges on the stringers recorded almost no strain except for when the trucks were near (within approximately 30.48 m, or 100 ft) the longitudinal location where the strain gauges were located. Consequently, only a relatively small amount of data points could be used to find the neutral axis if found using the same procedure as for the girders. Therefore, a different approach was used. The neutral axis location was calculated qualitatively by comparing the peak stress values in the top and bottom flanges for the two highest corresponding maximum and minimum values. This analysis only considered load paths whose transverse location passed directly over, or near the stringers. Only these circumstances were considered because the measured response for all other cases was in comparison, very small.

Non-composite action was observed between the stringers and the deck when the response in the top and bottom flanges were nearly equal and opposite. This behavior indicated that the neutral axis was at the centroid of the stringer, and that the stress response of the stringer was independent of the response for the deck. Conversely, composite action or partially composite action occurred when the magnitude of response in the top flange was a fraction of the magnitude of response in the bottom flange. This behavior indicated that the neutral axis was above the centroid of the stringer, and that the stringer acted compositely with the deck to resist the load. *Figure 3.24* demonstrates how the stringers acted with the deck, as determined by the response in the top and bottom flanges.

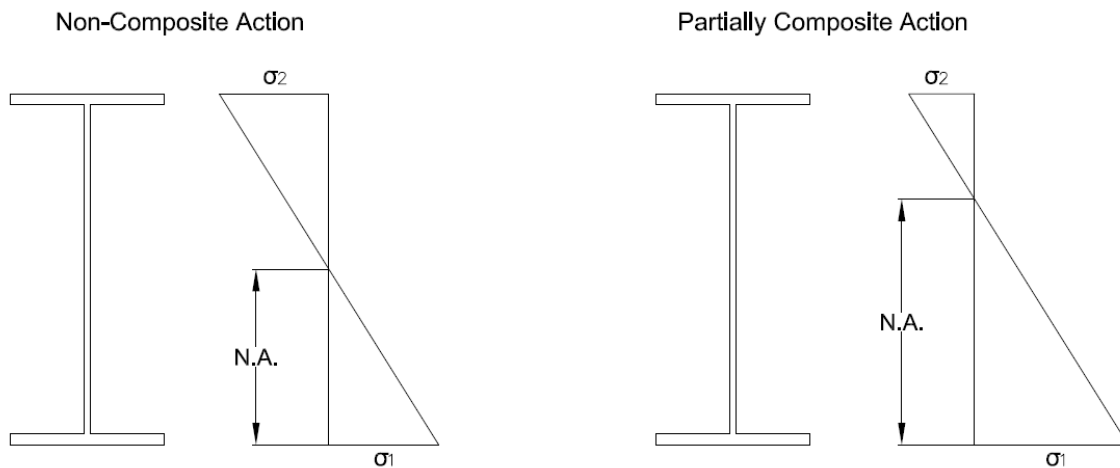


*Figure 3.24 Stinger-Deck Level of Composite Action*

The composite action between the deck and the stringers was observed to be partially composite and non-composite for S1, and S2, respectively. Partially composite action was observed when the ratio of stress fell between fully composite and non-composite baseline values. The baseline for composite action was determined by comparing the peak magnitudes of stress in the top and bottom flanges of the girders. This average ratio of the stress in the top

flange to the stress in the bottom flange of the girders was approximately 28%. The baseline value for non-composite action was a ratio of 100% between the magnitudes of stress in the top and bottom flanges of the stringers. As seen in *Table 3*, the average stress for S1 fell nearly half way between the non-composite and composite baseline ratios, indicating partially composite action. Additionally, the average stress ratio for S2 was 92.7%, indicating nearly complete non-composite action. *Table 3.3* shows the stringer-deck action.

*Table 3.3 Stringer-Deck Composite Action*

<b>Stringer</b>	<b>Average Ratio (<math>\sigma_2/\sigma_1</math>)</b>	<b>Observed Action</b>
S1	0.595	Partially Composite
S2	0.927	Non-Composite

The approach spans were intended to have minimal effect on the three main spans of the bridge. This was done by designing the approach spans as simply supported beams. This assumption was confirmed when, upon review of the data, the stresses in the structural members before the trucks crossed the expansion joint onto the first span were close to zero. This behavior is illustrated in *Figure 3.25*. *Figure 3.25* shows that the stress response in G1 at section A-A before the snoopers reached Span 1 is approximately 1.4 MPa (0.2 ksi).

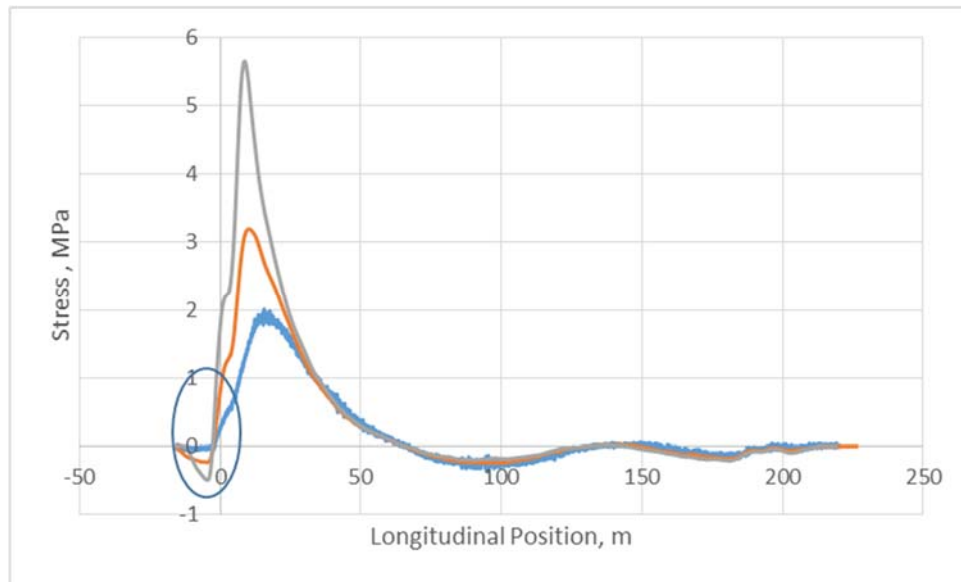


Figure 3.25 Response at Section A-A due to Approach Spans

The maximum stress response in the structural members under the different loading conditions was analyzed. The absolute maximum response in the girders due to the side-by-side, and tandem tests was approximately 1.6 times the response of the single snoopers load case. The maximum magnitude of negative stress was approximately 1.6 and 1.4 times the response of the single snoopers load case for the tandem and side-by-side cases, respectively. The largest magnitude of stress was 30.47 MPa (4.42 ksi), recorded in Girder 2 at section E-E during the side-by-side loading condition. *Table 3.4* shows the maximum and minimum responses in the girders, and *Table 3.5* shows the maximum and minimum responses in the stringers.

Table 3.4 Maximum and Minimum Girder Stress Responses

<b>Maximum/Minimum Girder Stress Responses (MPa)</b>				
<b>Load Case</b>	<b>Maximum Stress</b>	<b>Compared to Snoopers</b>	<b>Minimum Stress</b>	<b>Compared to Snoopers</b>
Snoopers	18.55	-	-8.69	-
Tandem	30.47	1.58	-14.07	1.61
Side-by-Side	29.30	1.64	-11.93	1.37

Table 3.5 Maximum and Minimum Stringer Stress Responses

<b>Maximum/Minimum Stringer Stress Responses (MPa)</b>				
<b>Load Case</b>	<b>Maximum Stress</b>	<b>Compared to Snooper</b>	<b>Minimum Stress</b>	<b>Compared to Snooper</b>
Snooper	21.65	-	-24.55	-
Tandem	24.89	1.15	-28.34	1.16
Side-by-Side	20.96	.97	-21.44	.87

For the normal speed test, the dynamic responses were found to be an average of about 7% of the static response for the girders and about 13% for stringers. The peak values were 13.5% for the girders and 25% for the stringers. These values were obtained by comparing the stress response in the normal speed test to the response of the crawl speed test. An example response of crawl speed versus dynamic loading is shown in *Figure 3.26*. In comparison, the AASHTO Standard Specifications (2002) suggest that impact fraction for a bridge with spans between 56.4 m (185 ft) and 73.2 m (240 ft) should be between 13% and 16%.

$$I = \frac{50}{L+125} \quad (3)$$

Where:

$I$ = impact fraction (maximum 30 percent)

$L$ = length in feet of the portion of the span that is loaded to produce the maximum stress

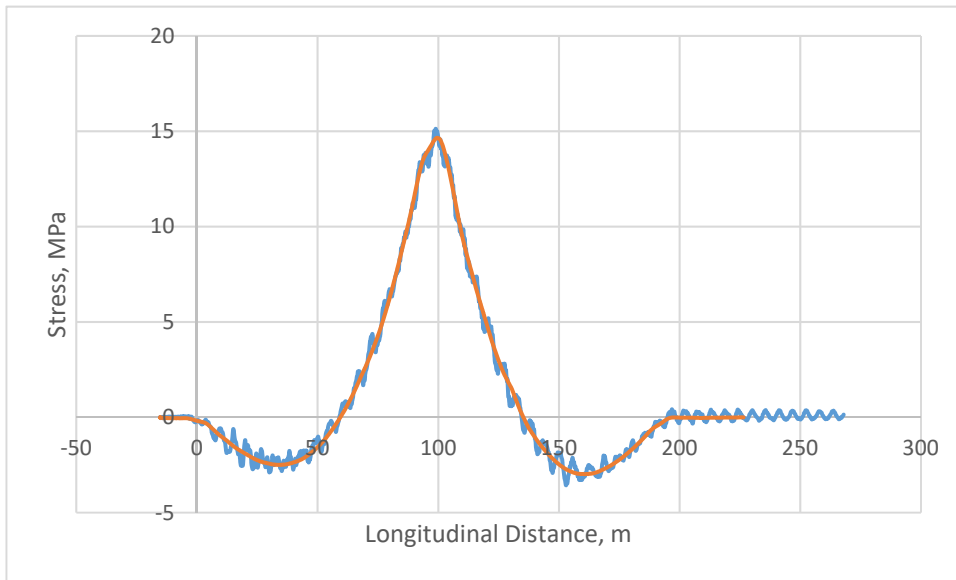


Figure 3.26 Response Comparison between Crawl Speed and Normal Speed Data

## CHAPTER 4. FINITE ELEMENT ANALYSIS

### 4.1 Description of Finite Element Model

The finite-element model for the SH-52 Bridge over the Snake River was created using CSiBridge 2015 version 17.3.0 (Computers and Structures, 2015). Frame, shell, and link elements were used to model the structural members. The composite behavior between the deck, and the girders and stringers, was modeled using joint constraints and link elements. Joint restraints were used to model the boundary conditions.

Frame elements connect two joints, and carry defined cross sectional properties between them. Frames “use . . . a general, three-dimensional, beam-column formulation which includes the effects of biaxial bending, torsion, axial deformation, and biaxial shear deformations” (Computers and Structures, 2015). For this model, frame elements were used to model girder and stringer flanges, vertical and transverse diaphragm members, pier caps, and piers.

Shell elements connect three or four joints, and cover an area with specified cross-sectional properties. “The Shell element is a type of area object that is used to model membrane, plate, and shell behavior in planar and three-dimensional structures” (Computers and Structures, 2015). The shell elements in this model were rectangular, and were used to model the girder and stringer webs, and the deck and curb concrete.

Link elements are objects that provide stiffness to the model for the degrees of freedom specified, between two joints. Link elements were used to model the bearings. Additionally, the partially composite behavior observed between stringer S1 and the deck was modeled using links.

Joint constraints were used to model composite and non-composite action between the deck and the girders G1 and G2, and stringer S2. Two joints were connected per constraint. For this model, the desired composite behavior was achieved by connecting the joint in the deck and the joint in the flange directly below it. “A Constraint is a group of joints that are connected. When a constraint is assigned to a joint, the joint becomes a part of the constraint and connects to other joints in the constraint” (Computers and Structures, 2015). Body constraints were used to model composite action. “A Body Constraint causes all of its constrained joints to move together as a three-dimensional rigid body” (Computers and Structures, 2015). Equal Constraints were used to model non-composite behavior between stringer S2 and the deck. “An Equal Constraint causes all of its constrained joints to move together with the same displacements for each chosen degree of freedom. The other degrees of freedom are unaffected. The Equal Constraint differs from the rigid-body types of Constraints in that there is *no coupling* between the rotations and the translations” (Computers and Structures, 2015).

Joint restraints were used to replicate boundary conditions at the bottoms of the piers. A fixed-end restraint was used to model the restraint on the bottom of the piers due to the piles and footings. “A joint restraint is . . . a rigid connection of the joint to the ground. Restraints are specified independently for each degree of freedom at a joint.” (Computers and Structures, 2015).

The finite-element model was developed to replicate the behavior of the three main spans, and not either of the approach spans. This was deemed appropriate because the approach spans were designed to be simply supported, and would theoretically not affect the three main spans. Additionally, based on the measured data, the approach spans were found to have little

effect on the main spans. For this model, spans 1 and 3 were 56.24 m (184.5 ft) long, and span 2 was 72.92 m (239.25 ft) long. The overall length of the bridge was 185.39 m (608.25 ft).

Joints pertaining to the deck, girders, and stringers were spaced longitudinally (x-direction) every 390.53 mm (15.38 in.) in spans 1 and 3, and 414.34 mm (16.31 in.) in span 2. For the remaining substructure of the bridge, longitudinal joints were spaced at increments of the bridge diaphragms and piers. For spans 1 and 3, joints were spaced every 6.25 m (20.5 ft), and for span 2 every 6.63 m (21.75 ft), for the diaphragms. The joints for the piers were placed at the following longitudinal locations (x-direction): 0 m, 56.24 m (184.5 ft), 129.16 m (423.75 ft), and 185.40 m (608.25 ft). Transversely (y-direction), joints were offset from the transverse center of the bridge. The joints pertaining to the centroid of the stringers were offset 1.12 m (44.25 in.) to either side. The joints for the girders were offset 3.43 m (135 in.) to either side, and the joints encompassing the curb were located 3.96 m (156 in.) and 4.65 m (183 in.) from the transverse center.

Vertically (z-direction), joints were offset in relation to the top of the deck. The vertical locations of the various joints were: the centroid of the deck (-82.55 mm, -3.25 in.), the top of the girders and stringers (-222.25 mm, -8.75 in.), the floor beam and bottom of the stringers (-0.60 m, -23.49 in.), near the vertical center of the girders where a link was connected to model the bearings (-1.75 m, -69.0 in.), the bottom of the girders (-3.24 m, -127.75 in.), the vertical center of the pier caps (-3.49 m, -137.5 in.), and the bottom of the piers. *Figure 4.1* shows a 3-D view of the SH-52 Bridge over the Snake River finite-element model.

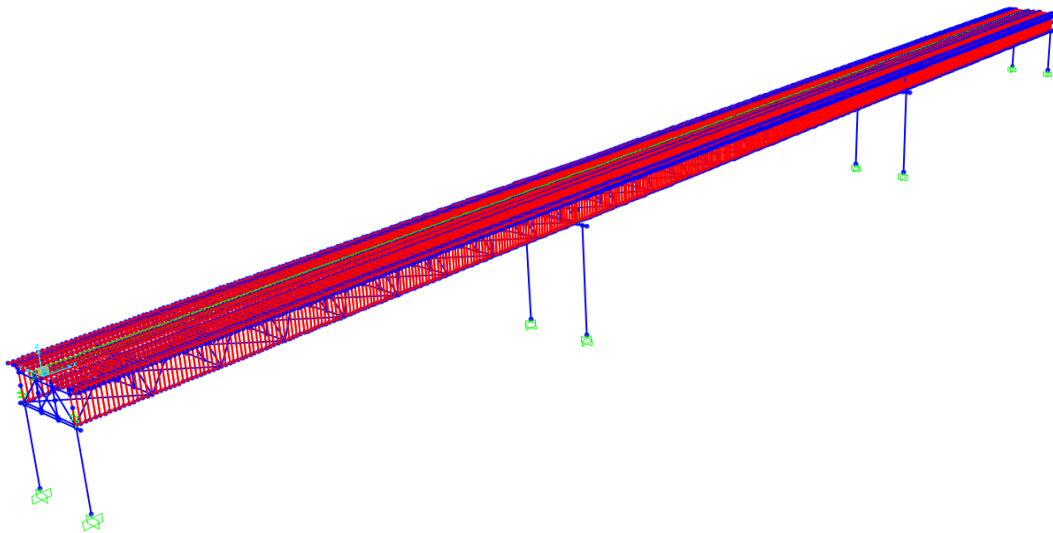
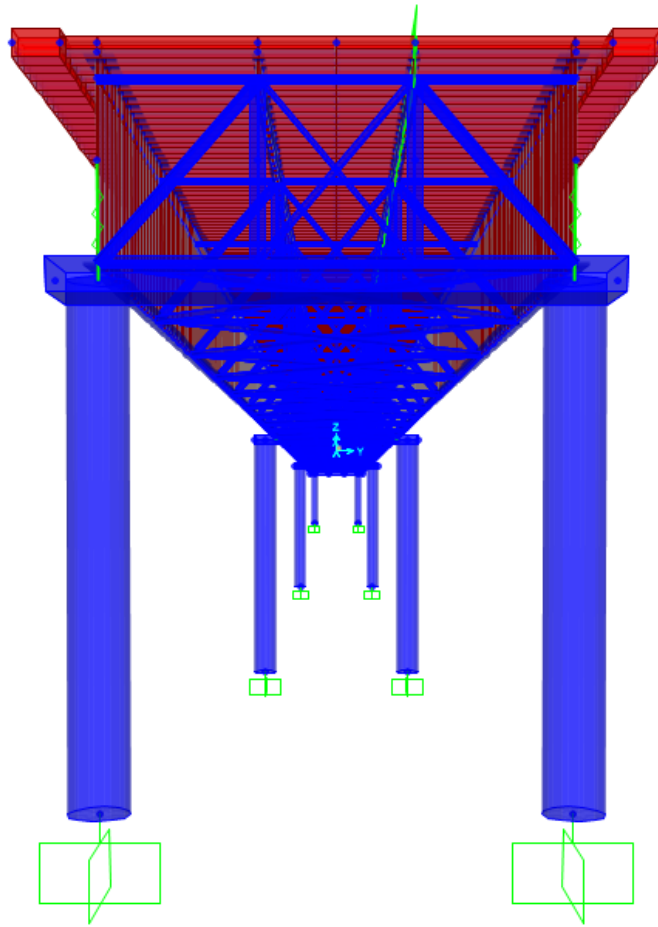


Figure 4.1 3-D View of SH-52 Bridge Over the Snake River Finite-Element Model

For piers 1 and 4, the joints corresponding to the bottom of the piers were placed at -11.19 m (-440.44 in.), and for piers 2 and 3, -16.71 m (-658 in.) and -16.99 m (-668.8 in.), respectively. The vertical joints at longitudinal locations, where the piers are not located, only include the joints from the bottom of the girders and upward. *Figure 4.2* shows the extruded substructure of the bridge.



*Figure 4.2 Extruded View of Bridge Substructure*

The finite-element model included varying frame, shell, and link element properties. The concrete for the superstructure was divided into deck concrete, and curb concrete. Both were modeled using shell elements. The deck concrete was 165.1 mm (6.5 in.) thick, and the curb concrete was 393.7 mm (15.5 in.) thick.

The top and bottom flanges of the girders and stringers were modeled as frame elements. The area of the girder flanges varied with longitudinal position. Because the girder flanges are overlain by cover plates near the piers, an effective flange thickness was used for the locations near the piers where the cover plates are located. The effective thickness was determined by

dividing the total area of the flange and cover plate(s) by the width of the cover plates, 508 mm (20 in.). The effective thickness was 50.04 mm (1.97 in.), 69.09 mm (2.72 in.), and 88.14 mm (3.47 in.) at the locations of 1, 2, and 3 cover plates, respectively. Because there were not joints at the exact locations of the cover plate transitions, the effective flange thickness transitions were taken at the joints closest the exact transition locations. *Figure 4.3* shows the cover plate

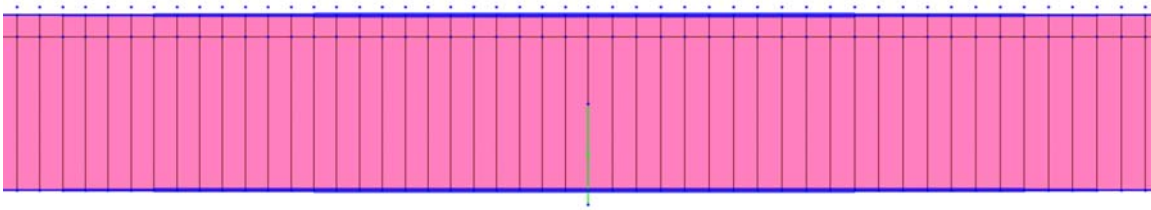


*Figure 4.3 Extruded View of Cover Plates near Piers 2 and 3*

transitions near piers 2 and 3.

Similar to the flanges, an effective width was calculated for the webs of the girders due to the presence of stiffeners. Vertical and longitudinal stiffeners provided additional stiffness to the girder webs. Neither the vertical nor longitudinal stiffeners were modeled explicitly; instead an effective web thickness was calculated to account for the additional steel. The added steel for the longitudinal stiffeners only took into account the stiffeners near the top of the girder web, and not those near the bottom of the web. This is due to the fact that the stiffeners at the top extend along the entire longitudinal length of the bridge and the bottom longitudinal stiffeners are only present near piers 2 and 3. The effective web thickness was found by summing the volume of steel over an interval length of consecutive vertical stiffeners (1.56 m, 61.5 in.) and dividing by the web height multiplied by the interval length. The calculated value for effective web thickness in spans 1 and 3 was 15.24 mm (0.60 in.). Although slightly different (14.99 mm, 0.59 in.), the

effective thickness used in the model for span 2 was also 15.24 mm (0.60 in.) because the two calculated values were very similar.

The webs and flanges of the stringers were modeled as uniform sections that did not vary with longitudinal position. Although three stringer sections were used on the bridge, only one was used in the model because their differences are very small. The stringer flanges are 14.22 mm (0.56 in.) thick by 178.82 mm (7.04 in.) wide. The web is 8.89 mm (0.35 in.) thick and 374.40 mm (14.74 in.) tall. These dimensions are based off the stringer section 16 WF 45.

The vertical diaphragm members were modeled as frame elements. Five frame sections were defined: Floor Beam 2Ls, 2Ls 6x3.5x3/8 double, 2Ls 4x3.5x5/16 double, 2Ls 4x4x3/8 double, and X Brace. Each was defined as either a single or double angle section, with its corresponding cross sectional dimensions and area. Floor Beam 2Ls, 2Ls 6x3.5x3/8 double, 2Ls 4x3.5x5/16 double, and 2Ls 4x4x3/8 double were defined as double angle sections that had total areas of 55.44 cm<sup>2</sup> (8.59 in<sup>2</sup>), 44.15 cm<sup>2</sup> (6.84 in<sup>2</sup>), 28.98 cm<sup>2</sup> (4.49 in<sup>2</sup>), and 36.90 cm<sup>2</sup> (5.72 in<sup>2</sup>), respectively. X Brace was a single angle section that had a total area of 16.03 cm<sup>2</sup> (2.48 in<sup>2</sup>). The angle sections used for the vertical diaphragms are shown below in *Figure 4.4*.

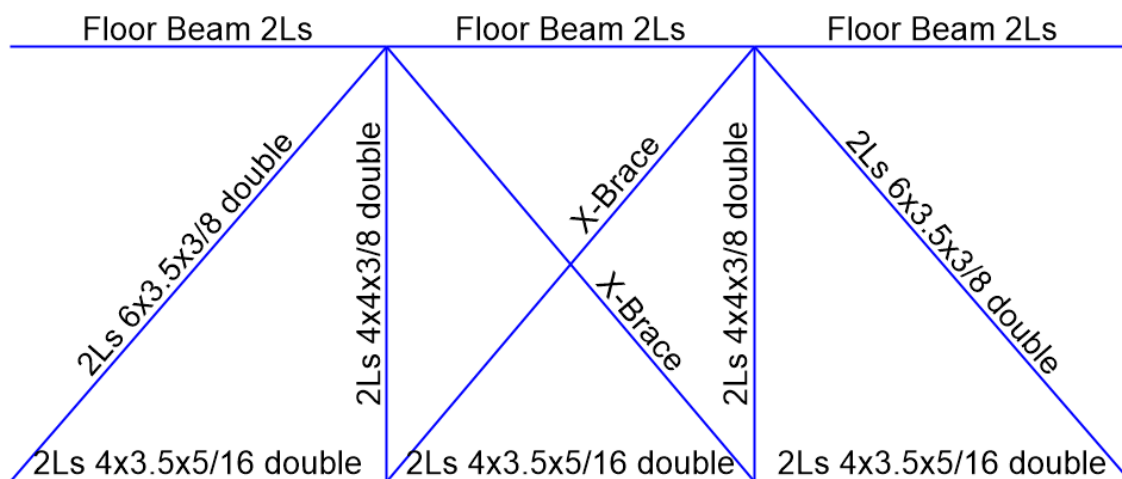


Figure 4.4 Bridge Vertical Diaphragm

The transverse diaphragm members were also modeled as frame elements. Seven different angle sections were used in the construction of the bridge. Their cross sectional areas ranged from 22.77 cm<sup>2</sup> (3.53 in<sup>2</sup>) to 45.48 cm<sup>2</sup> (7.05 in<sup>2</sup>). An intermediate value of 29.03 cm<sup>2</sup> (4.5 in<sup>2</sup>) was chosen for the model as a uniform cross sectional area instead of explicitly modeling each angle section.

Frame sections were used to model the columns and pier caps at each pier. The columns of piers 1 and 4 had a diameter of 0.91 m (36 in.), and were 7.69 m (25.25 ft) tall. Pier 2 was modeled with columns that had a diameter of 1.22 m (4 ft), and was 13.22 m (43.38 ft) tall. The diameter of columns for pier 3 was 1.22 m (4 ft), and it was 13.50 m (44.28 ft) tall. The cap at piers 1 and 4 was 482.6 mm (19 in) deep by 1.37 m (4.5 ft) wide. At pier 2 the cap was 533.4 mm (21 in.) deep by 1.60 m (5.25 ft) wide, and at pier 3 the cap was also 533.4 mm (21 in.) deep by 1.60 m (5.25 ft) wide.

The concrete for the deck and the curb had a specified concrete compressive strength,  $f'_c$  of 22.75 MPa (3.3 ksi) and a modulus of elasticity of 17.9 GPa (2,600 ksi). The concrete used for the piers and pier caps had a value of 22.75 MPa (3.3 ksi) for  $f'_c$  and 20.0 GPa (2,900 ksi) for modulus of elasticity. The modulus of elasticity was greater for the substructure concrete to account for the walls between piers, which were not modeled explicitly. Two different properties were specified for steel, ASTM 242-46 and A7-46. ASTM 242-46 steel has a minimum yield stress,  $F_y$  of 344.74 MPa (50 ksi) an ultimate yield stress,  $F_u$  of 448.16 MPa (65 ksi), and a modulus of elasticity of 199.95 GPa (29,000 ksi). A7-46 steel has a value for  $F_y$  of 206.84 MPa (30 ksi),  $F_u$  of 379.21 MPa (55 ksi), and for modulus of elasticity of 199.95 GPa (29,000 ksi).

The magnitudes of stiffness for the links used to model partially composite action between the deck and stringer S1 were determined during the model calibration phase of the research. These selected values minimized the difference between the finite-element and measured data. These links provided stiffness in three degrees of freedom: the longitudinal, transverse, and vertical translation directions (U1, U2, and U3). U1 was given a stiffness of 10.51 kN/mm (60 k/in.), U2 was given a stiffness of 350.25 kN/mm (2000 k/in.), and the link was fixed or infinitely stiff in the U3 direction. The links used to model the roller connection bearing at piers 1, 2, and 4 were stiffened in the U1 and U2 degrees of freedom. The stiffness for each direction was  $1.00 \times 10^8$  kN/mm ( $5.71 \times 10^8$  k/in.). The link used to model the pinned connection bearing on pier 3 was stiffened in the U1, U2, U3, and rotation about the 3-3 axis (R3) degrees of freedom. The stiffness value for U1, U2, and U3 was  $1.00 \times 10^8$  kN/mm ( $5.71 \times 10^8$  k/in.) and  $9.99 \times 10^{10} \frac{N*m}{\phi}$  ( $8.85 \times 10^{11} \frac{K*in.}{\phi}$ ) for R3.

#### 4.2 Finite Element Live-Load Test

The live-load test was reproduced in CSiBridge by defining trucks to replicate the snooper and gravel truck, and lanes to replicate the load paths. The snooper was defined by assigning the first axle as a “Leading Load” with a value of 91.72 kN (20.62 k), and an axle width of 2.21 m (87 in.). The back two axles were defined as “Fixed Length” with 5.0 m (197 in.) and 1.35 m (53 in.) between the first and second, and second and third axles, respectively. The back two axle loads were 81.29 kN (18.274 k), and had a width of 1.91 m (75 in.). Each axle width type was assigned as “Two Points”. This process was repeated for the gravel truck. The front axle was defined as a “Leading Load”. The front axle load was 67.45 kN (15.163 k) and

had a width of 2.01 m (79 in.). The back two axles were defined as “Fixed Length”, with axle loads of 83.50 kN (18.772 k), and axle widths of 1.83 m (72 in.). The axle width types were assigned as “Two Points”. The footprint of vehicle dimensions is shown in *Figure 3.20*.

The load paths were defined as lanes. The longitudinal length of the lanes was defined as the total length of the three main spans, 185.40 m (7299 in.). The width of the lanes was defined as the width of the widest snoopers axle, 2.22 m (87.5 in.). The transverse position of each lane was defined as an offset with respect to the transverse center of the bridge. Load paths Y1, Y2, and Y3 were offset 2.24 m (88.25 in.), 44.45 mm (1.75 in.), and -2.24 m (-88.25 in.), respectively. Because the vehicles traveled across the bridge in the westbound direction during the live-load test, the model was created with the trucks traveling from pier 4 to pier 1.

A “VEHICLE LIVE” load pattern was created for each load case, to simulate the live-load test. The self-weight multiplier was set to zero so that the response of the model would only be due to the loading experienced from the trucks. The load path for each load case was assigned by choosing one of the previously defined lanes. To reflect the direction and nearly static movement of the trucks across the bridge, the direction was set to “Forward”, and the speed was set to 38.1 cm/s (15 in./sec). The model was set to discretize every 0.5 seconds, and the loading duration was set to be long enough for the trucks to cross the bridge for the specified load case. For the snoopers and side-by-side load cases the duration was set for 510 seconds. For the tandem load case the duration was set for 600 seconds. The duration of the tandem case allowed enough time for the gravel truck to cross the bridge while traveling behind the snoopers with 5.11 m (16.75 ft) between the back axle of the snoopers and the front axle of the gravel truck. This distance between vehicles translated into the gravel truck beginning travel across the bridge

33.73 seconds after the snooper. *Figure 4.5* shows the snooper crossing the bridge during the finite-element live-load test.

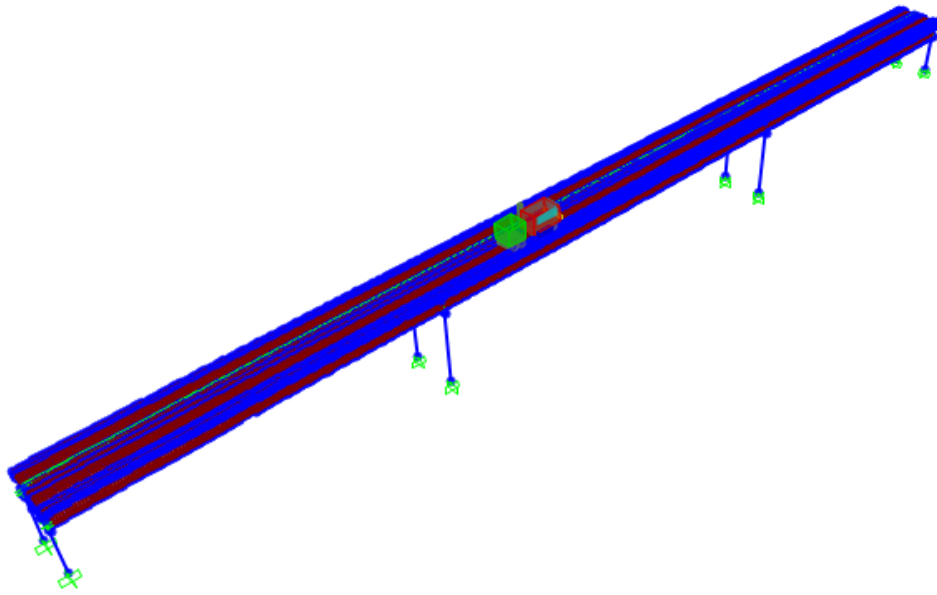


*Figure 4.5 Finite-Element Live-Load Test*

#### **4.3 FE Model Results**

Following the creation of the bridge structural elements and live-load test parameters, the finite-element analyses were performed. A multi-step linear static analysis was performed with the response being reported at the distance traveled for each discretization (190.5 mm, 7.5 in.) in 0.5 seconds. This corresponded to a rate of travel of 1.37 kph (0.85 mph). For the snooper and side-by-side load cases, the analysis was performed using 1,021 steps. For the tandem case, the analysis was performed using 1,201 steps. In all, the finite-element model was comprised of 8,947 joints, 4,170 frame elements, 6,496 shell elements, and 473 links. *Figure 4.6* shows the deformed shape of the bridge after the analysis.

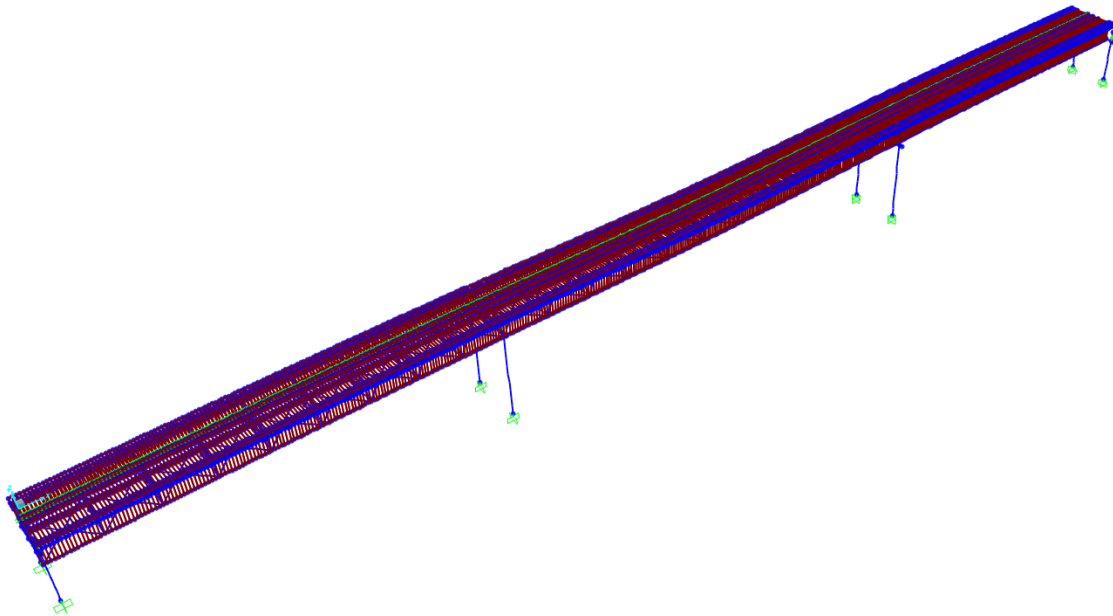


*Figure 4.6 Deformed Shape of Analyzed Bridge with Truck near Mid Span*

To quantify the changes in stress during the live-load test, at the various longitudinal and transverse locations, the frame elements where the strain gauges were attached were selected that corresponded to the top and bottom flange at the desired location. For some longitudinal locations, there were not joints that coincided to the exact locations of the strain gauges. However, no joint was longitudinally located further than 207.17 mm (8.16 in.) from the location of the actual strain gauges. With the desired frame elements selected, the stress response due to live-load was calculated with respect to the corresponding longitudinal position. This data was then analyzed so that the responses at the centroid of the top and bottom flanges could be displayed with respect to the longitudinal position of the truck.

Several model iterations were analyzed until an accurate correlation was obtained between the measured and finite-element data. Model iterations were required due to the

uncertainty of composite behavior for the girders and stringers. Requirements for an accurate correlation included: visual inspection of the graphed data,  $R^2$  coefficient of correlation, and the slope of the trend line between measured and finite-element data. After the model was created, it was decided that only certain bridge parameters could justifiably be modified, within a reasonable range, to increase the accuracy of the model. These factors included material properties, the stiffness of the links, and the type of joint constraint.

To determine the extent of correlation between the measured and finite-element data, an in-depth comparison was performed at each longitudinal cross section (A-A to I-I) where the bridge was instrumented for the live-load test. The measured changes in stress recorded during the live-load test were compared to the corresponding calculated values from the finite-element, live-load test for each load path and instrumented longitudinal location. Both sets of data were plotted on the same graph for visual inspection, and data points at 3.05 m (10 ft) increments were compared to quantify the  $R^2$  coefficients of correlation. For the  $R^2$  correlation analysis, any data points that were obvious outliers were disregarded.

While data from all loading conditions were compared, the in-depth analysis at each cross section was only performed for the snooper loading condition. *Figure 4.7* shows an example plot of stress response vs. longitudinal position for Girder 1 at section E-E when the snooper was in load path Y1. As the snooper crossed the bridge, Girder 1 acted as a continuous beam. In spans 1 and 3 the bottom flange experienced a negative moment, and in span 2 a positive moment. The moments experienced in the top flange were opposite of those in the bottom flange, positive in spans 1 and 3, and negative in span 2.

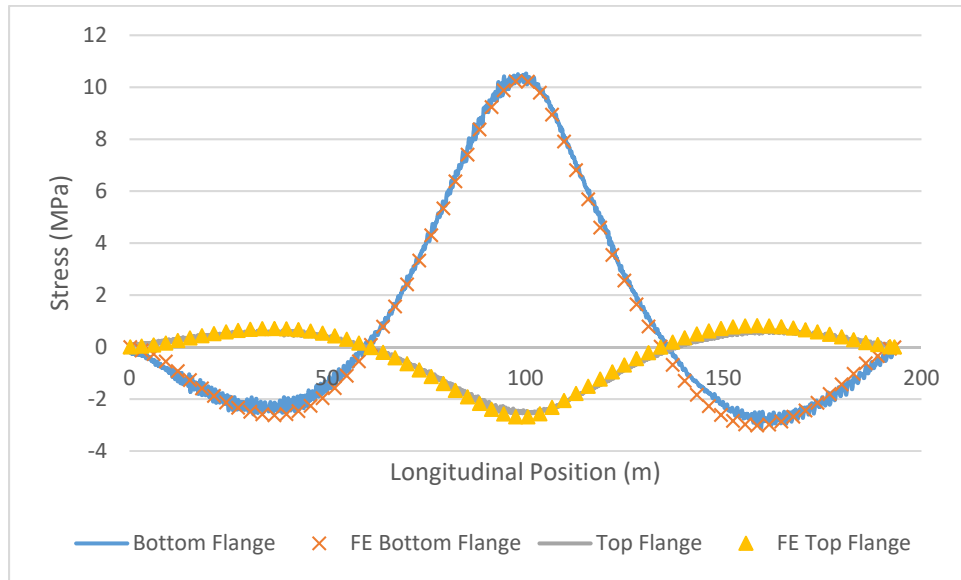


Figure 4.7 Stress Response vs. Longitudinal Position in Girder 1 at Section E-E

Figure 4.8 shows a plot of the finite-element data (x-axis) vs. measured data (y-axis) at 3.05 m (10 ft) increments, as well as the  $R^2$  coefficient of correlation value and slope of the trend line. The data correlated well for both the small and large magnitudes of stress.

Figure 4.9 shows the changes in stress due to the snooper loading in load path Y1, in Girder 2. Like Girder 1, Girder 2 acted as a continuous beam.

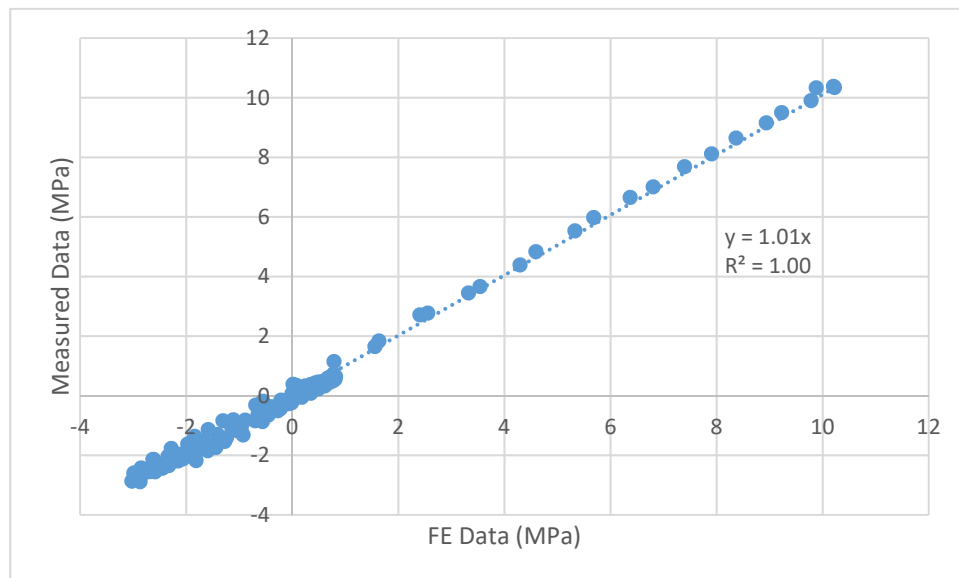


Figure 4.8  $R^2$  Correlation and Slope of Line for Measured vs. FE Data for Girder 1

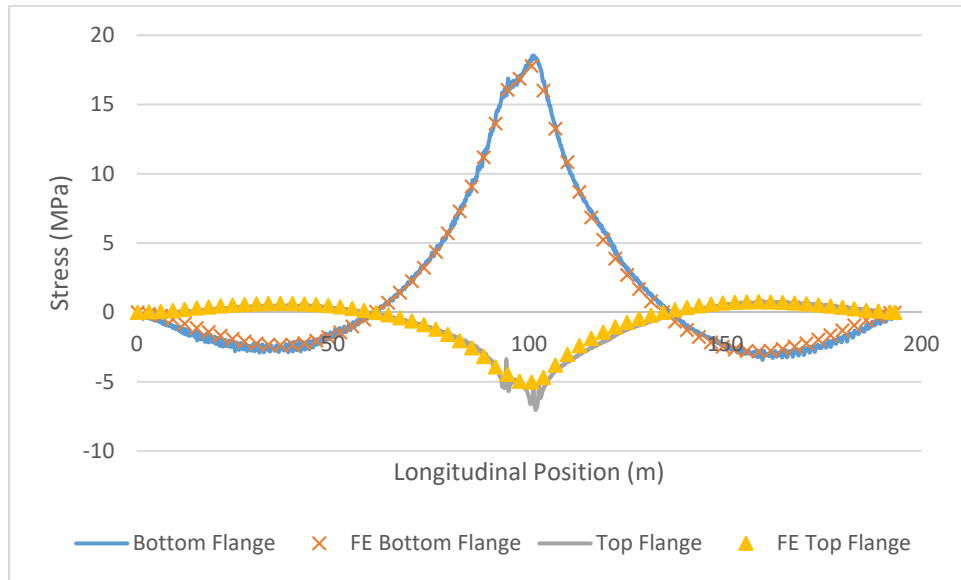


Figure 4.9 Stress Response vs. Longitudinal Position in Girder 2 at Section E-E

Figure 4.10 shows the correlation between the finite-element data and measured data for this loading for Girder 2. The data correlated well for both smaller and larger magnitudes of stress.

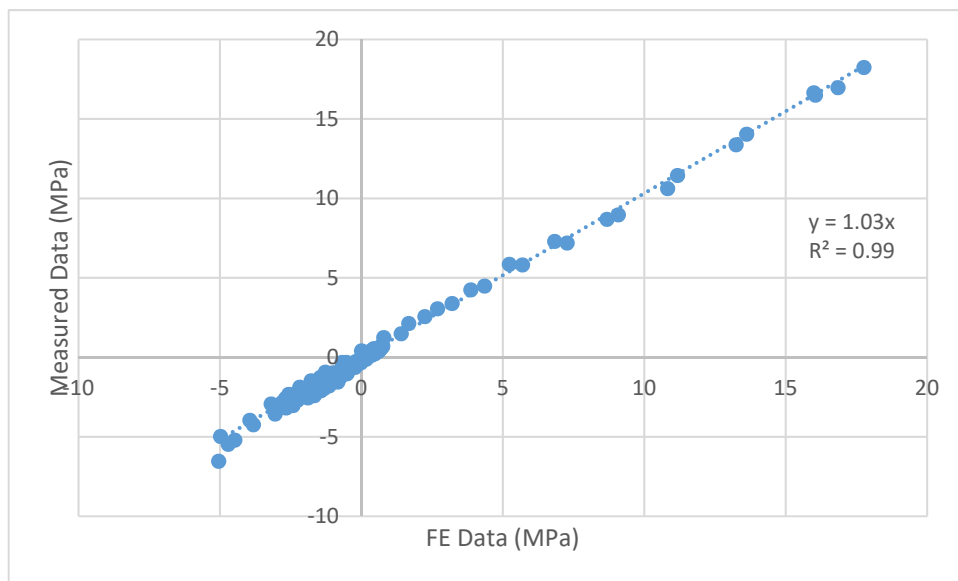


Figure 4.10  $R^2$  Correlation and Slope of Line for FE vs. Measured Data

Figure 4.11 shows the top and bottom stress response vs. longitudinal position for Stringer 1 at section E-E when the snooper was driven along load path Y2. The stress response was small except for the longitudinal locations when the snooper was near the strain gauges at section E-E.

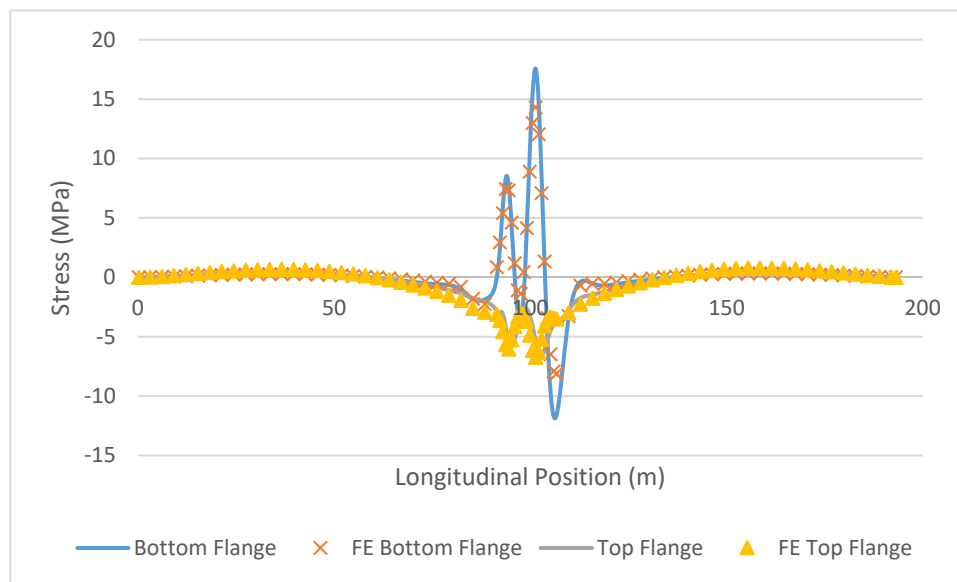


Figure 4.11 Stress Response vs. Longitudinal Position in Stringer 1 at Section E-E, Load Path Y2

Figure 4.12 shows the  $R^2$  correlation plot for the finite-element data vs. measured data for Stringer 1 at section E-E. An accurate correlation was found between the two sets of data.

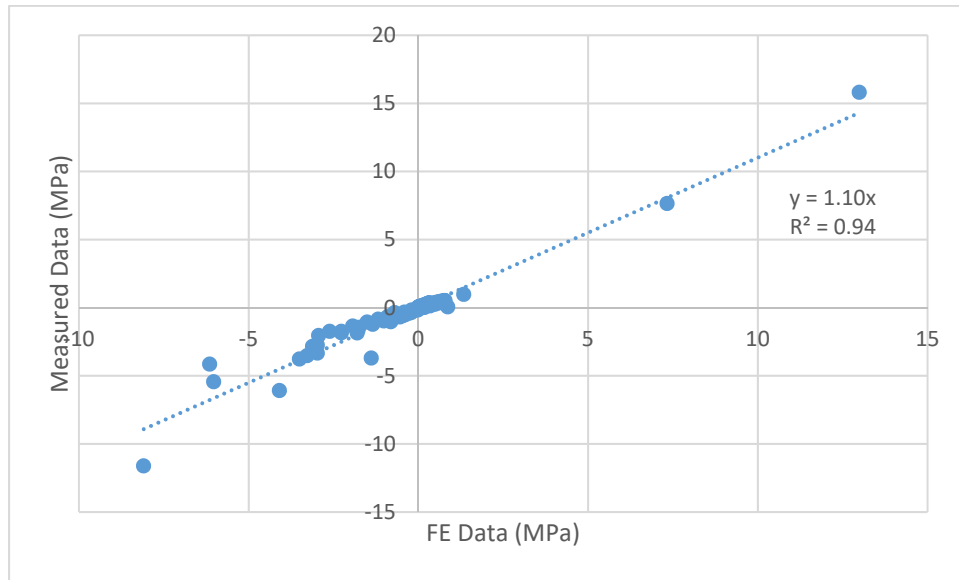


Figure 4.12  $R^2$  Correlation and Slope of Line for FE vs. Measured Data

Figure 4.13 shows the stress response vs. longitudinal position in Stringer 2 at section E-E when the snoopers were in load path Y2.

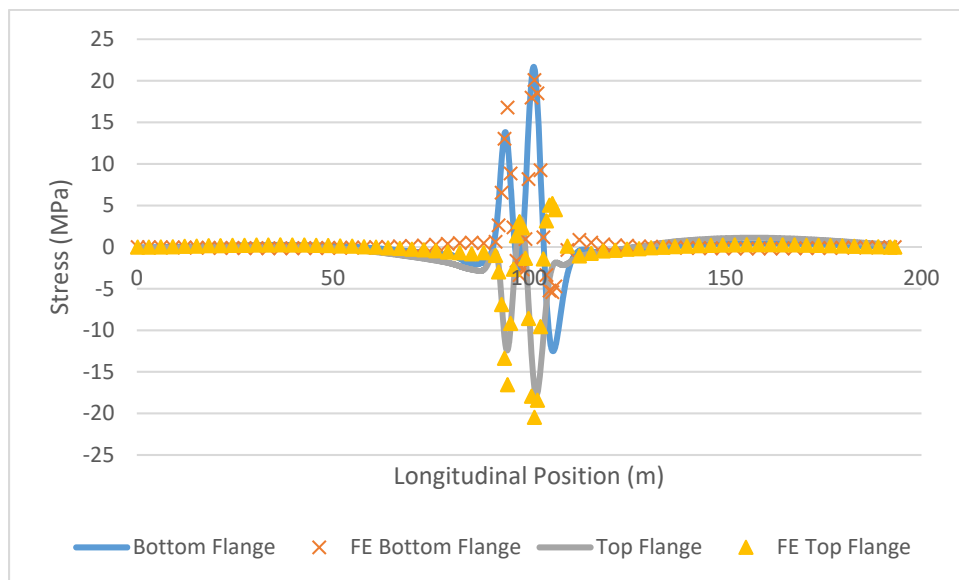


Figure 4.13 Stress Response vs. Longitudinal Position in Stringer 2 at Section E-E, Load Path Y2

Figure 4.14 shows the correlation between the measured and finite-element data for Stringer 2. While there was still a significant correlation between the data, it was not as strong as for the other beams.

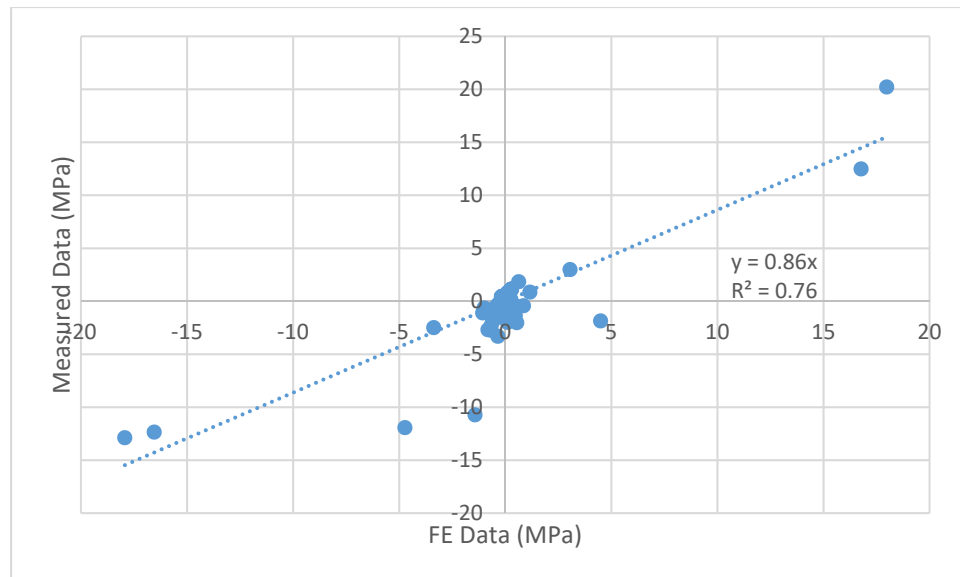
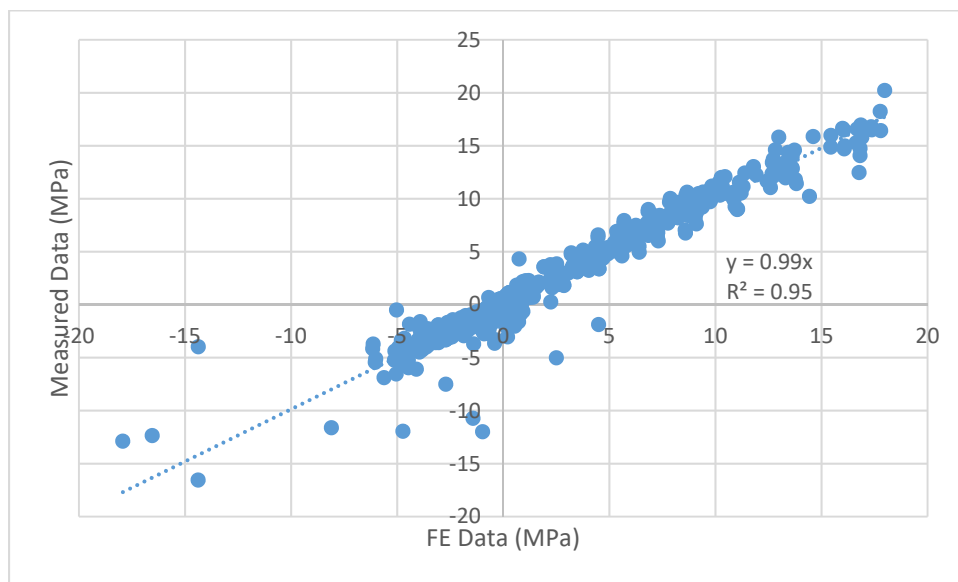


Figure 4.14  $R^2$  Correlation and Slope of Line for FE vs. Measured Data

Based on the  $R^2$  correlation value, slope of the trend line, and visual inspection, the finite-element data correlated well with the measured data for Girders 1 and 2, and Stringer 1. However, based on these same parameters the data for Stringer 2 did not correlate nearly as well, but was still reasonable. Many factors may potentially contribute to the lesser correlation between the measured and finite-element data for Stringer 2. These factors include the difficulty of modeling non-composite behavior in conjunction with fully composite, and partially composite behavior, the high variability of the stress response, as well as variability in material properties and boundary conditions.

Despite the reduced correlation between the data for Stringer 2, overall the model was found to be quite accurate in predicting the bridge response. *Figure 4.15* shows the combined data for the girders and stringers at the cross sections where the highest magnitudes were recorded for spans 1 and 2, which were located at B-B and E-E (only the cases when a wheel line passed over the stringer were included because the response in other load paths was very small and difficult to model). Data from 2,080 points were compared.



*Figure 4.15 Correlation for Girders at Sections E-E and B-B and for Stringers at Section E-E*

In addition to the influence lines that have been shown for each of the supporting structural members, the transverse diaphragm was also instrumented at Section F-F during the live-load test. As for the supporting structural members, a comparison analysis was performed to determine the correlation for the diaphragm members. The stress response at seven locations on the diaphragm members was compared to the measured response recorded during the live-load test. *Figure 4.16* is provided as a reference for the accompanying plots that analyzed several different diaphragm members.

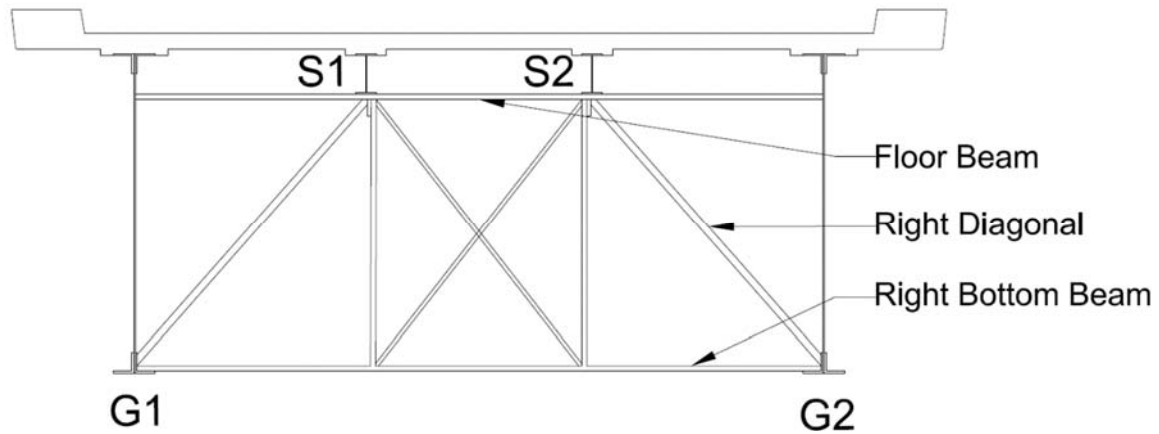


Figure 4.16 Diaphragm Reference Figure

Figure 4.17 shows an example plot of the finite-element and measured data for the floor beam. Similar to the stringers, the diaphragm members carried very little load except for the longitudinal locations when the snooper was near the cross-section where they were located.

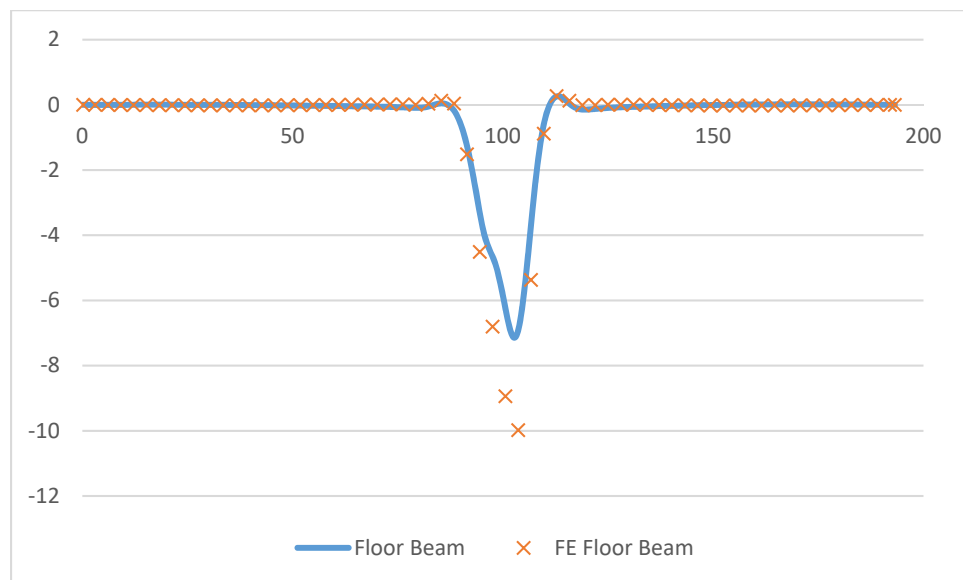


Figure 4.17 Stress Response vs. Longitudinal Position in Floor Beam

Figure 4.18 shows a response plot comparison for the right diagonal member. The finite-element data closely follows the shape and magnitude of the measured data.

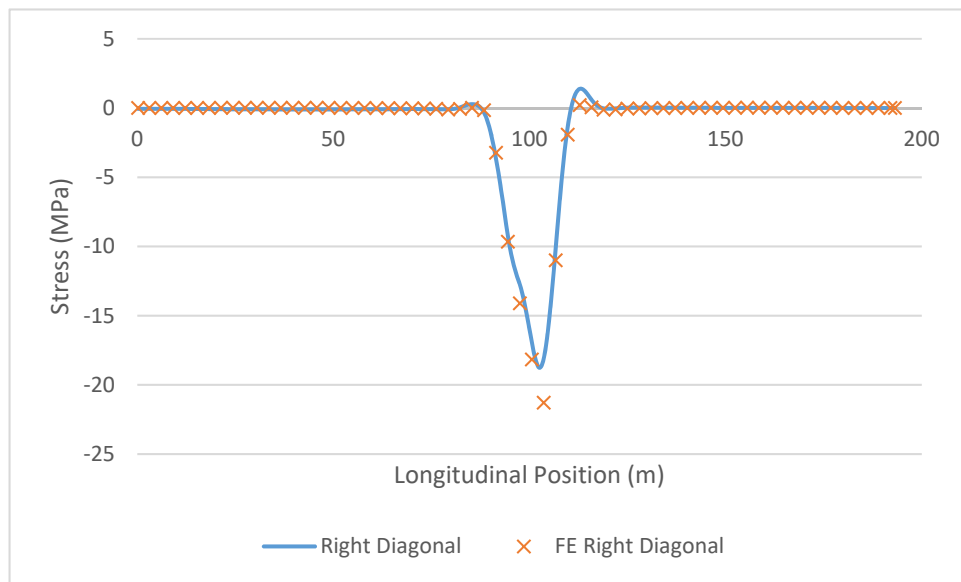


Figure 4.19 Example Stress Response in the Right Diagonal Diaphragm Member

Figure 4.19 shows a response plot comparison for the right bottom beam. The finite-

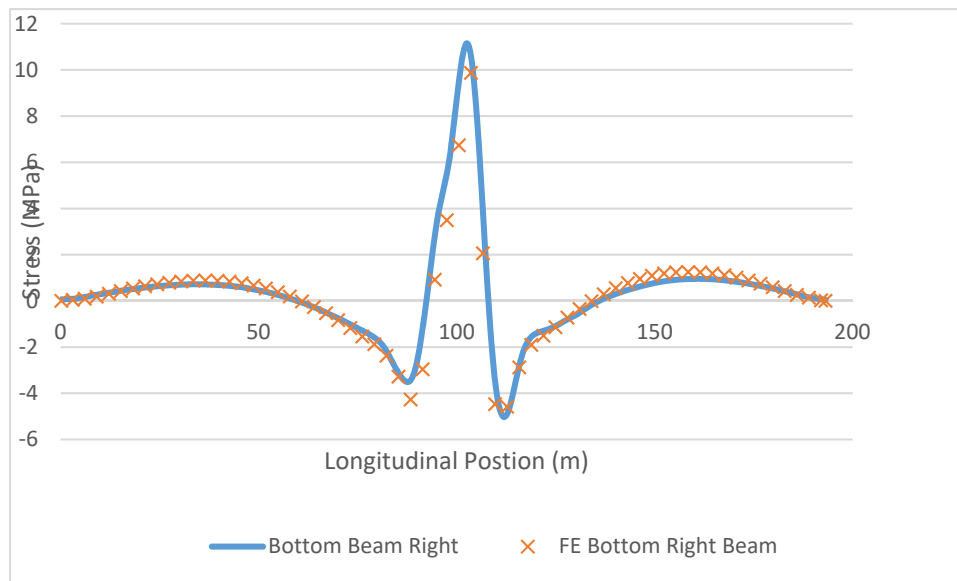
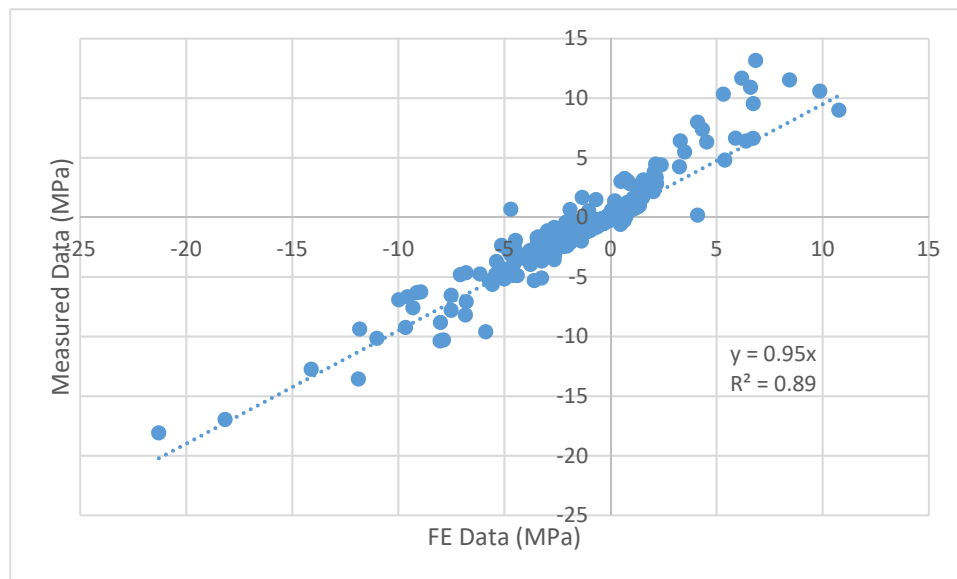


Figure 4.18 Example Stress Response in Bottom Right Beam

element data mirrors the magnitude and direction of the measured data.

To determine the combined coefficient of correlation for all the diaphragm members, data from 1,365 points were compared between the finite-element and measured data. This included data for all diaphragm members and all load paths, for a total coefficient of correlation of 0.89 and a slope of 0.95, as shown in *Figure 4.20*.



*Figure 4.20 Correlation of all Load Paths for Transverse Diaphragm Members*

Following the completion of comparisons for each individual supporting structural member and load path, a combined analysis was performed. This comparison accounted for all load paths for the girders and diaphragm members, and for the cases when the snooper traveled directly over the stringers. A total of 8,381 data points were compared between the finite-element and measured data. The combined  $R^2$  and linear correlation for all supporting structural members is 0.90 and 0.96, respectively. As previously discussed, the data sets correlated particularly well

for Girders 1 and 2, Stringer 1, and the diaphragm members, but not nearly as well for Stringer 2.

This data comparison is shown in *Figure 4.21*.

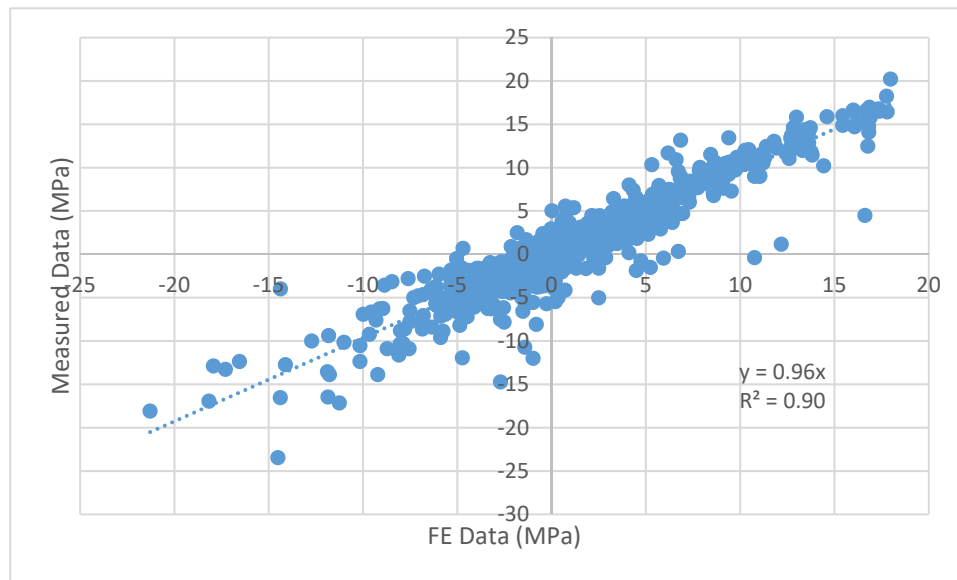


*Figure 4.21 R<sup>2</sup> Correlation for all Load Paths and all Structural Supporting Members*

#### 4.4 Transverse Comparison of Strain

In addition to comparing the stress response data, the transverse distribution of strain was also compared. The responses were only compared at one longitudinal cross-section, E-E because it was the only cross-section for which both girders and both stringers were instrumented with strain transducers. The comparison was performed for the response when the truck was at the maximum magnitude of strain, for each girder. For Girder 1 this location occurred at 100.60 m (330.04 ft) when the snoopers were in load path Y3, and 101.18 m (331.96 ft) when the snoopers were in load path Y1, for Girder 2. *Figures 4.22 and 4.23* show the finite-element vs. measured data in Girder 2 for the bottom and top flange, respectively. Just as with the stress response

comparison, it can be seen that the strain between the two data sets correlated very well for Girders 1 and 2, and Stringer 1, but not quite as well for Stringer 2. As seen in the figures, the

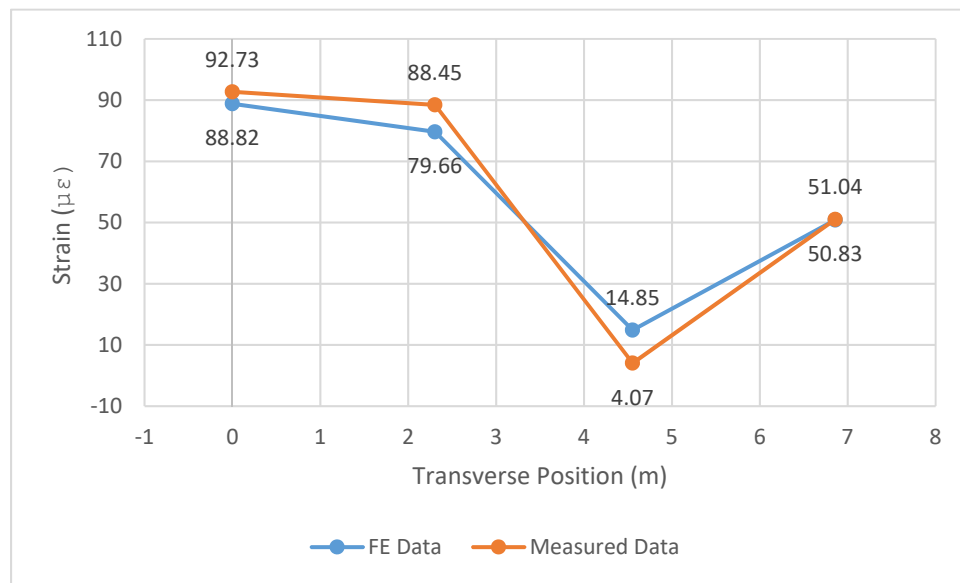


Figure 4.22 Transverse Strain Distribution in Bottom Flanges for Load Path Y1

strain distribution of the finite-element data follows the shape and relative magnitude of the measured strain. The transverse position is measured from Girder 2 (0 m) toward Girder 1 (6.86 m).

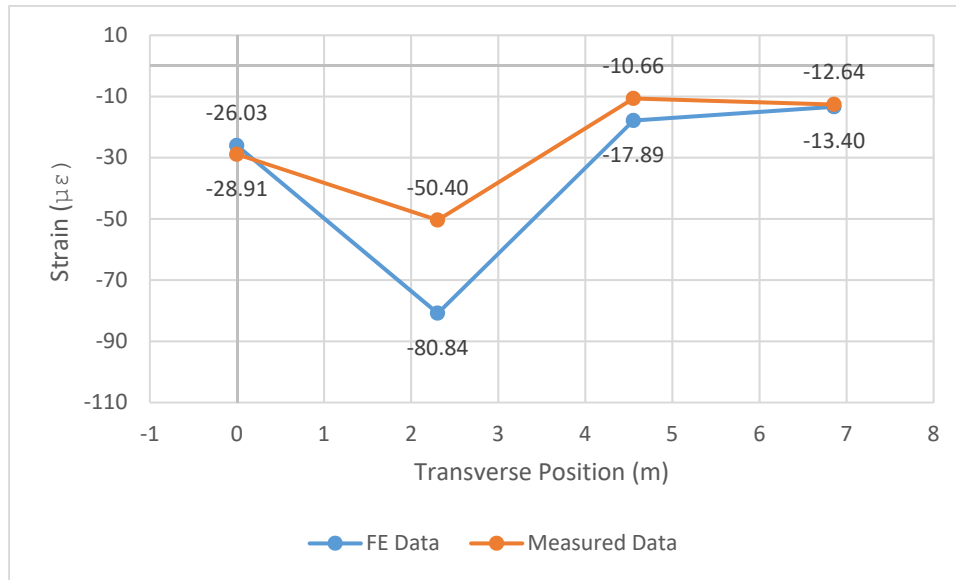


Figure 4.24 Transverse Strain Distribution in Top Flanges for Load Path Y1

Figures 4.24 and 4.25 show the transverse strain distribution for Girder 1 for the bottom and top flange, respectively. Despite some differences in the comparison for the top flange, it can be seen that the correlation of data for the bottom flange, where the highest values of strain were

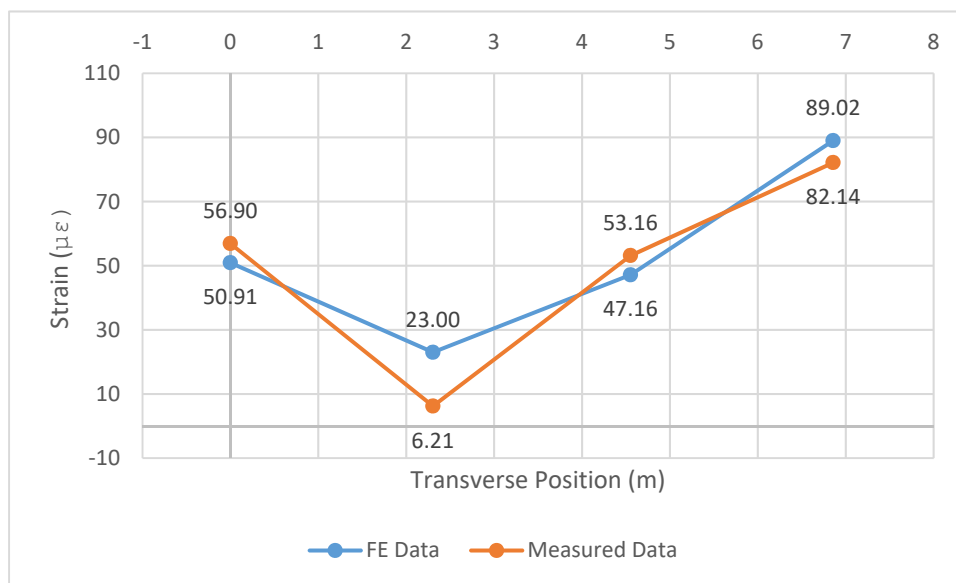


Figure 4.23 Transverse Strain Distribution in Bottom Flanges for Load Path Y

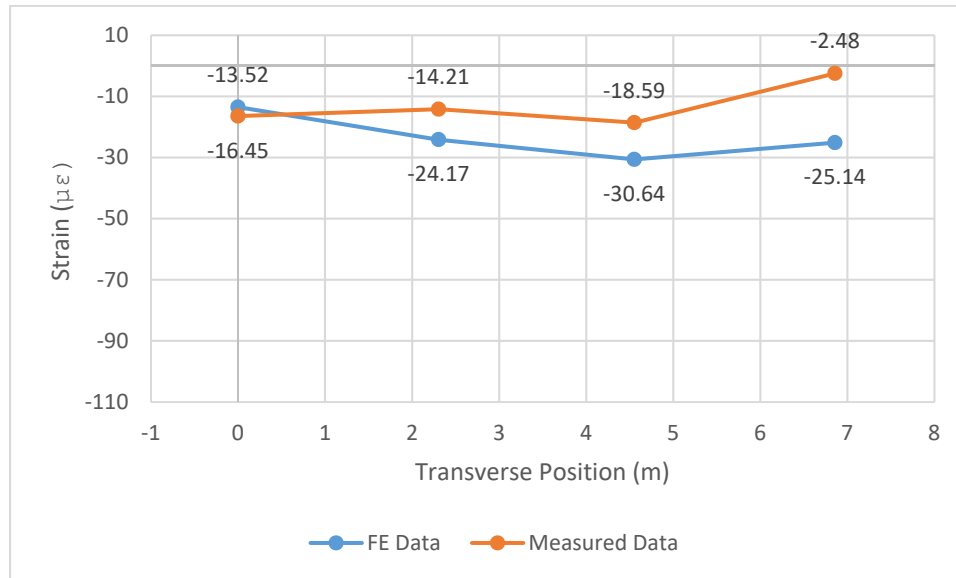


Figure 4.25 Transverse Strain Distribution for Top Flanges in Load Path Y3

recorded, is the best. Overall the distribution of finite-element strain correlated well with the distribution of measured strain.

In addition to the transverse strain distribution at the longitudinal locations that achieved the largest stress in the girders, the strain distribution was also analyzed when the truck was at a longitudinal position of 91.44 m (300 ft). *Figures 4.26 and 4.27* show the distribution of strain in Girder 2, when the load is in path Y1 for the bottom and top flange, respectively.

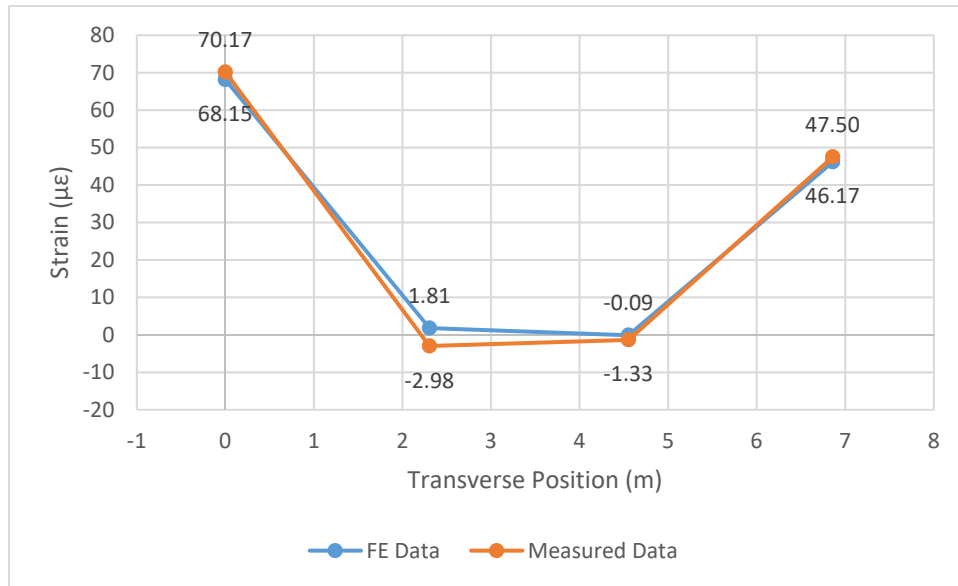


Figure 4.26 Transverse Strain Distribution in Top Flanges with Snooper at 91.44 m (300 ft) for Load Path Y1

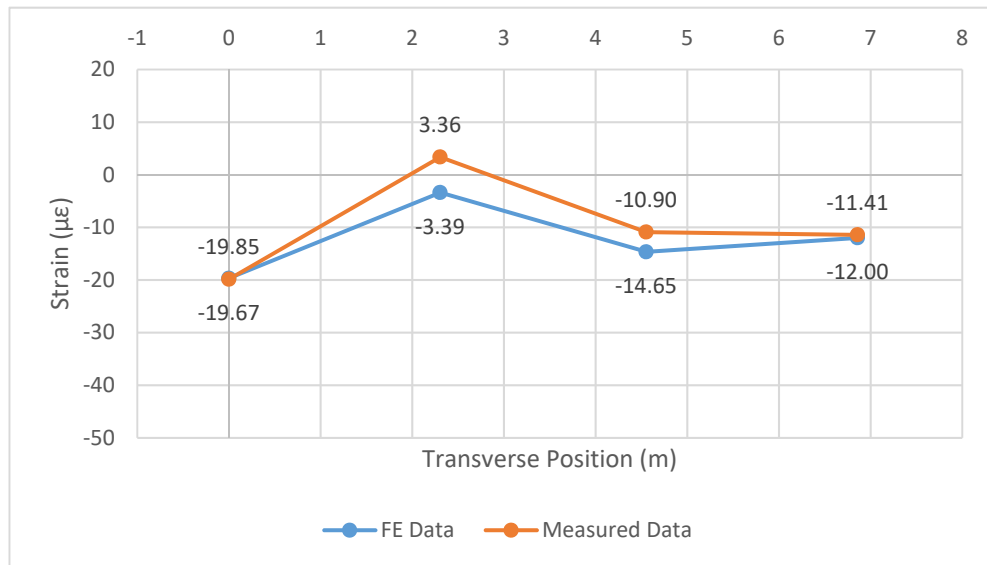


Figure 4.27 Transverse Strain Distribution in Top Flanges with Snooper at 91.44 m (300 ft) for Load Path Y1

Figures 4.28 and 4.29 show the distribution of strain when the load is in path Y3 for the bottom and top flange, respectively. Based on these figures, the distribution of strain from the finite-element data closely follows both the magnitude and shape of the distribution of strain of the measured data.

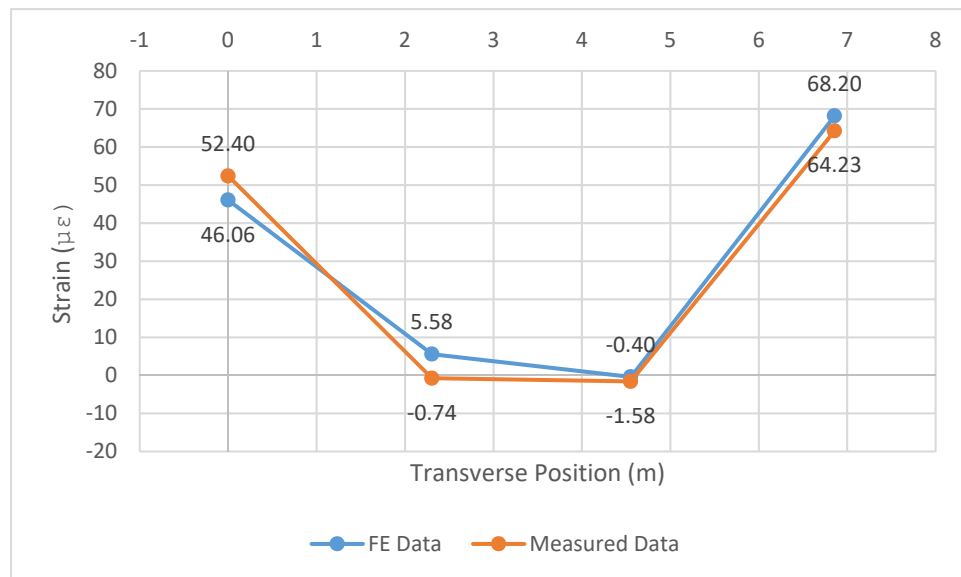


Figure 4.28 Strain Distribution in Bottom Flanges with Snooper at 91.44 m (300 ft) for Load Path Y3

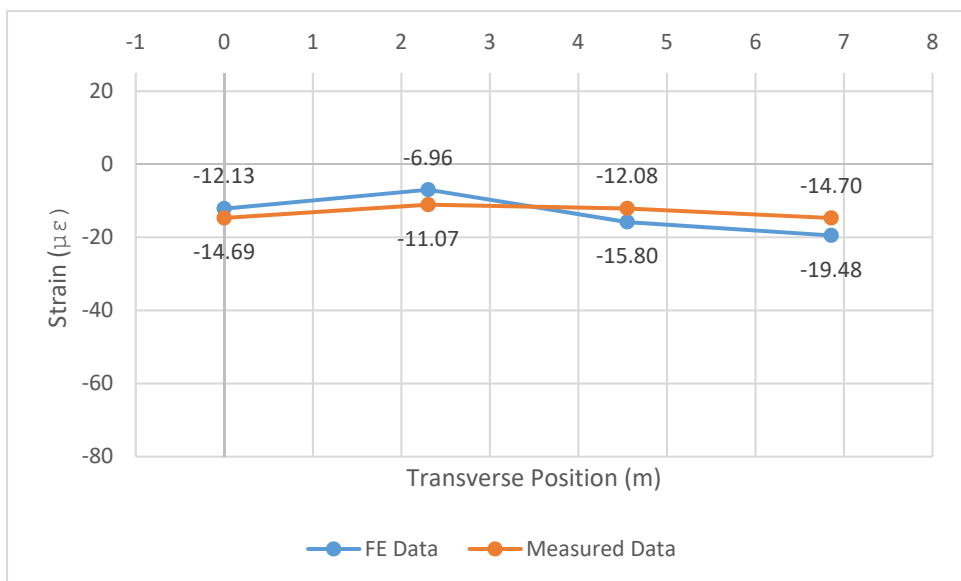


Figure 4.29 Transverse Strain Distribution in Top Flanges with Snooper at 91.44 m (300 ft) in Load Path Y3

## CHAPTER 5. DISTRIBUTION FACTORS AND LOAD RATINGS

### 5.1 Comparison of Distribution Factors

Once the model was deemed sufficiently accurate in predicting the live-load response of the bridge, the transverse distribution of moments was quantified. The AASHTO Standard Specifications for Highway Bridges (2002) and the AASHTO LRFD Specifications (2010) provide simplified equations to calculate the transverse distribution factors based on bridge type. These simplified equations eliminate the need of a finite-element analysis to determine the design moment for an individual beam. While these equations are intended to save time by simplifying the analysis, they have been found to be less accurate. For this research, the distribution factors for the SH-52 Bridge over the Snake River were calculated using the AASHTO Standard and AASHTO LRFD Specifications, and subsequently compared to the analytically obtained distribution factors using finite-element analysis.

The AASHTO Standard and LRFD Specifications use a multiple presence factor to account for different lane loading scenarios. The multiple presence factor is assigned based on the number of design lanes (which are not necessarily the same as the actual number of lanes that a bridge supports). The number of design lanes is the integer value of the roadway width divided by twelve. For this bridge there are two design lanes, so the distribution factors were calculated for the cases of single and double lane loading. The larger distribution factor is the controlling value. *Table 5.1* shows the multiple presence factor versus number of lanes loaded for the AASHTO Standard and AASHTO LRFD Specifications.

Table 5.1 Multiple Presence Factor vs. Lane Loading

<b>Multiple Presence Factor</b>		
	<b>AASHTO Specifications</b>	
<b>Lane Loading</b>	<b>Standard</b>	<b>LRFD</b>
Single	1.0	1.2
Double	1.0	1.0

The distribution factors calculated by the AASHTO Standard Specifications cannot be directly compared to the AASHTO LRFD or finite-element distribution factors. This is because the AASHTO Standard distribution factors are based on wheel line loads instead of axle loads. Therefore, the AASHTO Standard distribution factors must be divided by two for an equivalent comparison.

The AASHTO Standard Specifications provide expressions to calculate the distribution factors for an interior stringer for a steel I-girder bridge with a concrete deck using the equations in Table 3.23.1.

$$DF = \frac{S}{5.5} * MPF \quad (4)$$

Where:

$S$  = average stringer spacing in feet

$MPF$  = multiple presence factor

The distribution of moments for the exterior beams was calculated by applying the requirements of Section 3.23.2.3. The distribution factor was calculated using the lever rule (described with the AASHTO LRFD distribution factors), but could not exceed the result of Equation 5.

$$DF = \frac{S}{4.0 + 0.25 * S} * MPF \quad (5)$$

Where:

$S$  = average stringer spacing in feet

$MPF$  = multiple presence factor

The distribution factors calculated according to the AASHTO Standard Specifications are the same for both single and double lane loading, and are shown in *Table 5.2*.

*Table 5.2 Distribution Factors for AASHTO Standard Specifications*

<b>Structural Member:</b>	<b>Distribution Factor</b>
Girders	0.642
Stringers	0.679

Because the superstructure of the SH-52 Bridge over the Snake River is supported with steel members and the deck was cast-in-place, the cross-section was determined to be type “a” for the AASHTO LRFD Specifications (Table 4.6.2.2.1-1). As for the AASHTO Standard Specifications, the distribution factors for interior and exterior beams were calculated separately. For both types of beams the single and double lane loading cases were evaluated. The moment distribution factors for interior beams for the cases of single and double lane loading are calculated using *Equations 6* and *7*, respectively. The equations for distribution factors from the AASHTO LRFD Specifications account for the multiple presence factor internally.

Single Lane loading:

$$DFM_I^{One-lane} = 0.06 + \left(\frac{S}{14}\right)^{0.4} \left(\frac{S}{L}\right)^{0.3} \left(\frac{K_g}{12.0Lt_s^3}\right)^{0.1} \quad (6)$$

Double Lane Loading:

$$DFM_I^{Two-lane} = 0.075 + \left(\frac{S}{9.5}\right)^{0.6} \left(\frac{S}{L}\right)^{0.2} \left(\frac{K_g}{12.0Lt_s^3}\right)^{0.1} \quad (7)$$

These equations apply when:

$$3.5 \leq S \leq 16.0$$

$$4.5 \leq t_s \leq 12.0$$

$$20 \leq L \leq 240$$

$$N_b \leq 4$$

$$10,000 \leq K_g \leq 7,000,000$$

Where:

$S$  = transverse beam spacing

$t_s$  = depth of concrete slab

$L$  = span length

$N_b$  = number of beams

$K_g$  = longitudinal stiffness parameter;

$$K_g = n(+Ae_g^2)$$

$$n = \frac{E_b}{E_d}$$

$E_b$  = modulus of elasticity of beam material

$E_d$  = modulus of elasticity of deck material

$I$  = moment of inertia of the non-composite beam

$A$  = Area of the non-composite beam

$e_g$  = distance between the centers of gravity of the basic beam and the deck

The distribution factor for an exterior beam subjected to the single lane loading conditions is calculated using the lever rule. The lever rule is based on the assumption that a hinge is placed at the first interior beam that is adjacent to the exterior beam. The wheel lines of a truck that has an axle width of 1.83 m (6 ft) is placed on the roadway surface, with the center of the outside wheel being placed 0.61 m (2 ft) away from the edge of the roadway width. *Figure 5.1* shows a schematic drawing of the lever rule for the SH-52 Bridge over the Snake River.

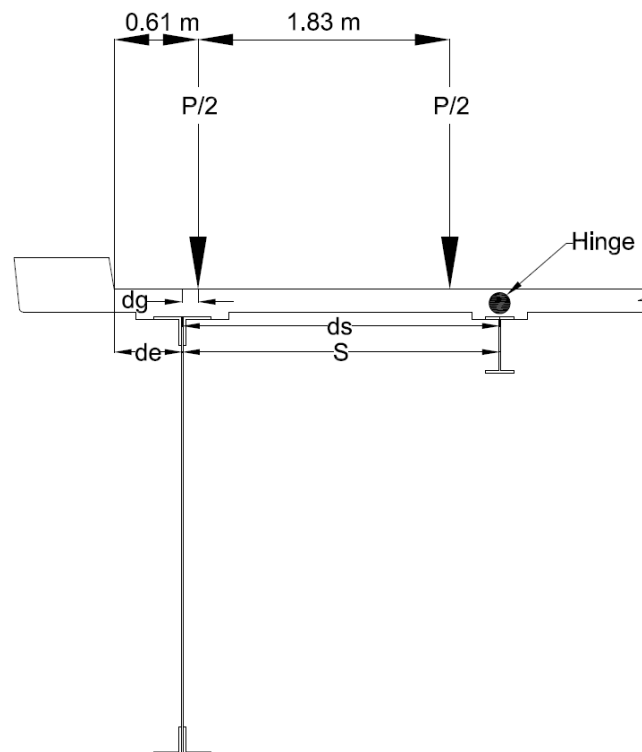


Figure 5.1 Schematic Drawing of the Lever Rule

The moment distribution factor for the single lane loading case is calculated by finding the fraction of the load  $P$  that is resisted by the exterior girder and multiplying by the multiple presence factor.

$$DFM_E^{One-lane} = R_E * MPF \quad (8)$$

Where:

$$R_E = \frac{((S-dg)+(S-ds))}{2*S} \quad (9)$$

$MPF$  = Multiple Presence Factor

When considering the distribution factor for when two lanes are loaded, the distribution factor is calculated based off of a modification factor which is multiplied by the value obtained for the interior beams.

$$DFM_E^{Two-lane} = e * DFM_I^{Two-lane} \quad (10)$$

Where:

$DFM_E^{Two-lane}$  = moment distribution factor for an exterior beam when 2 lanes are loaded

$DFM_I^{Two-lane}$  = moment distribution factor for an interior beam when 2 lanes are loaded

$$e = 0.77 + \frac{d_e}{9.1}$$

$d_e$  = overhang distance

The distribution factors calculated in accordance with the procedures in the AASHTO LRFD Specifications are presented in *Tables 5.3* and *5.4*. *Table 5.3* shows the distribution factors for spans 1 through 3 for the single lane loading case, and *Table 5.4* shows the distribution factors for spans 1 through 3 for the double lane loading case.

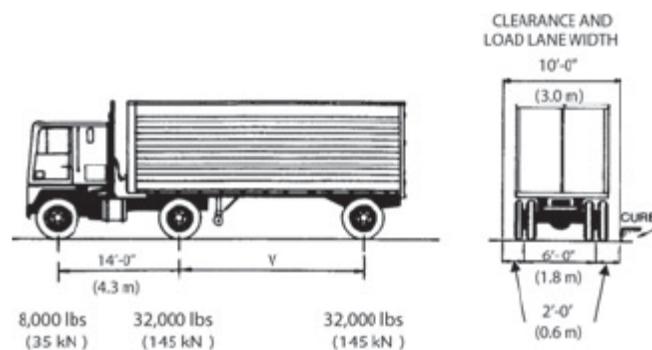
Table 5.3 AASHTO LRFD Distribution Factors for Single Lane Loading

<b>AASHTO LRFD Specifications Distribution Factors, 1 lane loaded</b>				
	<b>Girder</b>	<b>16 WF 45</b>	<b>16 WF 40</b>	<b>16 WF 36</b>
<b>Spans 1,3</b>	0.684	0.307	0.304	0.301
<b>Span 2</b>	0.684	0.282	0.280	0.277

Table 5.4 AASHTO LRFD Distribution Factors for Double Lane Loading

<b>AASHTO LRFD Specifications Distribution Factors, 2 lanes loaded</b>				
	<b>Girder</b>	<b>16 WF 45</b>	<b>16 WF 40</b>	<b>16 WF 36</b>
<b>Spans 1,3</b>	0.640	0.399	0.395	0.391
<b>Span 2</b>	0.597	0.375	0.371	0.367

To calculate the distribution factors based on the finite-element model of the bridge, the largest magnitude of moment caused by HS-20 truck loading in each of the supporting structural beams was required. The HS-20 truck has axle loads of 35.59 kN (8 k), 142.34 kN (32 k), and 142.34 (32 k) from front to back, respectively. The longitudinal spacing of axles was 4.27 m (14 ft) between the first and second, and second and third axles, and the axles were 1.83 m (6 ft) wide. *Figure 5.2* shows a schematic drawing of an HS-20 truck.



**These sketches illustrate the AASHTO-approved live loading specifications for standard H20 and HS20 trucks.**

Source: AASHTO Standard Specifications for Highway Bridges.

Figure 5.2 Schematic Drawing of an HS-20 Truck

The output of the finite-element model was stress. The distribution factors for the individual beams could not be simply obtained by taking the individual stress for a particular beam and dividing it by the sum of the total stress for all the beams because the cross section was not uniform. Therefore, the stress for each girder and stringer was converted to moments using *Equation 11*.

$$M = \frac{E\varepsilon * I}{y} \quad (11)$$

Where:

$M$  = the bending moment in the structural member

$\sigma$  = the stress response in the bottom flange, calculated in the finite-element analysis

$I$  = the moment of inertia of the structural members and tributary deck and curb widths due to composite action

$y$  = the distance from the centroid of the structural member or transformed section to its outermost fiber

The width of the deck attributed to the girders for the moment of inertia calculations was the value that was extrapolated from *Equation 2* (page 38). Both stringers were assumed to act non-compositely with the deck for this calculation.

The maximum girder or stringer response was obtained by systematically moving the transverse and longitudinal positions of the truck(s) across the bridge to find the location of maximum moment response. For the single lane loading case, the truck was moved transversely

anywhere except within 0.61 m (2 ft) of the edge of the roadway width to find the location that maximized the moment response for each member. For the double lane loading case, the trucks were moved within 3.66 m (12 ft) lanes which were also systematically moved across the width of the bridge. In accordance with the AASHTO specifications, the trucks were required to remain in their lanes and could not be closer than 0.61 m (2 ft) to either edge of their lane. To obtain the distribution factor for a particular beam, the transverse and longitudinal position that caused the maximum magnitude of moment were fixed, and the response in each of the other members were recorded. Equation 12 was then used to calculate the distribution factor.

$$DFM_i = \frac{M_i}{\Sigma M_i} * MPF \quad (12)$$

Where:

$DFM_i$  = the moment distribution factor for a particular supporting beam

$M_i$  = the bending moment in the desired supporting beam

$\Sigma M_i$  = the sum of the moments for all four supporting beams with the vehicle(s) at the critical transverse and longitudinal locations

$MPF$  = the AASHTO LRFD multiple presence factor

The positive moment distribution factors calculated based on the response of the finite-element model are shown below in *Table 5.5*.

*Table 5.5 Finite-Element Positive Moment Distribution Factors*

<b>Finite-Element Distribution Factors</b>				
	<b>Girder 1</b>	<b>Girder 2</b>	<b>Stringer 1</b>	<b>Stringer 2</b>
<b>1 Lane Loaded</b>	0.773	0.772	0.01	0.014
<b>2 Lanes Loaded</b>	0.533	0.532	0.005	0.008

The distribution factors from the AASHTO Standard Specifications, AASHTO LRFD Specifications, and finite-element analysis were compared for positive moment. The results are shown in *Table 5.6*. The controlling distribution factors are shaded.

*Table 5.6 Comparison of Positive Moment Distribution Factors*

	Distribution Factor Calculation					
	Standard Specifications		LRFD Specifications		Finite Element Calculations	
	Single	Double	Single	Double	Single	Double
<b>Lane Loading</b>						
<b>Girder 1</b>	0.642	0.642	0.684	0.640	0.773	0.533
<b>Girder 2</b>	0.642	0.642	0.684	0.640	0.772	0.532
<b>Stringer 1</b>	0.679	0.679	0.307	0.399	0.01	0.005
<b>Stringer 2</b>	0.679	0.679	0.307	0.399	0.014	0.008

Based on *Table 5.6* the controlling distribution factor from the AASHTO codes is 0.684 for the girders and 0.679 for the stringers. The controlling distribution factor from the finite-element analysis was 0.773 for the girders and 0.014 for the stringers.

In addition to finding the distribution factors for positive moment, the distribution factors for negative moment were also calculated and compared to the AASHTO distribution factors. Only the AASHTO LRFD and finite-element distribution factors had to be recalculated because the AASHTO Standard Specifications do not differentiate between positive and negative moment distribution factors. The calculation for the AASHTO LRFD Specifications was simple because the only parameter that had to be changed was the span length. For negative moments, the span length is taken as the average of the two adjacent spans. The negative moment, finite-element distribution factors were calculated in the same manner as for the positive moment region except that the response in each beam was maximized for negative moment. The resulting negative moment distribution factors are summarized below in *Table 5.7*.

Table 5.7 Comparison of Negative Moment Distribution Factors

	Distribution Factor Calculation					
	Standard Specifications		LRFD Specifications		Finite Element Calculations	
Lane Loading	Single	Double	Single	Double	Single	Double
<b>Girder 1</b>	0.642	0.642	0.684	0.617	0.730	0.527
<b>Girder 2</b>	0.642	0.642	0.684	0.617	0.728	0.525
<b>Stringer 1</b>	0.679	0.679	0.294	0.386	0.171	0.107
<b>Stringer 2</b>	0.679	0.679	0.294	0.386	0.225	0.141

The AASHTO distribution factors do a better job of approximating the distribution factors for negative moment regions than for positive moment regions. Despite the increased accuracy, there is still a significant discrepancy.

Overall, the code based distribution factors do not correlate well with the finite-element distribution factors for regions of positive or negative moment. The distribution factors for the girders are slightly unconservative and for the stringers they are overly conservative. This is likely due to the large difference in stiffness between the girders and stringers, and the differing composite behavior experienced between the deck and the girders, and the deck and the stringers.

## 5.2 Comparison of Distribution Factors with and without Diaphragm Bracing

An additional analysis was performed to quantify the influence of the intermediate diaphragm members. For this analysis, the previously calculated finite-element distribution factors were compared to the newly calculated distribution factors from a model that excluded all intermediate diaphragm members except the floor beams. As was the case with the full bridge analysis, the single truck loading case was the controlling distribution factor for each beam. Based on this analysis, the intermediate diaphragms were found to significantly impact the distribution of moments. The distribution factors for the girders were approximately 23% less

when the diaphragms were included for positive moment and 27% less for negative moment. The stringers were virtually unaffected by the cross bracing in positive moment, however the cross bracing significantly decreased the portion of the load carried in the stringers in negative moment by transferring it to the girders. *Table 5.8* shows the distribution factors for the cases when the intermediate diaphragm members are present and absent for positive moment. *Table 5.9* shows the distribution factors for the cases when the intermediate diaphragm members are present and absent for negative moment.

*Table 5.8 Finite-Element Positive Moment Distribution Factors with and without Diaphragm Members*

<b>Structural Member</b>	<b>Distribution Factor</b>	
	<b>Diaphragm Members Present</b>	<b>Diaphragm Members Absent</b>
Girder 1	0.773	1.00
Girder 2	0.771	1.00
Stringer 1	0.011	0.011
Stringer 2	0.015	0.011

*Table 5.9 Finite-Element Negative Moment Distribution Factors with and without Diaphragm Members*

<b>Structural Member</b>	<b>Distribution Factor</b>	
	<b>Diaphragm Members Present</b>	<b>Diaphragm Members Absent</b>
Girder 1	0.730	1.00
Girder 2	0.728	1.00
Stringer 1	0.171	0.017
Stringer 2	0.225	0.023

### 5.3 Load Ratings

Load ratings are numerical values assigned to a bridge that theoretically describe its capacity to carry standardized live-loads. The AASHTO LRFR manual (2003) states that a load rating is “the determination of the live load carrying capacity of an existing bridge”. Two load rating

factors are given to bridges: inventory and operating. The inventory level rating is defined as follows: “[g]enerally corresponds to the rating at the design level of reliability for new bridges... but reflects the existing bridge and material conditions with regard to deterioration and loss of section”. The operating level rating is the “[a]bsolute maximum load level to which a structure may be subjected for limited passages of the load. Generally corresponds to the rating at the Operating level of reliability in past load rating practice” (AASHTO LRFR, 2003). Load ratings guide decisions regarding which loads are permitted to cross a bridge, and if a bridge needs to be repaired or replaced.

Load ratings for the SH-52 Bridge over the Snake River were calculated based on the results of the finite-element model. The AASHTO LFD general load rating equation is:

$$RF = \frac{R_n - \gamma_D * D}{\gamma_L * L * (1 + I)} \quad (13)$$

Where:

$RF$  = load rating factor

$R_n$  = nominal capacity of the member

$\gamma_D$  = dead load factor; 1.3

$D$  = dead load effects of the bridge

$\gamma_L$  = live load factor; 1.3 operating and 2.17 inventory

$L$  = live load effects on the bridge

$I$  = impact factor due to dynamic loading

For this study the nominal capacity of the members was calculated using the AASHTO Standard Specifications. These calculations are described in more detail in the following pages.

The dead and live load effects were calculated using CSiBridge. Because this procedure used a calibrated finite-element model, it was not necessary to perform a beam-line analysis with distribution factors. For the dead load effects, a load case was created that included the self-weight of the structural members. An additional load was assigned to the deck and curb to account for the wearing surface and bridge railing, respectively; which were not modeled explicitly. The response in the bottom flange was converted to moments by multiplying the reported stress by the moment of inertia of the beam and tributary deck width due to composite action, then dividing by the distance to the neutral axis, as shown in *Equation 12*.

The live load effects were calculated by finding the maximum response due to the loading from two HS-20 trucks. The same transverse and longitudinal positions that maximized the stress response for the distribution factors was used to find the response for the live load effects. The same conversion from stress to moments that was used for the dead load effects was used for the live load effects.

The impact factor was calculated as the increase in stress due to dynamic loading compared to the stress response recorded during crawl speed loading. This comparison was performed at the longitudinal location where the peak magnitude of stress occurred during dynamic loading using the measured data. The maximum observed impact factor from the measured data was used to calculate the load ratings. For the girders, the observed impact factor was 0.135 and for the stringers 0.25.

To find the moment capacity for the girders and stringers, the procedures in the AASHTO Standard Specifications were applied. The calculations in the report provided by Bridge Diagnostics Inc. (B.D.I., 2013) were used as a guideline. The geometric properties for

each structural member were calculated or obtained from structural design manuals. Because the level of composite action between the deck and its supporting beams deteriorates over time, all capacities were calculated as if the beams were in a non-composite condition. The procedure to determine the capacity was based on the compactness of the section. To identify if the section was compact, the equations from parts a, b, and c in section 10.48.1.1 of the code were applied. For positive moments, the requirement for part c was met because the compression flange is continuously braced by the deck, and  $L_b$  was taken as zero. *Table 5.10* shows the input values for the compactness checks.

Section 10.48.1.1 compactness checks:

(a) Compression flange

$$\frac{b}{t} \leq \frac{4,110}{\sqrt{F_y}} \quad (14)$$

(b) Web thickness

$$\frac{D}{t_w} \leq \frac{19,230}{\sqrt{F_y}} \quad (15)$$

(c) Spacing of lateral bracing for compression flange

$$\frac{L_b}{r_y} \leq \frac{[3.6 - 2.2 * (\frac{M_1}{M_u})] * 10^6}{F_y} \quad (16)$$

Where:

$b$  = width of compression flange

$t$  = thickness of compression flange

$F_y$  = minimum specified yield strength of the steel

$D$  = clear distance between flanges

$t_w$  = web thickness

$L_b$  = distance between points of bracing of the compression flange (equal to zero because the compression flange is continuously braced by the deck)

$r_y$  = radius of gyration of the steel section with respect to the Y-Y axis

$M_l$  = smaller moment at the end of the unbraced length of the member (not shown in the table)

$M_u$  = ultimate moment at the other end of the unbraced length (not shown in the table)

Table 5.10 Input Values for Compactness Checks

Input Variable	Girder 0 cover plates	Girder 1 cover plates	Girder 2 cover plates	Girder 3 cover plates	16 WF 45	16 WF 40	16 WF 45
$b$	16.5	20	20	20	7.04	7	6.99
$t$	0.75	1.37	2.12	2.87	0.563	0.503	0.43
$F_y$	50,000	50,000	50,000	50,000	50,000	50,000	50,000
$D$	119	119.26	119.26	119.26	14.99	14.99	14.99
$t_w$	0.5	0.5	0.5	0.5	0.35	0.31	0.30
$L_b$	0	0	0	0	0	0	0
$r_y$	2.33	3.40	3.94	4.64	1.52	1.5	1.45

If any of the requirements for the compression flange, web thickness, or lateral bracing were not met, the entire section was considered non-compact. For non-compact sections, the procedure in Section 10.48.2 was applied. For compact sections, equations 10-103a, and 10-103c were applied.

Because the web thickness for the girders was non-compact, the girders were checked against the requirements of Section 10.48.2. The input values are given in *Table 5.11*.

(a) Compression flange

$$\frac{b}{t} \leq 24 \quad (17)$$

(b) Web thickness

$$\frac{D}{t_w} \leq \frac{73,000}{\sqrt{F_y}} \quad (18)$$

(c) Spacing of lateral bracing for compression flange

$$L_b \leq \frac{20,000,000 * A_f}{F_y * d} \quad (19)$$

Where:

$b$  = width of compression flange

$t$  = thickness of compression flange

$D$  = clear distance between flanges

$t_w$  = web thickness

$F_y$  = minimum specified yield strength of the steel

$A_f$  = flange area

$d$  = depth of beam or girder

Table 5.11 Input Values for Equations 17, 18, and 19

<b>Input Variable</b>	<b>Girder 0 cover plates</b>	<b>Girder 1 cover plates</b>	<b>Girder 2 cover plates</b>	<b>Girder 3 cover plates</b>
$b$	16.5	20	20	20
$t$	0.75	1.37	2.12	2.87
$D$	119	119.26	119.26	119.26
$t_w$	0.5	0.5	0.5	0.5
$F_y$	50,000	50,000	50,000	50,000
$A_f$	12.38	27.38	42.38	57.38
$d$	120.5	122	123.5	125

Since the girders met the requirements of parts a, and b, and the spacing of lateral bracing was equal to zero for part c, the moment capacity was calculated as the minimum of:

$$M_u = F_y * S_{xt} \quad (20)$$

and

$$M_u = F_{cr} * S_{xc} * R_b \quad (21)$$

Where:

$F_y$  = minimum yield stress of the steel

$S_{xt}$  = section modulus with respect to the tension flange

$$F_{cr} = (4,400 * \frac{t}{b})^2 \leq F_y \quad (22)$$

$t$  = compression flange thickness

$b$  = compression flange width

$S_{xc}$  = section modulus with respect to compression flange

To obtain  $R_b$ , values for  $k$  and  $f_b$  were first calculated. The value for  $k$  was calculated according to the requirements of Section 10.48.4.1. The value for  $f_b$  was calculated according to Section 10.61.1. The input values for the moment capacity equations are shown in *Table 5.12*.

$$\text{for } \frac{d_s}{D_c} \geq 0.4 \quad k = 5.17 * \left(\frac{D}{d_s}\right)^2 \geq 9 * \left(\frac{D}{D_c}\right)^2 \quad (23)$$

$$\text{for } \frac{d_s}{D_c} < 0.4 \quad k = 11.64 * \left(\frac{D}{D_c - d_s}\right)^2 \quad (24)$$

$$f_b \leq \frac{26,200,000 * k}{\left(\frac{D}{t_w}\right)^2} \leq F_{yw} \quad (25)$$

Where:

$d_s$  = distance from the gage line of an angle longitudinal stiffener to the inner surface or the leg of the compression flange component

$D_c$  = clear distance between the neutral axis and the compression flange

$D$  = the clear distance between flanges

$t_w$  = thickness of the web

$F_{yw}$  = specified minimum yield strength of the web

$R_b$  was then obtained in accordance with the requirements of Section 10.48.4.1.

$$R_b = 1$$

When:

$$\frac{D}{t_w} \leq 5,460 * \sqrt{\frac{k}{f_b}} \quad (26)$$

Table 5.12 Input Values for Girder Positive Moment Capacity

<b>Input Variable</b>	<b>Girder 0 cover plates</b>	<b>Girder 1 cover plates</b>	<b>Girder 2 cover plates</b>	<b>Girder 3 cover plates</b>
$F_y$	50,000	50,000	50,000	50,000
$S_{xt}$	3767	5528	7291	8990
$t$	0.75	1.37	2.12	2.87
$b$	16.5	20	20	20
$F_{cr}$	40,000	90,842	217,273	398,319
$S_{xc}$	3767	5528	7291	8990
$d_s$	28.25	28.25	28.25	28.25
$D_c$	59.5	59.63	59.63	59.63
$D$	119	119.26	119.26	119.26
$k$	91.74	92.14	92.14	92.14
$t_w$	0.5	0.5	0.5	0.5
$F_{yw}$	50,000	50,000	50,000	50,000
$R_b$	1.0	1.0	1.0	1.0

The positive moment capacity was only calculated for the case of zero cover plates because the additional cover plates were only present in the regions of negative moment near piers 2 and 3. The positive moment capacity is shown in *Table 5.13*.

*Table 5.13 Girder Positive Moment Capacity*

<b>Number of Cover Plates</b>	<b>Girder Positive Moment Capacity, kip*ft (kN*m)</b>
0	12,556 (17,024)

This process was repeated to determine the positive moment capacity of the stringers. Unlike the girders, the stringer sections were found to be compact.

Because the stringers are compact sections and meet the requirement:

$$\frac{D_c}{t_w} \leq \frac{\lambda}{\sqrt{F_y}} \quad (27)$$

$M_r$  was calculated using equation 10-103c (*Equation 28* below). The values input into *Equation 27* are shown in *Table 5.14*.

Where:

$D_c$  = clear distance between the neutral axis and the compression flange

$t_w$  = thickness of the web

$\lambda = 15,400$

$F_y$  = minimum specified yield strength

*Table 5.14 Input Values for the Requirement of Equation 27*

<b>Input Variable</b>	<b>16 WF 45</b>	<b>16 WF 40</b>	<b>16 WF 36</b>
$D_c$	7.5	7.5	7.5
$t_w$	0.35	0.31	0.30
$F_y$	50,000	50,000	50,000

$$M_r = 91 * 10^6 * C_b * \left(\frac{I_{yc}}{L_b}\right) * \sqrt{0.772 * \frac{J}{I_{yc}} + 9.87 * \left(\frac{d}{L_b}\right)^2} \leq M_y \quad (28)$$

The values for *Equation 28* are given in *Table 5.15*.

Where:

$C_b$  = bending coefficient (assumed value of 1.0)

$I_{yc}$  = moment of inertia of the compression flange

$L_b$  = unbraced length of the compression flange, (assumes bracing at midpoint of panel)

$J$  = torsional constant

$d$  = depth of the beam or girder

$$M_y = F_y * S_x$$

$F_y$  = minimum specified yield strength of the steel

$S_x$  = section modulus

*Table 5.15 Input Values for Equation 28*

<b>Input Variable</b>	<b>16 WF 45</b>	<b>16 WF 40</b>	<b>16 WF 36</b>
$C_b$	1.0	1.0	1.0
$I_{yc}$	16.36	14.4	12.2
$L_b$	10.88	10.88	10.88
$J$	1.11	0.79	0.55
$d$	16.12	16.0	15.85
$F_y$	50,000	50,000	50,000
$S_x$	72.4	64.4	56.3

The moment capacity,  $M_u$  was then found by multiplying  $M_r$  by the modification factor  $R_b$ . To find  $R_b$  for the stringers, *Equation 29* (equation 10-103b in the AASHTO code) was applied. The values used to calculate  $R_b$  are shown in *Table 5.16*.

$$R_b = 1 - 0.002 * \left( \frac{D_c * t_w}{A_{fc}} \right) * \left[ \frac{D_c}{t_w} - \frac{\lambda}{\sqrt{\frac{M_r}{S_{xc}}}} \right] \leq 1.0 \quad (29)$$

Where:

$D_c$  = depth of the web in compression

$t_w$  = thickness of web

$A_{fc}$  = area of compression flange

$M_r$  = previously calculated moment capacity

$S_{xc}$  = section modulus with respect to compression flange

$\lambda = 15,400$

Table 5.16 Input Values to obtain  $R_b$

Input Variable	16 WF 45	16 WF 40	16 WF 36
$D_c$	7.5	7.5	7.5
$t_w$	0.35	0.31	0.30
$A_{fc}$	3.96	3.52	2.99
$M_r$	301.7	268.3	234.6
$S_{xc}$	72.4	64.4	56.3
$R_b$	1.0	1.0	1.0

The positive moment capacity was calculated for each of the three stringer sections. The capacities are shown in Table 5.17.

Table 5.17 Stringer Positive Moment Capacities

Stringer Section	Positive Moment Capacity, $M_u$ kip*ft (kN*m)
16 WF 36	234.6 (318.1)
16 WF 40	268.3 (363.8)
16 WF 45	301.7 (409.1)

In addition to the capacity of the beams in positive moment, the capacity in negative moment was also calculated for the girders. (The stringers were assumed to have the same capacity for both positive and negative moments.) The compactness calculations to determine the capacities for the girders were the same, however, a different procedure was used to calculate the capacity of the girders because the unbraced length for negative moment did not meet the requirement of section 10.48.2. To determine the appropriate equation for capacity an additional requirement checked the slenderness of the web (*Equation 30*). The input values for *Equation 30* are given in *Table 5.18*.

$$\frac{D_c}{t_w} \leq \frac{\lambda}{\sqrt{F_y}} \quad (30)$$

Where:

$D_c$  = clear distance between the neutral axis and the compression flange

$t_w$  = thickness of the web

$\lambda = 15,400$

$F_y$  = minimum specified yield strength

*Table 5.18 Input Values for Equation 30*

<b>Input Variable</b>	<b>No Cover Plates</b>	<b>1 Cover Plate</b>	<b>2 Cover Plates</b>	<b>3 Cover Plates</b>
$D_c$	60.25	60.25	60.25	60.25
$t_w$	0.5	0.5	0.5	0.5
$F_y$	50,000	50,000	50,000	50,000

Since the web depth requirement was not met, *Equation 31* (equation 10-103e) was applied. *Table 5.19* shows the input variables for *Equation 31*.

$$M_r = C_b * F_y * S_{xc} * \left[ 1 - .5 * \left( \frac{L_b - L_p}{L_r - L_p} \right) \right] \quad (31)$$

Where:

$C_b$  = bending coefficient (assumed value 1.0)

$F_y$  = minimum specified yield strength

$S_{xc}$  = section modulus with respect to compression flange

$L_b$  = unbraced length

$L_p = 9500 * r' / F_y^{(0.5)}$

$r'$  = radius of gyration of compression flange about the vertical axis in the plane of the web

$$L_r = \sqrt{\frac{572 * 10^6 * I_{yc} * d}{F_y * S_{xc}}}$$

$d$  = depth of the web

Table 5.19 Input Values for Equation 31

Input Variable	No Cover Plates	1 Cover Plate	2 Cover Plates	3 Cover Plates
$C_b$	1.0	1.0	1.0	1.0
$F_y$	50,000	50,000	50,000	50,000
$S_{xc}$	3767	5528	7291	8990
$L_b$	21.75	21.75	21.75	21.75
$L_p$	202	245	245	245
$r'$	4.76	5.77	5.77	5.77
$L_r$	321	480	523	552
$d$	120.5	122	123.5	125

The resulting negative moment girder capacities for the cases of 0, 1, 2, and 3 cover plates are shown in Table 5.20.

Table 5.20 Girder Negative Moment Capacities

Number of Cover Plates	Girder Negative Moment Capacity, kip*ft (kN*m)
0	-11,801 (-16,000)
1	-22,263 (-30,185)
2	-29,520 (-40,024)
3	-36,496 (-49,482)

Table 5.21 shows the positive and negative moment capacities for the girders and stringers.

Table 5.21 Summary of Girder and Stringer Capacities

Structural Section	Positive Moment kip*ft (kN*m)	Negative Moment kip*ft (kN*m)
Girder no plates	12,556 (17,024)	-11,801 (-16,000)
Girder 1 plate	-	-22,263 (-30,185)
Girder 2 plates	-	-29,520 (-40,024)
Girder 3 plates	-	-36,496 (-49,482)
16 WF 36	234.6 (318.1)	-234.6 (-318.1)
16 WF 40	268.3 (363.8)	-268.3 (-363.8)
16 WF 45	301.7 (409.1)	-301.7 (-409.1)

After calculating the capacities and recording the dead and live load effects from the finite-element model, the load ratings were calculated. A summary of the capacities, dead load effects, live load effects, and inventory and operating ratings for the girders and stringers in positive moment is shown in Table 5.22. The same parameters for negative moment are shown in Table 5.23.

Table 5.22 Summary of Positive Moment Load Rating Parameters

Structural Members	Member Capacity	Dead Load Effects	Live Load Effects	Inventory Rating Factor	Operating Rating Factor
<b>Girders</b>	12556	4173.6	2297	1.26	2.10
<b>Stringers</b>	268.4	8.9	33.9	2.79	4.66

*Table 5.23 Summary of Negative Moment Load Rating Parameters*

<b>Structural Members</b>	<b>Member Capacity</b>	<b>Dead Load Effects</b>	<b>Live Load Effects</b>	<b>Inventory Rating Factor</b>	<b>Operating Rating Factor</b>
<b>Girders</b>	11801	-3651.8	-1326.8	2.16	3.60
<b>Stringers</b>	234.6	-12.7	-30.6	2.63	4.39

## CHAPTER 6. SUMMARY AND CONCLUSIONS

### 6.1 Summary

The SH-52 Bridge over the Snake River is a twin girder and twin stringer bridge located on the Idaho-Oregon border near Payette, Idaho. The bridge has been in service since the 1950's. The twin girders are built up I-girder sections. The twin stringers are rolled, wide-flange, I-beam sections. The bridge section is comprised of three continuous spans totaling 185.39 m (608.25 ft). Additionally, there are two 12.19 m (40.0 ft) approach spans. The bridge was designed to carry two lanes of traffic.

The Utah Transportation Center (UTC) in partnership with the Mountain Plains Consortium sponsored a study to investigate the distribution factors and load ratings for the SH-52 Bridge over the Snake River. Bridge Diagnostics Inc. (BDI) was contracted by the Idaho Transportation Department and performed a live-load test that provided the data as the basis for this study.

For the live-load test, the bridge was instrumented with 62 strain gauges at nine different longitudinal locations. In order to apply the live-load, two trucks were driven across the bridge. The two trucks were a snooper truck and a gravel truck. The snooper was driven individually, side-by-side, and in tandem with the gravel truck. The trucks were driven along three predetermined load paths that were chosen to maximize the response in the girders and stringers. The strain gauge response was recorded with the corresponding longitudinal position of the truck. BDI provided the bridge data to researchers at Utah State University, which was then used as a basis to calibrate a 3-D finite-element model of the bridge.

This study compared the distribution factors obtained from the AASHTO Standard and AASHTO LRFD Specifications to the distribution factors obtained based on the results of the live-load test and finite-element analysis. Additionally, inventory and operating ratings were calculated using the results of the calibrated finite-element model.

The distribution factors calculated using the AASHTO codes were slightly unconservative for the girders, and overly conservative for the stringers. Based on the results of the finite-element analysis the controlling inventory and operating ratings due to HS-20 loading for the girders were 1.26 and 2.10, respectively. The controlling inventory and operating ratings for the HS-20 loading for the stringers were 2.63 and 4.39, respectively.

## **6.2 Conclusions**

The results of the live-load test were analyzed and subsequently used as a basis to calibrate a 3-D finite-element model. The distribution factors obtained from the finite-element analysis were compared to the distribution factors calculated according to the AASHTO Standard Specifications and AASHTO LRFD Specifications. Additionally, load ratings were calculated using the results of the finite-element analysis. Based on the findings of this study, several conclusions were formed.

- The peak impact factor due to dynamic loading (0.25) was 55% higher than the impact factor calculated from AASHTO Standard Specifications (0.16), and 24% lower than the impact factor for the AASHTO LRFD Specifications (0.33).
- The finite-element model was found to be quite accurate in predicting the live-load response. A correlation of 0.90 was found between the finite-element and measured

- data. The slope of the trend line was found to be 0.96. This comparison included responses from all longitudinal cross sections, all strain gauges, and each load path.
- The controlling positive moment distribution factors calculated using finite-element analysis were 0.773 for the girders, and 0.011 for the stringers, and for negative moment they were 0.730 and 0.225, respectively.
  - The distribution factors calculated according to the AASHTO Standard Specifications (2002) and AASHTO LRFD Specifications (2010) do not accurately describe the moment distribution for a bridge that has large differences in stiffness between supporting beams. The code based distribution factors were unconservative for the girders and overly conservative for the stringers.
  - The intermediate diaphragm bracing was found to significantly impact the distribution of moments for the bridge. There was a 23% decrease in moment distribution in the girders when the diaphragm members were not present in the model.
  - The controlling inventory and operating load ratings based on the results of the finite-element analysis were 1.26 and 2.10 for the girders and 2.63 and 4.39 for the stringers, respectively.

### **6.3 Recommendations for Additional Research**

Additional research is needed to influence the AASHTO bridge design specifications for cases when there is a large difference in the stiffness between supporting beams. The AASHTO specifications should be able to accurately approximate the distribution of loads for the larger and smaller supporting members. Additionally, more research should be performed to quantify

the influence of intermediate diaphragms on the distribution of loads. Lastly, studies are needed that investigate the accuracy of a beam-line analysis versus the actual dead load and live load effects that a bridge experiences.

## CHAPTER 7. REFERENCES

- 2010 Interim Revisions to AASHTO LRFD Bridge Design Specifications.* (2010). *2010 Interim Revisions to AASHTO LRFD Bridge Design Specifications*, American Association of State Highway and Transportation Officials, Washington, D.C.
- Barnard, T., Hovell, C. G., Sutton, J. P., Mouras, J. M., Neuman, B. J., Samaras, V. A., Kim, J., Williamson, E. B., and Frank, K. H. (2010). “Modeling the Response of Fracture Critical Steel Box Girder Bridges.” *University of Texas at Austin, Texas Department of Transportation*.
- Bechtel, A., McConnell, J., and Chajes, M. (2011). “Ultimate Capacity Destructive Testing and Finite-Element Analysis of Steel I-Girder Bridges.” *Journal of Bridge Engineering*, 16(2), 197–206.
- B. D. I. (2013). *Field Testing and Load Rating Report: SH-52 Over the Snake River-Payette, ID.* rep., Bridge Diagnostics, Inc.
- Chajes, M. J., and Shenton, H. W. (2005). *Using Diagnostic Load Tests for Accurate Load Rating of Typical Bridges. Using Diagnostic Load Tests for Accurate Load Rating of Typical Bridges*, Structures Congress 2005: Metropolis and Beyond, tech., American Society of Civil Engineers.
- Computers and Structures, Inc. (2015). “Analysis Reference Manual.” Berkeley, California.
- Connor, R., Dexter, R., and Mahmoud, M. (2005). “Inspection and Management of Bridges with Fracture-Critical Details.” *Transportation Research Board Online Publications*, National Cooperative Highway Research Program.
- Hodson, D., Barr, P., and Pockels, L. (2013). *Live-Load Test Comparison and Load Ratings of a Posttensioned Box Girder Bridge. Live-Load Test Comparison and Load Ratings of a Posttensioned Box Girder Bridge*, tech., American Society of Civil Engineers.
- Idriss, R. L., and Jauregui, D. V. (1994). “Load Path Evaluation of the I-40 Bridge.” *The National Academies of Sciences, Engineering, Medicine*, The National Science Foundation.
- Manual for Condition Evaluation and Load and Resistance Factor Rating (LRFR) of Highway Bridges.* (2003). *Manual for Condition Evaluation and Load and Resistance Factor Rating (LRFR) of Highway Bridges*, American Association of State Highway and Transportation Officials, Washington, D.C.

*Standard Specifications for Highway Bridges. (2002). Standard Specifications for Highway Bridges, American Association of State Highway and Transportation Officials, Washington, D.C.*

Yanadori, N. (2004). "Static and dynamic behavior of a continuous steel I-girder bridge." thesis.

## CHAPTER 8. APPENDICES

### APPENDIX A: INSTRUMENTATION

Appendix A contains the instrumentation drawings for the cross sections not included in Chapter 3 (all cross sections except A-A and F-F). The instrumentation at these cross sections is shown in *Figures A1 to A7*.

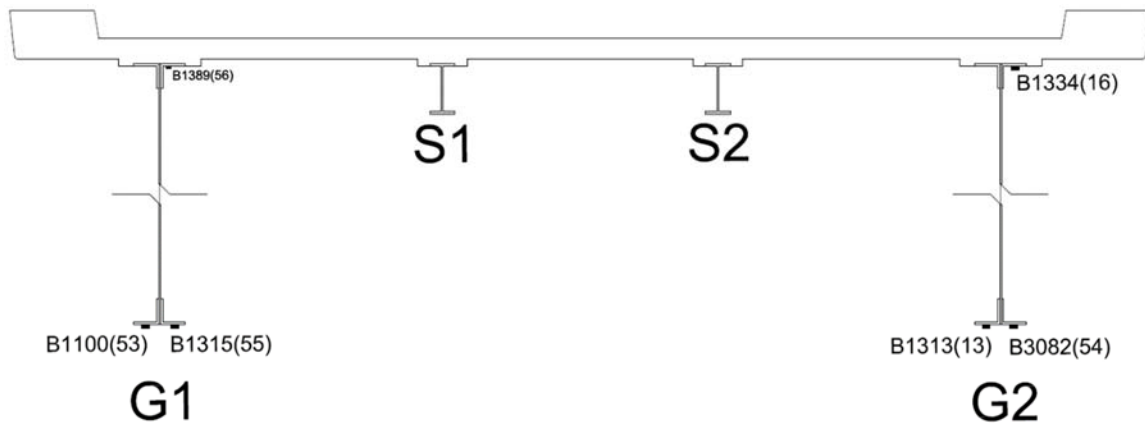


Figure A1 Instrumentation at Cross Section B-B

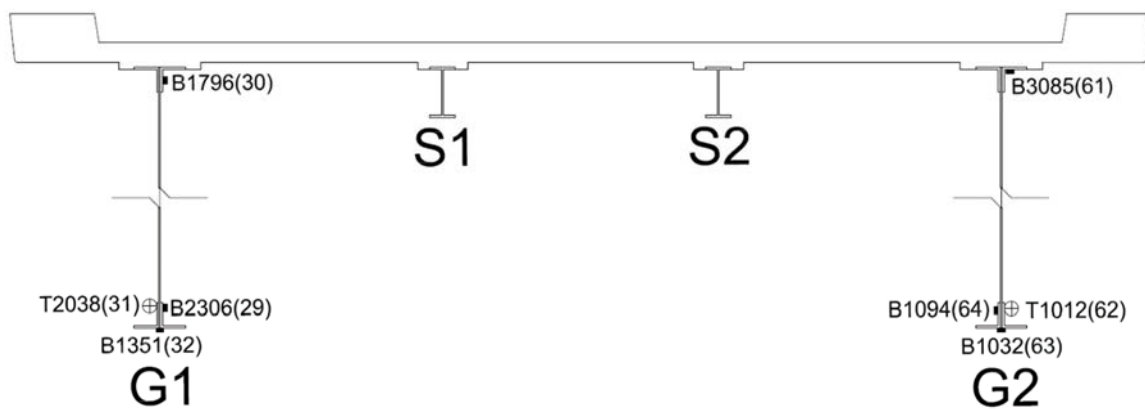


Figure A2 Instrumentation at Cross Section C-C

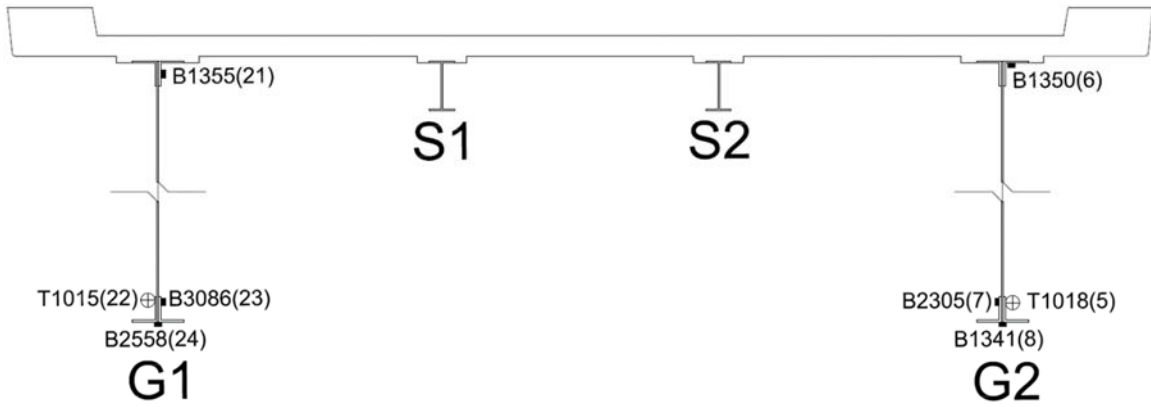


Figure A3 Instrumentation at Cross Section D-D

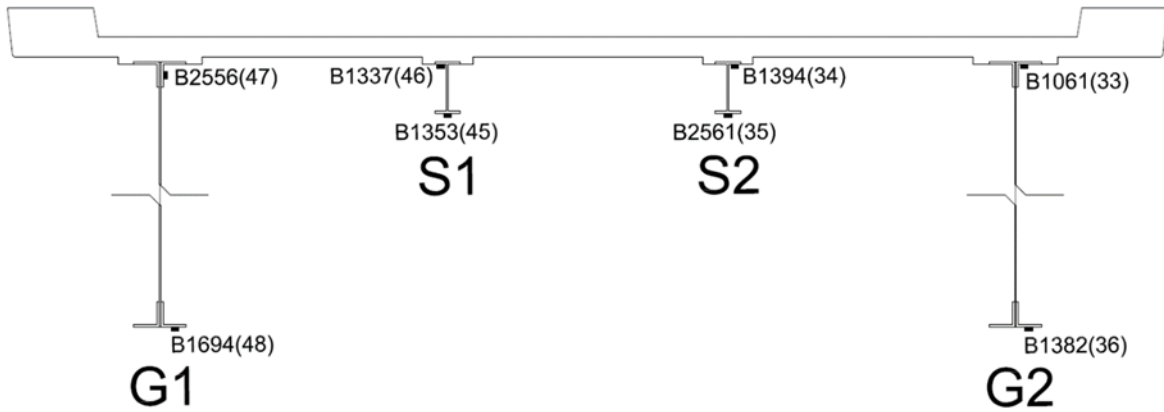


Figure A4 Instrumentation at Cross Section E-E

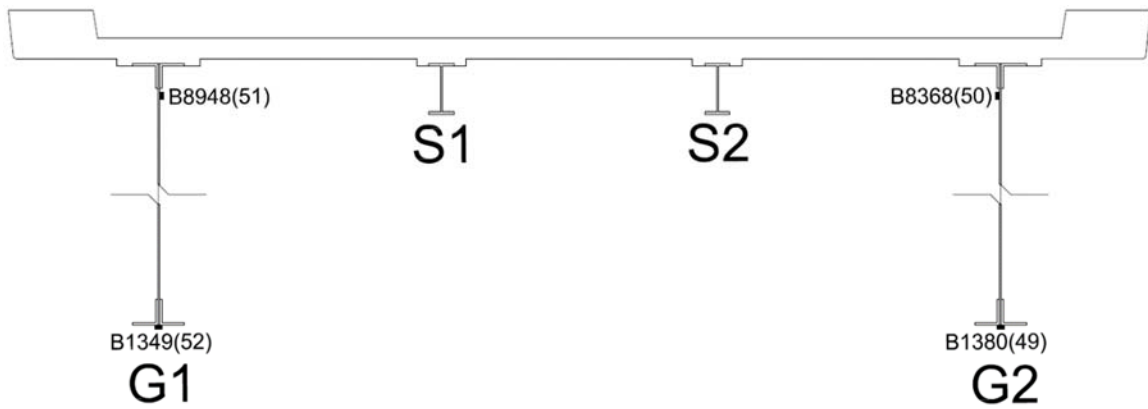


Figure A5 Instrumentation at Cross Section G-G

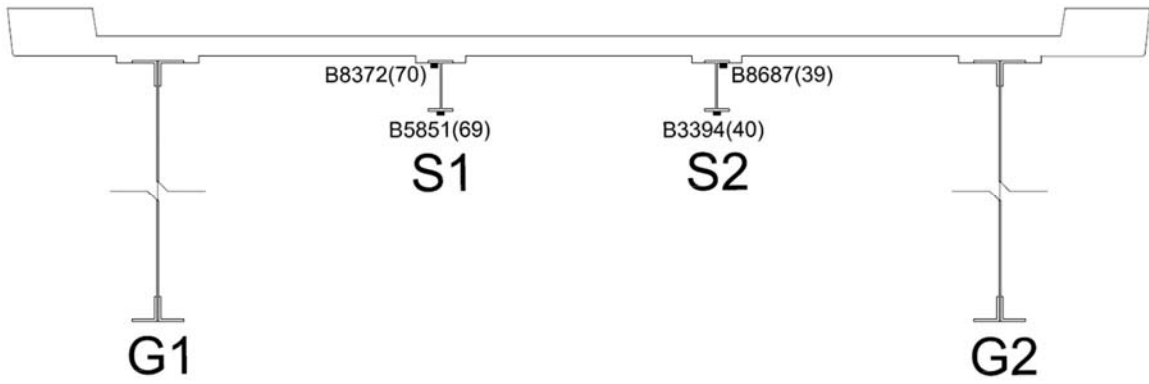


Figure A6 Instrumentation at Cross Section H-H

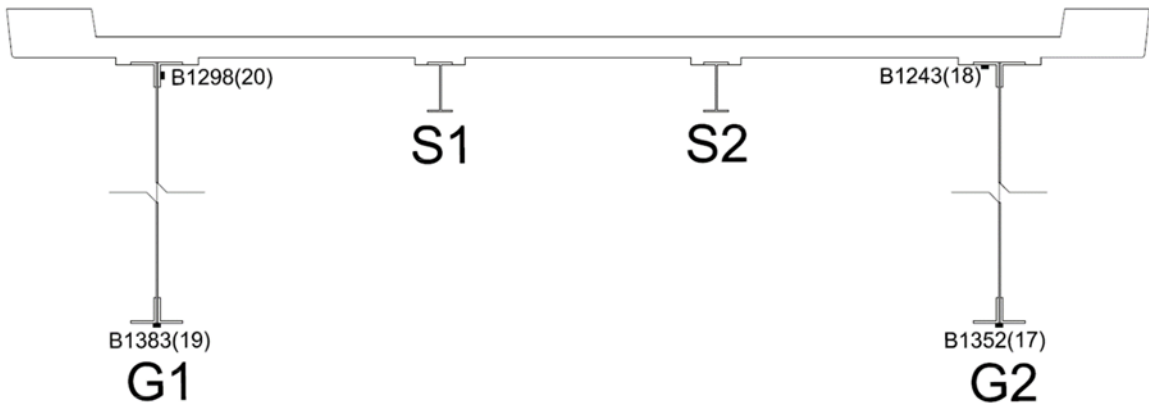


Figure A7 Instrumentation at Cross Section I-I

**Girder Capacity No Cover Plates**

$$\begin{array}{lll}
 F_Y := 50000 & d := 120.5 & I_x := \frac{21786659}{96} = 2.26944 \cdot 10^5 \\
 b := 16.5 & t_f := .75 & \\
 t := .75 & b_f := 16.5 & S_x := \frac{I_x}{\frac{d}{2}} = 3766.71145 \\
 D := 119 & d_s := 28.25 & \\
 t_w := 0.5 & D_c := 59.5 & 
 \end{array}$$

10.48.1.1

A) Flange

```

if  $\frac{b}{t} < \frac{4110}{\sqrt{F_Y}}$  = "Flange is non-compact"
"Flange is compact"
else
"Flange is non-compact"

```

B) Web

```

if  $\frac{D}{t_w} < \frac{19230}{\sqrt{F_Y}}$  = "Web is non-compact"
"Web is compact"
else
"Web is non-compact"

```

10.48.2.1

A) Compression Flange

```

if  $\frac{b}{t} < 24$  = "Compression Flange ok"
"Compression Flange ok"
else
"Compression Flange not ok"

```

B) Web thickness

```

if  $\frac{D}{t_w} < \frac{73000}{\sqrt{F_Y}}$  = "Web Thickness ok" eqn (10-109)
"Web Thickness ok"
else
"not ok"

```

C) Spacing of lateral bracing for compression flange

$$\begin{array}{ll}
 L_{bpos} := 0 & L_{bneg} := 21.75 \cdot 12 = 261 \\
 A_f := 16.5 \cdot 0.75 = 12.375 & 
 \end{array}$$

## APPENDIX B: CAPACITY CALCULATIONS

Positive Moment

$$\text{if } L_{bpos} \leq \frac{20000000 \cdot A_f}{F_y \cdot d} \quad = \text{"Lesser of } \mu F_y \cdot S_{xt}, \mu F_{cr} \cdot S_{xc} \cdot R_b \text{"}$$

"Lesser of  $\mu F_y \cdot S_{xt}, \mu F_{cr} \cdot S_{xc} \cdot R_b$ "

else

"Got to 10.48.4"

$$I_{yc} = \frac{t_f \cdot b_f^3}{12} = 280.75781$$

$$r' = \sqrt{\frac{I_{yc}}{b_f \cdot t_f}} = 4.76314$$

$$\frac{d_s}{D_c} = 0.47479 \quad d_s = 28.25$$

$$D_c = 59.5$$

$$L_p = 9500 \cdot \frac{r'}{\sqrt{F_y}} = 202.36338 \quad \frac{L_p}{12} = 16.86361$$

$$\text{if } L_{bpos} \leq L_p \quad = \text{"ok"}$$

"ok"

else

"different equation"

$$k = \text{if } 5.17 \cdot \left(\frac{D}{d_s}\right)^2 \geq 9 \cdot \left(\frac{D}{D_c}\right)^2 = 91.73764$$

$$5.17 \cdot \left(\frac{D}{d_s}\right)^2$$

else

$$9 \cdot \left(\frac{D}{D_c}\right)^2$$

$$F_{cr} = \text{if } \left(4400 \cdot \frac{t}{b}\right)^2 < F_y = 40000$$

$$\left(4400 \cdot \frac{t}{b}\right)^2$$

else

$$F_y$$

$$f_b = \frac{26200000 \cdot k}{\left(\frac{D}{t_w}\right)^2} = 42432.14034$$

$$R_b := \begin{cases} \text{if } \frac{D}{t_w} < 5460 \cdot \sqrt{\frac{k}{f_b}} & = 1 \\ 1 & \\ \text{else} & \\ \text{"other equation"} & \end{cases}$$

$$M_r := \frac{F_{cr} \cdot S_x \cdot R_b}{12000} = 12555.70482$$

$$M_{r1} := \frac{F_y \cdot S_x}{12000} = 15694.63102$$

$$M_u := \min(M_r, M_{r1}) = 12555.70482$$

10.48.4 (negative moment)

Negative Moment

$$\text{if } L_{b\text{neg}} \leq \frac{20000000 \cdot A_f}{F_y \cdot d} = \text{"Go to 10.48.4"} \\ \text{"mu=Fy*Sxt"} \\ \text{else} \\ \text{"Go to 10.48.4"}$$

$$\frac{L_{b\text{neg}}}{12} = 21.75$$

$$\lambda = 15400$$

Since:

$$\frac{\lambda}{\sqrt{F_y}} = 68.87089 < \frac{D_c}{t_w}$$

$$L_r := \sqrt{\frac{572 \cdot 10^6 \cdot I_{yc} \cdot d}{F_y \cdot S_x}} = 320.54668$$

$$\frac{L_p}{12} = 16.86361$$

Since  $L_r > L_b > L_p$

$$C_b := 1$$

$$M_r := C_b \cdot F_y \cdot S_x \cdot \left( 1 - 0.5 \cdot \left( \frac{L_{b\text{neg}} - L_p}{L_r - L_p} \right) \right) \cdot \frac{1}{12000} = 11801.18708$$

Girder Capacity One Cover Plates

$$\begin{array}{lll}
 F_Y := 50000 & d := 122 & I_x := \frac{32371919}{96} = 3.37207 \cdot 10^5 \\
 b := 20 & t_f := 1.37 & \\
 t := 1.37 & b_f := 20 & S_x := \frac{I_x}{\frac{d}{2}} = 5527.99163 \\
 D := d - 2 \cdot t_f = 119.26 & d_s := 28.25 & \\
 t_w := 0.5 & D_c := \frac{D}{2} = 59.63 & 
 \end{array}$$

10.48.1.1

A) Flange

$$\begin{array}{ll}
 \text{if } \frac{b}{t} < \frac{4110}{\sqrt{F_Y}} & = \text{"Flange is compact"} \\
 \text{"Flange is compact"} & \\
 \text{else} & \\
 \text{"Flange is non-compact"} & 
 \end{array}$$

B) Web

$$\begin{array}{ll}
 \text{if } \frac{D}{t_w} < \frac{19230}{\sqrt{F_Y}} & = \text{"Web is non-compact"} \\
 \text{"Web is compact"} & \\
 \text{else} & \\
 \text{"Web is non-compact"} & 
 \end{array}$$

10.48.2.1

A) Compression Flange

$$\begin{array}{ll}
 \text{if } \frac{b_f}{t_f} < 24 & = \text{"Compression Flange ok"} \\
 \text{"Compression Flange ok"} & \\
 \text{else} & \\
 \text{"Compression Flange not ok"} & 
 \end{array}$$

B) Web thickness

$$\begin{array}{ll}
 \text{if } \frac{D}{t_w} < \frac{73000}{\sqrt{F_Y}} & = \text{"Web Thickness ok"} \quad \text{eqn (10-109)} \\
 \text{"Web Thickness ok"} & \\
 \text{else} & \\
 \text{"not ok"} & 
 \end{array}$$

C) Spacing of lateral bracing for compression flange

$$\begin{array}{ll}
 L_{bpos} := 0 & L_{bneg} := 21.75 \cdot 12 = 261 \\
 A_f := 16.5 \cdot 0.75 = 12.375 & 
 \end{array}$$

10.48.4 (negative moment)

Negative Moment

$$\text{if } L_{\text{bneg}} \leq \frac{20000000 \cdot A_f}{F_Y \cdot d} = \text{"Go to 10.48.4"}$$

"mu=Fy\*Sxt"

else

"Go to 10.48.4"

$$\frac{L_{\text{bneg}}}{12} = 21.75$$

$$\lambda := 15400$$

Since:

$$\frac{\lambda}{\sqrt{F_Y}} = 68.87089 < \frac{D_c}{t_w}$$

$$L_r := \sqrt{\frac{572 \cdot 10^6 \cdot I_{yc} \cdot d}{F_Y \cdot S_x}} = 480.20192$$

$$L_p := 9500 \cdot \frac{r'}{\sqrt{F_Y}} = 245.28895$$

$$\frac{L_p}{12} = 20.44075$$

Since  $L_r > L_b > L_p$

$$C_b := 1$$

$$M_r := C_b \cdot F_Y \cdot S_x \cdot \left( 1 - .5 \cdot \left( \frac{L_{\text{bneg}} - L_p}{L_r - L_p} \right) \right) \cdot \frac{1}{12000} = 22263.0613$$

(Negative Moment)

**Girder Capacity Two Cover Plates**

$$\begin{aligned}
 F_Y &:= 50000 & d &:= 123.5 & I_x &:= \frac{43220699}{96} = 4.50216 \cdot 10^5 \\
 b &:= 20 & t_f &:= 2.12 \\
 t &:= 2.12 & b_f &:= 20 & S_x &:= \frac{I_x}{\frac{d}{2}} = 7290.94113 \\
 D &:= d - 2 \cdot t_f = 119.26 & d_s &:= 28.25 \\
 t_w &:= 0.5 & D_c &:= \frac{D}{2} = 59.63
 \end{aligned}$$

10.48.1.1

A) Flange

```

if  $\frac{b}{t} < \frac{4110}{\sqrt{F_Y}}$            = "Flange is compact"
"Flange is compact"
else
"Flange is non-compact"

```

B) Web

```

if  $\frac{D}{t_w} < \frac{19230}{\sqrt{F_Y}}$        = "Web is non-compact"
"Web is compact"
else
"Web is non-compact"

```

10.48.2.1

A) Compression Flange

```

if  $\frac{b_f}{t_f} < 24$                  = "Compression Flange ok"
"Compression Flange ok"
else
"Compression Flange not ok"

```

B) Web thickness

```

if  $\frac{D}{t_w} < \frac{73000}{\sqrt{F_Y}}$        = "Web Thickness ok"      eqn (10-109)
"Web Thickness ok"
else
"not ok"

```

C) Spacing of lateral bracing for compression flange

$$\begin{aligned}
 L_{bpos} &:= 0 & L_{bneg} &:= 21.75 \cdot 12 = 261 \\
 A_f &:= 16.5 \cdot 0.75 = 12.375
 \end{aligned}$$

10.48.4 (negative moment)

Negative Moment

$$\text{if } L_{b\text{neg}} \leq \frac{20000000 \cdot A_f}{F_y \cdot d} = \text{"Go to 10.48.4"}$$

"mu=Fy\*Sxt"

else

"Go to 10.48.4"

$$\frac{L_{b\text{neg}}}{12} = 21.75$$

$$\lambda = 15400$$

Since:

$$\frac{\lambda}{\sqrt{F_y}} = 68.87089 < \frac{D_c}{t_w}$$

$$L_r := \sqrt{\frac{572 \cdot 10^6 \cdot I_{yc} \cdot d}{F_y \cdot S_x}} = 523.33164$$

$$L_p := 9500 \cdot \frac{r'}{\sqrt{F_y}} = 245.28895$$

$$\frac{L_p}{12} = 20.44075$$

Since  $L_r > L_b > L_p$

$$C_b := 1$$

$$M_r := C_b \cdot F_y \cdot S_x \cdot \left( 1 - .5 \cdot \left( \frac{L_{b\text{neg}} - L_p}{L_r - L_p} \right) \right) \cdot \frac{1}{12000} = 29520.62712$$

(Negative Moment)

**Girder Capacity Three Cover Plates**

$$\begin{aligned}
 F_y &:= 50000 & d &:= 125 & I_x &:= \frac{54336239}{96} = 5.66002 \cdot 10^5 \\
 b &:= 20 & t_f &:= 2.87 & S_x &:= \frac{I_x}{\frac{d}{2}} = 9056.03983 \\
 t &:= 2.87 & b_f &:= 20 & d_s &:= 28.25 \\
 D &:= d - 2 \cdot t_f = 119.26 & t_w &:= 0.5 & D_c &:= \frac{D}{2} = 59.63
 \end{aligned}$$

10.48.1.1

A) Flange

$$\begin{aligned}
 &\text{if } \frac{b}{t} < \frac{4110}{\sqrt{F_y}} && \text{"Flange is compact"} \\
 &\text{"Flange is compact"} \\
 &\text{else} \\
 &\text{"Flange is non-compact"}
 \end{aligned}$$

B) Web

$$\begin{aligned}
 &\text{if } \frac{D}{t_w} < \frac{19230}{\sqrt{F_y}} && \text{"Web is non-compact"} \\
 &\text{"Web is compact"} \\
 &\text{else} \\
 &\text{"Web is non-compact"}
 \end{aligned}$$

10.48.2.1

A) Compression Flange

$$\begin{aligned}
 &\text{if } \frac{b_f}{t_f} < 24 && \text{"Compression Flange ok"} \\
 &\text{"Compression Flange ok"} \\
 &\text{else} \\
 &\text{"Compression Flange not ok"}
 \end{aligned}$$

B) Web thickness

$$\begin{aligned}
 &\text{if } \frac{D}{t_w} < \frac{73000}{\sqrt{F_y}} && \text{"Web Thickness ok"} && \text{eqn (10-109)} \\
 &\text{"Web Thickness ok"} \\
 &\text{else} \\
 &\text{"not ok"}
 \end{aligned}$$

C) Spacing of lateral bracing for compression flange

$$\begin{aligned}
 L_{bpos} &:= 0 & L_{bneg} &:= 21.75 \cdot 12 = 261 \\
 A_f &:= 16.5 \cdot 0.75 = 12.375
 \end{aligned}$$

10.48.4 (negative moment)

Negative Moment

$$\text{if } L_{\text{bneg}} \leq \frac{20000000 \cdot A_f}{F_Y \cdot d} = \text{"Go to 10.48.4"}$$

"mu=Fy\*Sxt"

else

"Go to 10.48.4"

$$\frac{L_{\text{bneg}}}{12} = 21.75$$

$$\lambda := 15400$$

Since:

$$\frac{\lambda}{\sqrt{F_Y}} = 68.87089 < \frac{D_c}{t_w}$$

$$L_r := \sqrt{\frac{572 \cdot 10^6 \cdot I_{yc} \cdot d}{F_Y \cdot S_x}} = 549.66005$$

$$L_p := 9500 \cdot \frac{r'}{\sqrt{F_Y}} = 245.28895$$

$$\frac{L_p}{12} = 20.44075$$

Since  $L_r > L_b > L_p$

$$C_b := 1$$

$$M_r := C_b \cdot F_Y \cdot S_x \cdot \left( 1 - .5 \cdot \left( \frac{L_{\text{bneg}} - L_p}{L_r - L_p} \right) \right) \cdot \frac{1}{12000} = 36759.63375$$

(Negative Moment)

16 WF 36

$$\begin{array}{lll}
 F_y := 50000 & b_f := 6.992 & I_y := 22.1 \\
 d := 15.85 & t_f := 0.428 & J := 0.545 \\
 A := 10.59 & D := d - 2 \cdot t_f = 14.994 & D_c := \frac{D}{2} = 7.497 \\
 I_x := 446.3 & r_y := 1.45 & \\
 S_x := 56.3 & t_w := 0.299 & 
 \end{array}$$

10.48.1

a) Compression Flange (AASHTO 10-93)

$$\begin{array}{l}
 \text{if } \frac{b_f}{t_f} \leq \frac{4110}{\sqrt{F_y}} \quad = \text{"compact"} \\
 \text{"compact"} \\
 \text{else} \\
 \text{"non-compact"}
 \end{array}$$

b) Web thickness

$$\begin{array}{l}
 \text{if } \frac{D}{t_w} \leq \frac{19230}{\sqrt{F_y}} \quad = \text{"compact"} \\
 \text{"compact"} \\
 \text{else} \\
 \text{"non-compact"}
 \end{array}$$

c) lateral bracing

$$L_b := \frac{21.75}{2} \cdot 12 = 130.5 \quad \text{assume braced at mid point of bay}$$

$$\begin{array}{l}
 \text{if } L_b \leq \frac{20000000 \cdot b_f \cdot t_f}{F_y \cdot d} = \text{"go to 10.48.4.1"} \\
 \text{"meets 10-101"} \\
 \text{else} \\
 \text{"go to 10.48.4.1"}
 \end{array}$$

10.48.4.1

$$I_{yc} := \frac{1}{12} \cdot t_f \cdot b_f^3 = 12.19177 \quad I_y = 22.1$$

$$\begin{array}{l}
 \text{if } \frac{I_{yc}}{I_y} \leq 0.9 \quad = \text{"Capacity calculated as Mu=Mr*Rb"} \\
 \text{"Capacity calculated as Mu=Mr*Rb"} \\
 \text{else} \\
 \text{"use different equation"}
 \end{array}$$

$$\lambda := 15400$$

$$\text{if } \frac{D_c}{t_w} \leq \frac{\lambda}{\sqrt{F_Y}} \quad = \text{"meets 10-103c"} \\ \text{"meets 10-103c"} \\ \text{else} \\ \text{"doesn't meet 10-103c"}$$

$$C_b := 1.0$$

$$M_r := 91 \cdot 10^6 \cdot C_b \cdot \frac{I_{yc}}{L_b} \cdot \sqrt{0.772 \cdot \frac{J}{I_{yc}} + 9.87 \cdot \left(\frac{d}{L_b}\right)^2} = 3.60798 \cdot 10^6$$

$$M_y := F_y \cdot S_x = 2.815 \cdot 10^6$$

$$R_{b1} := 1 - .002 \cdot \left(\frac{D_c \cdot t_w}{b_f \cdot t_f}\right) \cdot \left(\frac{D_c}{t_w} - \frac{\lambda}{\sqrt{\frac{M_r}{S_x}}}\right) = 1.05357$$

$$R_b := \text{if } R_{b1} > 1.0 = 1 \\ 1.0 \\ \text{else} \\ R_{b1}$$

$$M_u := \frac{\min((M_r, M_y)) \cdot R_b}{12000} = 234.58333$$

$$M_u = 234.58333$$

16 WF 40

$$\begin{array}{lll}
 F_y := 50000 & b_f := 7 & I_y := 26.5 \\
 d := 16 & t_f := 0.503 & J := 0.794 \\
 A := 11.77 & D := d - 2 \cdot t_f = 14.994 & D_c := \frac{D}{2} = 7.497 \\
 I_x := 515.5 & r_y := 1.50 & \\
 S_x := 64.4 & t_w := 0.307 & 
 \end{array}$$

10.48.1

a) Compression Flange (AASHTO 10-93)

$$\begin{array}{l}
 \text{if } \frac{b_f}{t_f} \leq \frac{4110}{\sqrt{F_y}} = \text{"compact"} \\
 \text{"compact"} \\
 \text{else} \\
 \text{"non-compact"}
 \end{array}$$

b) Web thickness

$$\begin{array}{l}
 \text{if } \frac{D}{t_w} \leq \frac{19230}{\sqrt{F_y}} = \text{"compact"} \\
 \text{"compact"} \\
 \text{else} \\
 \text{"non-compact"}
 \end{array}$$

c) lateral bracing

$$L_b := \frac{21.75}{2} \cdot 12 = 130.5 \quad \text{assume braced at mid point of bay}$$

$$\begin{array}{l}
 \text{if } L_b \leq \frac{20000000 \cdot b_f \cdot t_f}{F_y \cdot d} = \text{"go to 10.48.4.1"} \\
 \text{"meets 10-101"} \\
 \text{else} \\
 \text{"go to 10.48.4.1"}
 \end{array}$$

10.48.4.1

$$I_{yc} := \frac{1}{12} \cdot t_f \cdot b_f^3 = 14.37742 \quad I_y = 26.5$$

$$\begin{array}{l}
 \text{if } \frac{I_{yc}}{I_y} \leq 0.9 = \text{"Capacity calculated as Mu=Mr*Rb"} \\
 \text{"Capacity calculated as Mu=Mr*Rb"} \\
 \text{else} \\
 \text{"use different equation"}
 \end{array}$$

$$\lambda := 15400$$

```

if  $\frac{D_c}{t_w} \leq \frac{\lambda}{\sqrt{F_Y}}$  = "meets 10-103c"
  "meets 10-103c"
else
  "doesn't meet 10-103c"

```

$$C_b := 1.0$$

$$M_r := 91 \cdot 10^6 \cdot C_b \cdot \frac{I_{yc}}{L_b} \cdot \sqrt{0.772 \cdot \frac{J}{I_{yc}} + 9.87 \cdot \left(\frac{d}{L_b}\right)^2} = 4.38156 \cdot 10^6$$

$$M_y := F_Y \cdot S_x = 3.22 \cdot 10^6$$

$$R_{b1} := 1 - .002 \cdot \left(\frac{D_c \cdot t_w}{b_f \cdot t_f}\right) \cdot \left(\frac{D_c}{t_w} - \frac{\lambda}{\sqrt{\frac{M_r}{S_x}}}\right) = 1.04526$$

```

R_b := if R_b1 > 1.0 = 1
      1.0
      else
      R_b1

```

$$M_u := \frac{\min((M_r, M_y)) \cdot R_b}{12000} = 268.33333$$

$M_u = 268.33333$
-------------------

16 WF 45

$$\begin{aligned}
 F_Y &:= 50000 & b_f &:= 7.039 & I_Y &:= 30.5 \\
 d &:= 16.12 & t_f &:= 0.563 & J &:= 1.11 \\
 A &:= 13.24 & D &:= d - 2 \cdot t_f = 14.994 & D_c &:= \frac{D}{2} = 7.497 \\
 I_x &:= 583.3 & r_y &:= 1.52 & & \\
 S_x &:= 72.4 & t_w &:= 0.346 & & 
 \end{aligned}$$

10.48.1

a) Compression Flange (AASHTO 10-93)

$$\begin{aligned}
 &\text{if } \frac{b_f}{t_f} \leq \frac{4110}{\sqrt{F_Y}} = \text{"compact"} \\
 &\quad \text{"compact"} \\
 &\text{else} \\
 &\quad \text{"non-compact"}
 \end{aligned}$$

b) Web thickness

$$\begin{aligned}
 &\text{if } \frac{D}{t_w} \leq \frac{19230}{\sqrt{F_Y}} = \text{"compact"} \\
 &\quad \text{"compact"} \\
 &\text{else} \\
 &\quad \text{"non-compact"}
 \end{aligned}$$

c) lateral bracing

$$L_b := \frac{21.75}{2} \cdot 12 = 130.5 \quad \text{assume braced at mid point of bay}$$

$$\begin{aligned}
 &\text{if } L_b \leq \frac{20000000 \cdot b_f \cdot t_f}{F_Y \cdot d} = \text{"go to 10.48.4.1"} \\
 &\quad \text{"meets 10-101"} \\
 &\text{else} \\
 &\quad \text{"go to 10.48.4.1"}
 \end{aligned}$$

10.48.4.1

$$I_{yc} := \frac{1}{12} \cdot t_f \cdot b_f^3 = 16.36289 \quad I_Y = 30.5$$

$$\begin{aligned}
 &\text{if } \frac{I_{yc}}{I_Y} \leq 0.9 = \text{"Capacity calculated as Mu=Mr*Rb"} \\
 &\quad \text{"Capacity calculated as Mu=Mr*Rb"} \\
 &\text{else} \\
 &\quad \text{"use different equation"}
 \end{aligned}$$

$$\lambda := 15400$$

```

if  $\frac{D_c}{t_w} \leq \frac{\lambda}{\sqrt{F_Y}}$  = "meets 10-103c"
  "meets 10-103c"
else
  "doesn't meet 10-103c"

```

$$C_b := 1.0$$

$$M_r := 91 \cdot 10^6 \cdot C_b \cdot \frac{I_{yc}}{L_b} \cdot \sqrt{0.772 \cdot \frac{J}{I_{yc}} + 9.87 \cdot \left(\frac{d}{L_b}\right)^2} = 5.14052 \cdot 10^6$$

$$M_y := F_Y \cdot S_x = 3.62 \cdot 10^6$$

$$R_{b1} := 1 - .002 \cdot \left(\frac{D_c \cdot t_w}{b_f \cdot t_f}\right) \cdot \left(\frac{D_c}{t_w} - \frac{\lambda}{\sqrt{\frac{M_r}{S_x}}}\right) = 1.04729$$

```

R_b := if R_b1 > 1.0 = 1
      1.0
      else
      R_b1

```

$$M_u := \frac{\min(M_r, M_y) \cdot R_b}{12000} = 301.66667$$

$$M_u = 301.66667$$

## APPENDIX C: DISTRIBUTION FACTOR CALCULATIONS

### AASHTO Standard Specifications Distribution Factors

#### Girder Distribution Factors

Using empirical equation for distribution factor

$$G_{1df} := \frac{7.5625}{2 \cdot (4 + .25 \cdot 7.5625)} = 0.64191 \quad \text{Section 3.23.2.3.1.5}$$

Using lever rule for girder distribution factor

$$P := 1$$

$$DFM_{g1} := 1.0 \cdot \left( \frac{P}{2} \cdot \left( 1 - \frac{3}{90.75} \right) + \frac{P}{2} \cdot \left( 1 - \frac{75}{90.75} \right) \right) = 0.57025$$

#### Stringer Distribution Factors

$$S1_{df} := \frac{7.46875}{(5.5)} = 1.35795$$

$$S1_{stan} := \frac{S1_{df}}{2} = 0.67898$$

Controlling Distribution Factors from AASHTO Standard Specifications:

Girders:

$$G_{1df} = 0.64191$$

Stringers:

$$S1_{stan} = 0.67898$$

AASHTO LRFD Specifications

$$E_c := \frac{57000 \cdot \sqrt{3300}}{1000} = 3274.40071$$

$$E_s := 29000$$

$$n := \frac{E_s}{E_c} = 8.85658$$

$$S_g := 7.78125$$

$$S_s := 7.46875$$

$$t_s := 6.5$$

$$L_{13} := 184.5$$

$$L_2 := 239.25$$

$$A_g := 4 \cdot (8 \cdot .75 + 7.25 \cdot .75) + 120.5 \cdot .5 = 106$$

$$A_{16wf45} := 13.24$$

$$A_{16wf40} := 11.77$$

$$A_{16wf36} := 10.59$$

$$e_{g45} := 60.25 + \frac{6.5}{2} = 63.5$$

$$e_{g40} := \frac{16.12}{2} + \frac{6.5}{2} = 11.31$$

$$e_{g36} := 8 + \frac{6.5}{2} = 11.25$$

$$e_{g36} := \frac{15.85}{2} + \frac{6.5}{2} = 11.175$$

Moment of Inertia, Girder

$$I_w := \frac{1}{12} \cdot .5 \cdot 120.5^3 = 72903.7552$$

$$I_{Bangle} := \frac{1}{12} \cdot 7.25 \cdot .75^3 + 7.25 \cdot .75 \cdot \left( .375 - \frac{120.5}{2} \right)^2 + \frac{1}{12} \cdot .75 \cdot 8^3 + .75 \cdot 8 \cdot \left( \frac{120.5}{2} - 4 \right)^2 = 38510.1523$$

$$I_{Tangle} := I_{Bangle} = 38510.1523$$

$$I_g := I_w + 2 \cdot I_{Tangle} + 2 \cdot I_{Bangle} = 2.2694 \cdot 10^5$$

$$I_{45} := 583.3$$

$$I_{40} := 515.5$$

$$I_{36} := 446.3$$

$$Kg_g := n \cdot \left( I_g + A_g \cdot eg_g^2 \right) = 5.79542 \cdot 10^6$$

$$Kg_{45} := n \cdot \left( I_{45} + A_{16wf45} \cdot eg_{45}^2 \right) = 20165.63385$$

$$Kg_{40} := n \cdot \left( I_{40} + A_{16wf40} \cdot eg_{45}^2 \right) = 17899.7953$$

$$Kg_{36} := n \cdot \left( I_{36} + A_{16wf36} \cdot eg_{36}^2 \right) = 15665.39752$$

### 2 Lanes Loaded

$$DFM_{4513} := 0.075 + \left( \frac{S_s}{9.5} \right)^{0.6} \cdot \left( \frac{S_s}{L_{13}} \right)^{0.2} \cdot \left( \frac{Kg_{45}}{12 \cdot L_{13} \cdot t_s^3} \right)^{0.1} = 0.39922$$

$$DFM_{452} := 0.075 + \left( \frac{S_s}{9.5} \right)^{0.6} \cdot \left( \frac{S_s}{L_2} \right)^{0.2} \cdot \left( \frac{Kg_{45}}{12 \cdot L_2 \cdot t_s^3} \right)^{0.1} = 0.3749$$

$$DFM_{4013} := 0.075 + \left( \frac{S_s}{9.5} \right)^{0.6} \cdot \left( \frac{S_s}{L_{13}} \right)^{0.2} \cdot \left( \frac{Kg_{40}}{12 \cdot L_{13} \cdot t_s^3} \right)^{0.1} = 0.39537$$

$$DFM_{402} := 0.075 + \left( \frac{S_s}{9.5} \right)^{0.6} \cdot \left( \frac{S_s}{L_2} \right)^{0.2} \cdot \left( \frac{Kg_{40}}{12 \cdot L_2 \cdot t_s^3} \right)^{0.1} = 0.37135$$

$$DFM_{3613} := 0.075 + \left( \frac{S_s}{9.5} \right)^{0.6} \cdot \left( \frac{S_s}{L_{13}} \right)^{0.2} \cdot \left( \frac{Kg_{36}}{12 \cdot L_{13} \cdot t_s^3} \right)^{0.1} = 0.39113$$

$$DFM_{362} := 0.075 + \left( \frac{S_s}{9.5} \right)^{0.6} \cdot \left( \frac{S_s}{L_2} \right)^{0.2} \cdot \left( \frac{Kg_{36}}{12 \cdot L_2 \cdot t_s^3} \right)^{0.1} = 0.36742$$

$$DFM_{g13} := 0.075 + \left( \frac{S_g}{9.5} \right)^{0.6} \cdot \left( \frac{S_g}{L_{13}} \right)^{0.2} \cdot \left( \frac{Kg_g}{12 \cdot L_{13} \cdot t_s^3} \right)^{0.1} = 0.6651$$

Negative Moment Distribution Factors

$$S_s = 7.46875 \quad L_n = 211.875$$

2 Lanes Loaded

$$DFM_{45n} := 0.075 + \left(\frac{S_s}{9.5}\right)^{0.6} \cdot \left(\frac{S_s}{L_n}\right)^{0.2} \cdot \left(\frac{Kg_{45}}{12 \cdot L_n \cdot t_s^3}\right)^{0.1} = 0.38604$$

$$DFM_{40n} := 0.075 + \left(\frac{S_s}{9.5}\right)^{0.6} \cdot \left(\frac{S_s}{L_n}\right)^{0.2} \cdot \left(\frac{Kg_{40}}{12 \cdot L_n \cdot t_s^3}\right)^{0.1} = 0.38235$$

$$DFM_{36n} := 0.075 + \left(\frac{S_s}{9.5}\right)^{0.6} \cdot \left(\frac{S_s}{L_n}\right)^{0.2} \cdot \left(\frac{Kg_{36}}{12 \cdot L_n \cdot t_s^3}\right)^{0.1} = 0.37828$$

$$DFM_{gin} := 0.075 + \left(\frac{S_g}{9.5}\right)^{0.6} \cdot \left(\frac{S_g}{L_n}\right)^{0.2} \cdot \left(\frac{Kg_g}{12 \cdot L_n \cdot t_s^3}\right)^{0.1} = 0.64111$$

$$d_e = 1.75$$

$$e = 0.77 + \frac{d_e}{9.1} = 0.96231$$

$$DFM_{gn} := DFM_{gin} \cdot e = 0.61694$$

1 Lane Loaded

$$DFM_{45n1} := 0.06 + \left(\frac{S_s}{9.5}\right)^{0.4} \cdot \left(\frac{S_s}{L_n}\right)^{0.3} \cdot \left(\frac{Kg_{45}}{12 \cdot L_n \cdot t_s^3}\right)^{0.1} = 0.29357$$

$$DFM_{40n1} := 0.06 + \left(\frac{S_s}{9.5}\right)^{0.4} \cdot \left(\frac{S_s}{L_n}\right)^{0.3} \cdot \left(\frac{Kg_{40}}{12 \cdot L_n \cdot t_s^3}\right)^{0.1} = 0.2908$$

$$DFM_{36n1} := 0.06 + \left(\frac{S_s}{9.5}\right)^{0.4} \cdot \left(\frac{S_s}{L_n}\right)^{0.3} \cdot \left(\frac{Kg_{36}}{12 \cdot L_n \cdot t_s^3}\right)^{0.1} = 0.28775$$

$$DFM_{g1} := 1.2 \cdot \left(\frac{P}{2} \cdot \left(1 - \frac{3}{90.75}\right) + \frac{P}{2} \cdot \left(1 - \frac{75}{90.75}\right)\right) = 0.6843$$

Controlling Negative Moment Distribution Factors from AASHTO LRFD Specifications:

Girders:

$DFM_{g1} = 0.6843$
---------------------

Stringers:

$DFM_{45n} = 0.38604$
-----------------------

Finite-Element Distribution Factors

Girder Section Modulus

$$E_s := 29000$$

$$f'c := 3300$$

$$E_c := \frac{57000 \cdot \sqrt{f'c}}{1000} = 3274.40071$$

$$n := \frac{E_s}{E_c} = 8.85658$$

$$b_{\text{curb}} := \frac{1}{n} \cdot 27 = 3.04858$$

$$y_0 := 2 \cdot \left( .75 \cdot 8 \cdot .375 + .75 \cdot 7.25 \cdot \left( .75 + \frac{7.25}{2} \right) \right) + .5 \cdot 120.5 \cdot \frac{120.5}{2} = 3682.14062$$

$$y_1 := 2 \cdot \left( .75 \cdot 7.25 \cdot \left( 120.5 - .75 - \frac{7.25}{2} \right) + .75 \cdot 8 \cdot (120.5 - .375) \right)$$

$$y_2 := \frac{1}{n} \cdot 6.5 \cdot 141.25 \cdot \left( 120.5 + \frac{6.5}{2} \right) \quad y_3 := \frac{1}{n} \cdot 9 \cdot 27 \cdot (120.5 + 6.5 + 4.5)$$

$$y := y_0 + y_1 + y_2 + y_3 = 22823.1412$$

$$a := 2 \cdot (.75 \cdot 8 + .75 \cdot 7.25) + 120.5 \cdot .5 + 2 \cdot (.75 \cdot 8 + .75 \cdot 7.25) + \frac{1}{n} \cdot (141.25 \cdot 6.5 + 9 \cdot 27) = 237.10305$$

$$y_{\text{bar}} := \frac{y}{a} = 96.25832$$

$$b_d := \frac{1}{n} \cdot 141.25 = 15.94859$$

$$I_w := \frac{1}{12} \cdot .5 \cdot 120.5^3 + .5 \cdot 120.5 \cdot (y_{\text{bar}} - 60.25)^2 = 1.51024 \cdot 10^5$$

$$I_{ba} := 2 \cdot \left( \frac{1}{12} \cdot 8 \cdot .75^3 + 8 \cdot .75 \cdot (y_{\text{bar}} - .375)^2 + \frac{1}{12} \cdot .75 \cdot 7.25^3 + .75 \cdot 7.25 \cdot \left( y_{\text{bar}} - .75 - \frac{7.25}{2} \right)^2 \right) = 2.02184 \cdot 10^5$$

$$I_{ta} := 2 \cdot \left( \frac{1}{12} \cdot .75 \cdot 7.25^3 + .75 \cdot 7.25 \cdot (116.125 - y_{\text{bar}})^2 + \frac{1}{12} \cdot 8 \cdot .75^3 + 8 \cdot .75 \cdot (120.125 - y_{\text{bar}})^2 \right) = 11175.8186$$

$$I_d := \frac{1}{12} \cdot b_d \cdot 6.5^3 + b_d \cdot 6.5 \cdot (123.75 - y_{\text{bar}})^2 = 78714.85307$$

$$I_{\text{curb}} := \frac{1}{12} \cdot b_{\text{curb}} \cdot 9^3 + b_{\text{curb}} \cdot 9 \cdot (131.5 - y_{\text{bar}})^2 = 34261.57235$$

$$I_g := I_w + I_{ba} + I_{ta} + I_d + I_{\text{curb}} = 4.7736 \cdot 10^5$$

$$S_g := \frac{I_g}{y_{\text{bar}}} = 4959.15877$$

16 WF 36 Section Modulus

16 WF 36

$$I_{36} := 446.3$$

$$Y_{36} := \frac{15.85}{2} = 7.925$$

$$S_{36} := \frac{I_{36}}{Y_{36}} = 56.31546 \quad \text{Assuming non-composite action}$$

16 WF 40 Section Modulus

16 WF 40

$$I_{40} := 515.5$$

$$Y_{40} := 8$$

$$S_{40} := \frac{I_{40}}{Y_{40}} = 64.4375 \quad \text{assuming non-composite action}$$

**Girder 1 DF's**2 Lanes loaded**Positive Moment**

$$\sigma_{g1} := 5.5582$$

$$\sigma_{s1} := 3.389$$

$$\sigma_{s2} := 3.8956$$

$$\sigma_{g2} := 4.7831$$

$$M_{g1} := \sigma_{g1} \cdot \frac{S_{g1}}{12} = 2296.99969$$

$$M_{s1} := \sigma_{s1} \cdot \frac{S_{40}}{12} = 18.19822$$

$$M_{s2} := \sigma_{s2} \cdot \frac{S_{40}}{12} = 20.91856$$

$$M_{g2} := \sigma_{g2} \cdot \frac{S_{g1}}{12} = 1976.67936$$

$$DF2_{g1} := \frac{M_{g1}}{M_{g1} + M_{s1} + M_{s2} + M_{g2}} = 0.5326$$

**Negative Moment**

$$\sigma_{g1} := -3.2124$$

$$\sigma_{s1} := 0.3395$$

$$\sigma_{s2} := -0.1597$$

$$\sigma_{g2} := -2.8893$$

$$M_{g1} := \sigma_{g1} \cdot \frac{S_g}{12} = -1327.5668$$

$$M_{s1} := \sigma_{s1} \cdot \frac{S_{36}}{12} = 1.59326$$

$$M_{s2} := \sigma_{s2} \cdot \frac{S_{36}}{12} = -0.74946$$

$$M_{g2} := \sigma_{g2} \cdot \frac{S_g}{12} = -1194.04145$$

$$DF2_{g1} := \frac{M_{g1}}{M_{g1} + M_{s1} + M_{s2} + M_{g2}} = 0.52665$$

Single Lane Loaded**Positive Moment**

$$MPF := 1.2$$

$$\sigma_{g1} := 3.3867$$

$$\sigma_{s1} := 1.6161$$

$$\sigma_{s2} := 0.805$$

$$\sigma_{g2} := 1.8362$$

$$M_{g1} := \sigma_{g1} \cdot \frac{S_g}{12} = 1399.59858$$

$$M_{s1} := \sigma_{s1} \cdot \frac{S_{40}}{12} = 8.67812$$

$$M_{s2} := \sigma_{s2} \cdot \frac{S_{40}}{12} = 4.32268$$

$$M_{g2} := \sigma_{g2} \cdot \frac{S_g}{12} = 758.83395$$

$$DF1_{g1} := MPF \cdot \frac{M_{g1}}{M_{g1} + M_{s1} + M_{s2} + M_{g2}} = 0.77346$$

**Negative Moment**

$$\sigma_{g1} := -1.8499$$

$$\sigma_{s1} := .173$$

$$\sigma_{s2} := -.0645$$

$$\sigma_{g2} := -1.1917$$

$$M_{g1} := \sigma_{g1} \cdot \frac{S_g}{12} = -764.49565$$

$$M_{s1} := \sigma_{s1} \cdot \frac{S_{36}}{12} = 0.81188$$

$$M_{s2} := \sigma_{s2} \cdot \frac{S_{36}}{12} = -0.3027$$

$$M_{g2} := \sigma_{g2} \cdot \frac{S_g}{12} = -492.48579$$

$$DF1_{g1} := MPF \cdot \frac{M_{g1}}{M_{g1} + M_{s1} + M_{s2} + M_{g2}} = 0.73014$$

**Girder 2 Distribution factors**

2 lanes loaded

**Positive Moment**

$$\sigma_{g2} := 5.5474$$

$$\sigma_{s2} := 3.9921$$

$$\sigma_{s1} := 3.3407$$

$$\sigma_{g1} := 4.7937$$

$$M_{g1} := \sigma_{g1} \cdot \frac{S_g}{12} = 1981.05995$$

$$M_{s1} := \sigma_{s1} \cdot \frac{S_{40}}{12} = 17.93886$$

$$M_{s2} := \sigma_{s2} \cdot \frac{S_{40}}{12} = 21.43675$$

$$M_{g2} := \sigma_{g2} \cdot \frac{S_g}{12} = 2292.53645$$

$$DF2_{g2} := \frac{M_{g2}}{M_{g1} + M_{s1} + M_{s2} + M_{g2}} = 0.53154$$

**Negative Moment**

$$\sigma_{g2} := -3.203$$

$$\sigma_{s2} := -0.178$$

$$\sigma_{s1} := 0.3353$$

$$\sigma_{g1} := -2.8984$$

$$M_{g1} := \sigma_{g1} \cdot \frac{S_g}{12} = -1197.80215$$

$$M_{s1} := \sigma_{s1} \cdot \frac{S_{36}}{12} = 1.57355$$

$$M_{s2} := \sigma_{s2} \cdot \frac{S_{36}}{12} = -0.83535$$

$$M_{g2} := \sigma_{g2} \cdot \frac{S_g}{12} = -1323.68213$$

$$DF2_{g1} := \frac{M_{g2}}{M_{g1} + M_{s1} + M_{s2} + M_{g2}} = 0.52512$$

Single Lane Loaded**Positive Moment**

$$\sigma_{g2} := 3.3829$$

$$\sigma_{s2} := 1.9968$$

$$\sigma_{s1} := 0.5557$$

$$\sigma_{g1} := 1.8429$$

$$MPF := 1.2$$

$$\sigma_{g2} := 3.3829$$

$$\sigma_{s1} := 0.5557$$

$$\sigma_{s2} := 1.9968$$

$$\sigma_{g1} := 1.8429$$

$$M_{g1} := \sigma_{g1} \cdot \frac{S_g}{12} = 761.60281$$

$$M_{s1} := \sigma_{s1} \cdot \frac{S_{40}}{12} = 2.98399$$

$$M_{s2} := \sigma_{s2} \cdot \frac{S_{40}}{12} = 10.7224$$

$$M_{g2} := \sigma_{g2} \cdot \frac{S_g}{12} = 1398.02818$$

$$DF1_{g1} := MPF \cdot \frac{M_{g2}}{M_{g1} + M_{s1} + M_{s2} + M_{g2}} = 0.77192$$

### Negative Moment

$$\sigma_{g2} := -1.8456$$

$$\sigma_{s2} := -0.1023$$

$$\sigma_{s1} := 0.1637$$

$$\sigma_{g1} := -1.1957$$

$$M_{g1} := \sigma_{g1} \cdot \frac{S_g}{12} = -494.13885$$

$$M_{s1} := \sigma_{s1} \cdot \frac{S_{36}}{12} = 0.76824$$

$$M_{s2} := \sigma_{s2} \cdot \frac{S_{36}}{12} = -0.48009$$

$$M_{g2} := \sigma_{g2} \cdot \frac{S_g}{12} = -762.71862$$

$$DF1_{g2} := MPF \cdot \frac{M_{g2}}{M_{g1} + M_{s1} + M_{s2} + M_{g2}} = 0.72838$$

### Stringer 1 DF's

2 Lanes Loaded

### Positive Moment

$$\sigma_{s1} := 4.3402$$

$$\sigma_{g1} := 5.3141$$

$$\sigma_{s2} := 5.6318$$

$$\sigma_{g2} := 4.9175$$

$$M_{g1} := \sigma_{g1} \cdot \frac{S_g}{12} = 2196.12214$$

$$M_{s1} := \sigma_{s1} \cdot \frac{S_{40}}{12} = 23.30597$$

$$M_{s2} := \sigma_{s2} \cdot \frac{S_{40}}{12} = 30.24159$$

$$M_{g2} := \sigma_{g2} \cdot \frac{S}{12} = 2032.22194$$

$$DF2_{s1} := \frac{M_{s1}}{M_{g1} + M_{s1} + M_{s2} + M_{g2}} = 0.00544$$

### Negative Moment

$$\sigma_{s1} := -4.9974$$

$$\sigma_{s2} := -5.94$$

$$\sigma_{g1} := -0.2114$$

$$\sigma_{g2} := -0.1943$$

$$M_{g1} := \sigma_{g1} \cdot \frac{S}{12} = -87.36385$$

$$M_{s1} := \sigma_{s1} \cdot \frac{S_{36}}{12} = -23.45257$$

$$M_{s2} := \sigma_{s2} \cdot \frac{S_{36}}{12} = -27.87615$$

$$M_{g2} := \sigma_{g2} \cdot \frac{S}{12} = -80.29705$$

$$DF2_{s1} := \frac{M_{s1}}{M_{g1} + M_{s1} + M_{s2} + M_{g2}} = 0.10709$$

### Single Lane Loaded

#### Positive Moment

$$\sigma_{s1} := 3.1734 \quad \text{MPF} := 1.2$$

$$\sigma_{s2} := 3.6683$$

$$\sigma_{g2} := 2.4488$$

$$\sigma_{g1} := 2.5933$$

$$M_{g1} := \sigma_{g1} \cdot \frac{S}{12} = 1071.71554$$

$$M_{s1} := \sigma_{s1} \cdot \frac{S_{40}}{12} = 17.0405$$

$$M_{s2} := \sigma_{s2} \cdot \frac{S_{40}}{12} = 19.69801$$

$$M_{g2} := \sigma_{g2} \cdot \frac{S}{12} = 1011.999$$

$$DF1_{s1} := \text{MPF} \cdot \frac{M_{s1}}{M_{g1} + M_{s1} + M_{s2} + M_{g2}} = 0.00964$$

**Negative Moment**

$$\sigma_{s1} := -3.6015$$

$$\sigma_{g1} := -0.1$$

$$\sigma_{s2} := -3.8729$$

$$\sigma_{g2} := -0.1014$$

$$M_{g1} := \sigma_{g1} \cdot \frac{S}{12} = -41.32632$$

$$M_{s1} := \sigma_{s1} \cdot \frac{S}{12} = -16.90168$$

$$M_{s2} := \sigma_{s2} \cdot \frac{S}{12} = -18.17534$$

$$M_{g2} := \sigma_{g2} \cdot \frac{S}{12} = -41.90489$$

$$DF1_{s1} := MPF \cdot \frac{M_{s1}}{M_{g1} + M_{s1} + M_{s2} + M_{g2}} = 0.17143$$

**Stringer 2 DF's**2 Lanes Loaded**Positive Moment**

$$\sigma_{s2} := 6.3105$$

$$\sigma_{g1} := 4.9299$$

$$\sigma_{g2} := 5.3022$$

$$\sigma_{s1} := 3.9556$$

$$M_{g1} := \sigma_{g1} \cdot \frac{S}{12} = 2037.3464$$

$$M_{s1} := \sigma_{s1} \cdot \frac{S}{12} = 21.24075$$

$$M_{s2} := \sigma_{s2} \cdot \frac{S}{12} = 33.88607$$

$$M_{g2} := \sigma_{g2} \cdot \frac{S}{12} = 2191.2043$$

$$DF2_{s2} := \frac{M_{s2}}{M_{g1} + M_{s1} + M_{s2} + M_{g2}} = 0.00791$$

**Negative Moment**

$$\sigma_{s2} := -6.616$$

$$\sigma_{s1} := -4.4858$$

$$\sigma_{g1} := -0.1857$$

$$\sigma_{g2} := -0.2203$$

$$M_{g1} := \sigma_{g1} \cdot \frac{S_g}{12} = -76.74298$$

$$M_{s1} := \sigma_{s1} \cdot \frac{S_{36}}{12} = -21.05166$$

$$M_{s2} := \sigma_{s2} \cdot \frac{S_{36}}{12} = -31.04859$$

$$M_{g2} := \sigma_{g2} \cdot \frac{S_g}{12} = -91.04189$$

$$DF2_{s2} := \frac{M_{s2}}{M_{g1} + M_{s1} + M_{s2} + M_{g2}} = 0.1412$$

Single Lane Loading**Positive Moment**

$$\sigma_{s2} := 4.5537$$

$$\sigma_{s1} := 2.6647$$

$$\sigma_{g1} := 2.4558$$

$$\sigma_{g2} := 2.5872$$

$$M_{g1} := \sigma_{g1} \cdot \frac{S_g}{12} = 1014.89184$$

$$M_{s1} := \sigma_{s1} \cdot \frac{S_{40}}{12} = 14.30888$$

$$M_{s2} := \sigma_{s2} \cdot \frac{S_{40}}{12} = 24.45242$$

$$M_{g2} := \sigma_{g2} \cdot \frac{S_g}{12} = 1069.19463$$

$$DF1_{s2} := MPF \cdot \frac{M_{s2}}{M_{g1} + M_{s1} + M_{s2} + M_{g2}} = 0.01382$$

**Negative Moment**

$$\sigma_{s2} := -4.7684$$

$$\sigma_{s1} := -2.923$$

$$\sigma_{g1} := -0.0956$$

$$\sigma_{g2} := -0.1062$$

$$M_{g1} := \sigma_{g1} \cdot \frac{S_g}{12} = -39.50796$$

$$M_{s1} := \sigma_{s1} \cdot \frac{S_{36}}{12} = -13.71751$$

$$M_{s2} := \sigma_{s2} \cdot \frac{S_{36}}{12} = -22.37789$$

$$M_{g2} := \sigma_{g2} \cdot \frac{S_g}{12} = -43.88856$$

$$DF1_{s2} := MPF \cdot \frac{M_{s2}}{M_{g1} + M_{s1} + M_{s2} + M_{g2}} = 0.22473$$

**Controlling distribution factors**

Girders:

**Positive Moment**

G1 Single lane loading

**Negative Moment**

G1 Single lane loading

Stringers:

**Positive Moment**

S2 single lane loading

**Negative Moment**

S2 single lane loading

## APPENDIX D: DISTRIBUTION FACTORS CALCULATIONS WITHOUT CROSS BRACING

### Girder 1 DF's

2 Lanes loaded

#### Positive Moment

$$\sigma_{g1} := 6.2605$$

$$\sigma_{s1} := 4.2011$$

$$\sigma_{s2} := 3.0153$$

$$\sigma_{g2} := 4.4515$$

$$M_{g1} := \sigma_{g1} \cdot \frac{S_g}{12} = 2587.23446$$

$$M_{s1} := \sigma_{s1} \cdot \frac{S_{40}}{12} = 22.55903$$

$$M_{s2} := \sigma_{s2} \cdot \frac{S_{40}}{12} = 16.19153$$

$$M_{g2} := \sigma_{g2} \cdot \frac{S_g}{12} = 1839.64127$$

$$DF2_{g1} := \frac{M_{g1}}{M_{g1} + M_{s1} + M_{s2} + M_{g2}} = 0.57937$$

**Negative Moment**

$$\sigma_{g1} := -3.6297$$

$$\sigma_{s1} := 0.3119$$

$$\sigma_{s2} := -.1759$$

$$\sigma_{g2} := -2.5966$$

$$M_{g1} := \sigma_{g1} \cdot \frac{S_g}{12} = -1500.02155$$

$$M_{s1} := \sigma_{s1} \cdot \frac{S_{36}}{12} = 1.46373$$

$$M_{s2} := \sigma_{s2} \cdot \frac{S_{36}}{12} = -0.82549$$

$$M_{g2} := \sigma_{g2} \cdot \frac{S_g}{12} = -1073.07931$$

$$DF2_{g1} := \frac{M_{g1}}{M_{g1} + M_{s1} + M_{s2} + M_{g2}} = 0.58311$$

Single Lane Loaded**Positive Moment**

$$MPF := 1.2$$

$$\sigma_{g1} := 4.519$$

$$\sigma_{s1} := 1.6085$$

$$\sigma_{s2} := 0.786$$

$$\sigma_{g2} := .8608$$

$$M_{g1} := \sigma_{g1} \cdot \frac{S_g}{12} = 1867.53654$$

$$M_{s1} := \sigma_{s1} \cdot \frac{S_{40}}{12} = 8.63731$$

$$M_{s2} := \sigma_{s2} \cdot \frac{S_{40}}{12} = 4.22066$$

$$M_{g2} := \sigma_{g2} \cdot \frac{S_g}{12} = 355.73699$$

$$DF1_{g1} := MPF \cdot \frac{M_{g1}}{M_{g1} + M_{s1} + M_{s2} + M_{g2}} = 1.0022$$

**Negative Moment**

$$\sigma_{g1} := -2.592$$

$$\sigma_{s1} := 0.194$$

$$\sigma_{s2} := -0.071$$

$$\sigma_{g2} := -0.5226$$

$$M_{g1} := \sigma_{g1} \cdot \frac{S_g}{12} = -1071.1783$$

$$M_{s1} := \sigma_{s1} \cdot \frac{S_{36}}{12} = 0.91043$$

$$M_{s2} := \sigma_{s2} \cdot \frac{S_{36}}{12} = -0.3332$$

$$M_{g2} := \sigma_{g2} \cdot \frac{S_g}{12} = -215.97136$$

$$DF1_{g1} := MPF \cdot \frac{M_{g1}}{M_{g1} + M_{s1} + M_{s2} + M_{g2}} = 0.9991$$

**Girder 2 Distribution factors**2 lanes loaded**Positive Moment**

$$\sigma_{g2} := 6.2693$$

$$\sigma_{s2} := 3.089$$

$$\sigma_{s1} := 4.2411$$

$$\sigma_{g1} := 4.4418$$

$$M_{g1} := \sigma_{g1} \cdot \frac{S_g}{12} = 1835.63262$$

$$M_{s1} := \sigma_{s1} \cdot \frac{S_{40}}{12} = 22.77382$$

$$M_{s2} := \sigma_{s2} \cdot \frac{S_{40}}{12} = 16.58729$$

$$M_{g2} := \sigma_{g2} \cdot \frac{S_g}{12} = 2590.87118$$

$$DF2_{g2} := \frac{M_{g2}}{M_{g1} + M_{s1} + M_{s2} + M_{g2}} = 0.58015$$

**Negative Moment**

$$\sigma_{g2} := -3.6267$$

$$\sigma_{s2} := -0.1964$$

$$\sigma_{s1} := 0.2662$$

$$\sigma_{g1} := -2.5988$$

$$M_{g1} := \sigma_{g1} \cdot \frac{S_g}{12} = -1073.98849$$

$$M_{s1} := \sigma_{s1} \cdot \frac{S_{36}}{12} = 1.24926$$

$$M_{s2} := \sigma_{s2} \cdot \frac{S_{36}}{12} = -0.9217$$

$$M_{g2} := \sigma_{g2} \cdot \frac{S_g}{12} = -1498.78176$$

$$DF2_{g1} := \frac{M_{g2}}{M_{g1} + M_{s1} + M_{s2} + M_{g2}} = 0.58263$$

Single Lane Loaded**Positive Moment**

$$\sigma_{g2} := 3.3829$$

$$\sigma_{s2} := 1.9968$$

$$\sigma_{s1} := 0.5557$$

$$\sigma_{g1} := 1.8429$$

$$MPF := 1.2$$

$$\sigma_{g2} := 4.5226$$

$$\sigma_{s1} := 1.1425$$

$$\sigma_{s2} := 1.4091$$

$$\sigma_{g1} := 0.8591$$

$$M_{g1} := \sigma_{g1} \cdot \frac{S_g}{12} = 355.03444$$

$$M_{s1} := \sigma_{s1} \cdot \frac{S_{40}}{12} = 6.13499$$

$$M_{s2} := \sigma_{s2} \cdot \frac{S_{40}}{12} = 7.56657$$

$$M_{g2} := \sigma_{g2} \cdot \frac{S_g}{12} = 1869.02429$$

$$DF1_{g1} := MPF \cdot \frac{M_{g2}}{M_{g1} + M_{s1} + M_{s2} + M_{g2}} = 1.00227$$

### Negative Moment

$$\sigma_{g2} := -2.5899$$

$$\sigma_{s2} := -.1125$$

$$\sigma_{s1} := .1025$$

$$\sigma_{g1} := -.5231$$

$$M_{g1} := \sigma_{g1} \cdot \frac{S_g}{12} = -216.178$$

$$M_{s1} := \sigma_{s1} \cdot \frac{S_{36}}{12} = 0.48103$$

$$M_{s2} := \sigma_{s2} \cdot \frac{S_{36}}{12} = -0.52796$$

$$M_{g2} := \sigma_{g2} \cdot \frac{S_g}{12} = -1070.31044$$

$$DF1_{g2} := MPF \cdot \frac{M_{g2}}{M_{g1} + M_{s1} + M_{s2} + M_{g2}} = 0.99832$$

### Stringer 1 DF's

2 Lanes Loaded

### Positive Moment

$$\sigma_{s1} := 5.1933$$

$$\sigma_{g1} := 5.7891$$

$$\sigma_{s2} := 3.899$$

$$\sigma_{g2} := 4.8828$$

$$M_{g1} := \sigma_{g1} \cdot \frac{S_g}{12} = 2392.42217$$

$$M_{s1} := \sigma_{s1} \cdot \frac{S_{40}}{12} = 27.88694$$

$$M_{s2} := \sigma_{s2} \cdot \frac{S_{40}}{12} = 20.93682$$

$$M_{g2} := \sigma_{g2} \cdot \frac{S}{12} = 2017.88171$$

$$DF2_{s1} := \frac{M_{s1}}{M_{g1} + M_{s1} + M_{s2} + M_{g2}} = 0.00625$$

#### Negative Moment

$$\sigma_{s1} := -2.4285$$

$$\sigma_{s2} := -1.3196$$

$$\sigma_{g1} := -0.8256$$

$$\sigma_{g2} := -0.7573$$

$$M_{g1} := \sigma_{g1} \cdot \frac{S}{12} = -341.19012$$

$$M_{s1} := \sigma_{s1} \cdot \frac{S_{36}}{12} = -11.39684$$

$$M_{s2} := \sigma_{s2} \cdot \frac{S_{36}}{12} = -6.19282$$

$$M_{g2} := \sigma_{g2} \cdot \frac{S}{12} = -312.96424$$

$$DF2_{s1} := \frac{M_{s1}}{M_{g1} + M_{s1} + M_{s2} + M_{g2}} = 0.01697$$

#### Single Lane Loaded

#### Positive Moment

$$\sigma_{s1} := 3.699 \quad \text{MPF} := 1.2$$

$$\sigma_{s2} := 2.5211$$

$$\sigma_{g2} := 2.4917$$

$$\sigma_{g1} := 2.8069$$

$$M_{g1} := \sigma_{g1} \cdot \frac{S}{12} = 1159.98856$$

$$M_{s1} := \sigma_{s1} \cdot \frac{S_{40}}{12} = 19.86286$$

$$M_{s2} := \sigma_{s2} \cdot \frac{S_{40}}{12} = 13.53778$$

$$M_{g2} := \sigma_{g2} \cdot \frac{S}{12} = 1029.72799$$

$$DF1_{s1} := \text{MPF} \cdot \frac{M_{s1}}{M_{g1} + M_{s1} + M_{s2} + M_{g2}} = 0.01072$$

**Negative Moment**

$$\sigma_{s1} := -1.5966$$

$$\sigma_{g1} := -0.4085$$

$$\sigma_{s2} := -.8305$$

$$\sigma_{g2} := -.8501$$

$$M_{g1} := \sigma_{g1} \cdot \frac{S_g}{12} = -168.81803$$

$$M_{s1} := \sigma_{s1} \cdot \frac{S_{36}}{12} = -7.49277$$

$$M_{s2} := \sigma_{s2} \cdot \frac{S_{36}}{12} = -3.8975$$

$$M_{g2} := \sigma_{g2} \cdot \frac{S_g}{12} = -351.31507$$

$$DF1_{s1} := MPF \cdot \frac{M_{s1}}{M_{g1} + M_{s1} + M_{s2} + M_{g2}} = 0.01692$$

**Stringer 2 DF's**2 Lanes Loaded**Positive Moment**

$$\sigma_{s2} := 5.2619$$

$$\sigma_{g1} := 4.7543$$

$$\sigma_{g2} := 5.6538$$

$$\sigma_{s1} := 4.6431$$

$$M_{g1} := \sigma_{g1} \cdot \frac{S_g}{12} = 1964.77738$$

$$M_{s1} := \sigma_{s1} \cdot \frac{S_{40}}{12} = 24.93248$$

$$M_{s2} := \sigma_{s2} \cdot \frac{S_{40}}{12} = 28.25531$$

$$M_{g2} := \sigma_{g2} \cdot \frac{S_g}{12} = 2336.50766$$

$$DF2_{s2} := \frac{M_{s2}}{M_{g1} + M_{s1} + M_{s2} + M_{g2}} = 0.00649$$

**Negative Moment**

$$\sigma_{s2} := -1.6967$$

$$\sigma_{s1} := -1.3839$$

$$\sigma_{g1} := -0.6298$$

$$\sigma_{g2} := -0.7542$$

$$M_{g1} := \sigma_{g1} \cdot \frac{S}{12} \cdot g = -260.27318$$

$$M_{s1} := \sigma_{s1} \cdot \frac{S}{12} \cdot 36 = -6.49458$$

$$M_{s2} := \sigma_{s2} \cdot \frac{S}{12} \cdot 36 = -7.96254$$

$$M_{g2} := \sigma_{g2} \cdot \frac{S}{12} \cdot g = -311.68313$$

$$DF2_{s2} := \frac{M_{s2}}{M_{g1} + M_{s1} + M_{s2} + M_{g2}} = 0.01358$$

Single Lane Loading**Positive Moment**

$$\sigma_{s2} := 3.7875$$

$$\sigma_{s1} := 3.1705$$

$$\sigma_{g1} := 2.4251$$

$$\sigma_{g2} := 2.7447$$

$$M_{g1} := \sigma_{g1} \cdot \frac{S}{12} \cdot g = 1002.20466$$

$$M_{s1} := \sigma_{s1} \cdot \frac{S}{12} \cdot 40 = 17.02492$$

$$M_{s2} := \sigma_{s2} \cdot \frac{S}{12} \cdot 40 = 20.33809$$

$$M_{g2} := \sigma_{g2} \cdot \frac{S}{12} \cdot g = 1134.28359$$

$$DF1_{s2} := MPF \cdot \frac{M_{s2}}{M_{g1} + M_{s1} + M_{s2} + M_{g2}} = 0.01123$$

**Negative Moment**

$$\sigma_{s2} := -1.1757$$

$$\sigma_{s1} := -0.8998$$

$$\sigma_{g1} := -0.3223$$

$$\sigma_{g2} := -0.3642$$

$$M_{g1} := \sigma_{g1} \cdot \frac{S_g}{12} = -133.19474$$

$$M_{s1} := \sigma_{s1} \cdot \frac{S_{36}}{12} = -4.22272$$

$$M_{s2} := \sigma_{s2} \cdot \frac{S_{36}}{12} = -5.51751$$

$$M_{g2} := \sigma_{g2} \cdot \frac{S_g}{12} = -150.51047$$

$$DF1_{s2} := MPF \cdot \frac{M_{s2}}{M_{g1} + M_{s1} + M_{s2} + M_{g2}} = 0.02256$$

**Controlling distribution factors**

Girders:

**Positive Moment**

G1 Single lane loading

**Negative Moment**

G1 Single lane loading

Stringers:

**Positive Moment**

S2 single lane loading

**Negative Moment**

S2 single lane loading

## APPENDIX E: LOAD RATING CALCULATIONS

Finite-Element Load ratings

### Girders

#### **Positive Moment**

$$R_n := 12556 \quad \gamma_D := 1.3$$

$$D := 4173.6 \quad \gamma_{LI} := 2.17$$

$$L := 2297 \quad \gamma_{LO} := 1.3$$

$$IM := .135$$

$$RF_I := \frac{R_n - \gamma_D \cdot D}{\gamma_{LI} \cdot L \cdot (1 + IM)} = 1.26035 \quad \text{Inventory Rating}$$

$$RF_O := \frac{R_n - \gamma_D \cdot D}{\gamma_{LO} \cdot L \cdot (1 + IM)} = 2.10382 \quad \text{Operating Rating}$$

#### **Negative Moment**

$$R_n := 11801 \quad \gamma_D := 1.3$$

$$D := 3651.8 \quad \gamma_{LI} := 2.17$$

$$L := 1326.8 \quad \gamma_{LO} := 1.3$$

$$IM := .135$$

$$RF_I := \frac{R_n - \gamma_D \cdot D}{\gamma_{LI} \cdot L \cdot (1 + IM)} = 2.15851 \quad \text{Inventory Rating}$$

$$RF_O := \frac{R_n - \gamma_D \cdot D}{\gamma_{LO} \cdot L \cdot (1 + IM)} = 3.60305 \quad \text{Operating Rating}$$

Stringers**Positive Moment**

$$R_n := 268.4 \quad \gamma_D := 1.3$$

$$D := 8.9 \quad \gamma_{LI} := 2.17$$

$$L := 33.9$$

$$IM := .25 \quad \gamma_{LO} := 1.3$$

$$RF_I := \frac{R_n - \gamma_D \cdot D}{\gamma_{LI} \cdot L \cdot (1 + IM)} = 2.79303$$

Inventory Rating

$$RF_O := \frac{R_n - \gamma_D \cdot D}{\gamma_{LO} \cdot L \cdot (1 + IM)} = 4.66222$$

Operating Rating

**Negative Moment**

$$R_n := 234.6 \quad \gamma_D := 1.3$$

$$D := 12.7 \quad \gamma_{LI} := 2.17$$

$$L := 30.6$$

$$IM = 0.25 \quad \gamma_{LO} := 1.3$$

$$RF_I := \frac{R_n - \gamma_D \cdot D}{\gamma_{LI} \cdot L \cdot (1 + IM)} = 2.62751$$

Inventory Rating

$$RF_O := \frac{R_n - \gamma_D \cdot D}{\gamma_{LO} \cdot L \cdot (1 + IM)} = 4.38592$$

Operating Rating